STARS

University of Central Florida
STARS

Electronic Theses and Dissertations, 2004-2019

2018

Evaluating Hydrologic Fluxes Through Stormwater Treatment Systems: Implication to Freshwater Springs in a Karst Environment

Nyle Rice
University of Central Florida

 Part of the Environmental Engineering Commons
Find similar works at: https://stars.library.ucf.edu/etd
University of Central Florida Libraries http://library.ucf.edu

This Masters Thesis (Open Access) is brought to you for free and open access by STARS. It has been accepted for inclusion in Electronic Theses and Dissertations, 2004-2019 by an authorized administrator of STARS. For more information, please contact STARS@ucf.edu.

STARS Citation
Rice, Nyle, "Evaluating Hydrologic Fluxes Through Stormwater Treatment Systems: Implication to Freshwater Springs in a Karst Environment" (2018). *Electronic Theses and Dissertations, 2004-2019*. 5996.
https://stars.library.ucf.edu/etd/5996

EVALUATING HYDROLOGIC FLUXES THOUGH STORMWATER TREATMENT SYSTEMS: IMPLICATION TO FRESHWATER SPRINGS IN A KARST ENVIRONMENT

by

NYLE J. RICE
B.S. University of Central Florida, 2016

A thesis submitted in partial fulfillment of the requirements
for the degree of Master of Science
in the Department of Civil, Environmental, and Construction Engineering
in the College of Engineering and Computer Science
at the University of Central Florida
Orlando, Florida

Summer Term
2018

Major Professor: Kelly Kibler

ABSTRACT

In recent years, concentrations of nutrients such as nitrogen and phosphorus have increased in surface and groundwater resources, due in part to non-point source pollution associated with stormwater runoff. The elevated nutrient concentrations found in stormwater runoff have prompted the design of best management practices (BMP's) to mitigate the problem. The overall objective within this thesis is to analyze the performance of innovative surface BMPs and investigate connections between the BMPs and groundwater flows to freshwater springs within a karst environment. The performance of two stormwater BMPs, blanket filters and vertical reactors containing Bio-sorption Activated Media (BAM), are assessed in terms of hydraulic retention time. Capture efficiency is also evaluated for the blanket filters. Blanket filters captured, at minimum 68% of the stormwater runoff entering a stormwater basin in one year. Water content monitoring indicates that BAM is affected by the surrounding water table. The vertical reactors are more appropriate technologies for small contributing areas. Tracking a conservative tracer from an injection point within a stormwater basin to nearby Silver Springs reveals several unique flowpaths and velocities of groundwater. Subsurface velocities observed in the basin ranged from 0.1 m/d to 1.4 m/d, while velocities from the injection well to the spring vary from 2.3 m/d to 13.5 m/d. The fastest travel times observed in the spring may represent flowpaths that include macropore/conduit flow through karst features, while the slower peaks may be more representative of matrix flow. Interaction with karst features may reduce retention time of stormwater in aquifers, altering expected nutrient transformations. Understanding the variable pathways stormwater may take from the surface to spring discharge may assist environmental managers in preserving water quality in springs and other waterbodies in karst systems.

ACKNOWLEDGMENTS

Writing this thesis, over a period of two years, has been a time of intensive learning for me, both scientifically and personally. I have experienced growth and accomplishments that I never thought I would achieve and would like to reflect on the people who have supported and helped me thus far. I would first like to thank the Florida Department of Transportation (FDOT) and the Florida Department of Environmental Protection (FDEP) for providing funding to this research. I would then like to thank my thesis advisor and committee chair, Dr. Kelly Kibler of the Civil, Environmental, and Construction Engineering Department at the University of Central Florida. She provided me with a tremendous amount of guidance. Her door was always open for me whenever I had any questions, comments, or concerns with my research. She allowed this paper to be my own work and guided me in the right direction whenever needed.

I would also like to thank other experts and students that were heavily involved in helping me present my research in a professional manner: Dr. Ni-Bin Chang, Dr. Martin Wanielista, Dr. Dingbao Wang, Dan Wen, Yuan Gao, and Mohammad Shokri. Without their passion, expertise, and input this research could not have been successfully completed.

Finally, I would like to express deepest gratitude to my parents for providing me with the support and encouragement throughout my two years of coursework, the process of conducting research, and composing this thesis. When times were hard they provided me with the love and support I needed. They are truly my ultimate role models. This accomplishment would have not been possible without them. Thank you!

TABLE OF CONTENTS

LIST OF FIGURES

LIST OF TABLES

CHAPTER 1: INTRODUCTION AND LITERATURE REVIEW

1.1 Problem Statement and Literature Review

In recent years, loadings of nutrients such as nitrogen and phosphorus have increased in natural water resources, including surface water and groundwater. Agriculture, wastewater, fossil fuels, and stormwater runoff from highways and roads are some sources of pollution to surface water bodies that can make their way into groundwater sources. Excess nitrogen and phosphorus in surface water bodies have been shown to stimulate plant growth to include algae. Algal growth may decrease dissolved oxygen levels and causes changes in the biotic community, known as eutrophication (EPA, 2015). Additionally, exposure to nitrates in drinking water is linked to cancer, diabetes, birth defects, and respiratory and neurological problems (Ward, 2005), as well as methemoglobinemia, or blue baby syndrome (Majumdar, 2003). In Florida, most of the water supply is groundwater from the Floridan Aquifer. The Environmental Protection Agency (EPA) set the maximum contaminant level (MCL) for nitrate, a form of nitrogen, at 10 mg/L (10 parts per million) (Fan & Steinberg, 1996).

Many surface water bodies are connected to groundwater, therefore the quality of surface waters may influence groundwater quality (Winter, 1999). Groundwater is also discharged as surface water through streams, rivers, lakes, wetlands, and springs. Springs are focused points of groundwater discharge where groundwater flow lines converge through vents (Van der Kamp, 1995). The groundwater that emerges at the springs becomes surface water and travels along rivers or streams. However, flow is quite different within karst springs. Karst springs may carry large amounts of nutrients at higher concentrations and velocities relative to normal groundwater

(Vesper & White, 2003). Springs are areas of concern because they provide a way to monitor groundwater quality throughout an entire watershed area (Quinlan, 1989) rather than in one specific location. Due to their heterogeneity, orthodox methods, like well installation and sampling, do not completely represent the groundwater quality in a karst aquifer (Vesper & White, 2003). Springs are important because they are connection points between groundwater and surface water where humans and wildlife can both interact and become exposed to contamination problems (Vesper & White, 2003) as well as being important areas for local ecology and recreation. Excess nutrients in springs can cause eutrophication, toxicity, changes in the natural habits of many animals, and even lead to mortality of aquatic organisms (Jacoby et al, 2008). Due to the connections between surface water and groundwater, there is concern that stormwater runoff should be treated before it infiltrates into groundwater systems, particularly in systems of karst hydrogeology. However, many questions remain regarding the potential cost-effectiveness of various stormwater Best Management Practices (BMPs) and in particular, mechanisms of flow and contaminant transport in regions characterized by karst hydrogeology.

1.1.1 Stormwater Runoff

Stormwater runoff may be generated by overland flow from impervious surfaces, pervious area excess overland flow, and return flow. Infiltration is based on the concept that runoff begins when precipitation events deliver water at a rate faster than the soil infiltration capacity, so the water begins to pond and flow as overland flow (Lyon, et al., 2006). Saturation excess overland flow describes soil saturation due to precipitation events (from above) and groundwater flow (from below) (Sivapalan et al., 1987). Return flow describes the return of groundwater to the surface, through thin locations in the soil to add to overland flow (Tarboton, 2003). On impervious surfaces,

water cannot infiltrate and thus flows as surface runoff after initial abstraction. Increasing the number of impervious surfaces in urban areas reduces infiltration, which allows water to penetrate into the groundwater and not flow as surface runoff (Askarizadeh et al., 2015). Impervious surfaces, such as roofs and roads, increase the volume of water entering storm drainage systems, thus decreasing the amount of water that is able to flow from the surface into the groundwater (Burns et al., 2005; Rose & Peters, 2001). In regards to quantity and quality and on a state basis in the US. Nearly 30% of the cases of polluted water quality were attributed to stormwater in urban environments (US EPA, 1992). Urban stream syndrome refers to the ecological degradation of streams draining from urban areas (Walsh et al., 2005). Some of the symptoms of this include an increase in the nutrient and contaminant loads as well as an increase in runoff flows which are believed to be attributed to runoff generation from impervious areas (Roy & Bickerton, 2011; Halstead et al., 2014; Paul & Meyer 2001). During runoff events, the volume of water that is delivered quickly to streams increases and the time between rainfall and runoff generation decreases, resulting in higher peak flows (Askarizadeh et al., 2015). There have been ongoing efforts to combat this problem, including channel reconfiguration and stream restoration, but neither have been effective to improve runoff signatures (Vietz et al., 2016), as these measures do not influence the true source of the problem.

In addition to altering hydrologic delivery to waterbodies, stormwater runoff also may contain high concentrations of pollutants, which may degrade water quality. Degradation in water quality is due to chemical and manure fertilizers, poultry waste disposal, ammonia generated by poultry lagoons (Mallin et al., 2009), improper disposal of waste generated from wastewater treatment plants, and pet waste. Roadways can also contain large amounts of suspended solids, metals, and inorganic

and organic compounds (Lee, et al., 2005) from vehicle emissions, oil leaks, construction zones, residential areas, parks, and asphalt road surfaces such as parking lots. In urban areas, when storm events occur, pollutants from the sources listed above flow down roadways, to stormwater systems (Brown & Peake, 2006). EPA's Nationwide Urban Runoff Program (NURP), operated from 1978 to 1983, analyzed urban runoff for over 2,300 storm events at 81 different sites. The median event mean concentration (EMC) for nitrate and nitrite in residential, commercial, rural, and mixed areas are 736 µg/L, 572 µg/L, 543 µg/L, and 588 µg/L, respectively (US EPA, 1983). The median event mean concentration for total phosphorus (TP) in residential, commercial, rural, and mixed areas are 383 µg/L, 201 µg/L, 121 µg/L, and 263 µg/L, respectively (US EPA, 1983). These data indicate significant differences in runoff pollutant loads between urban and rural (non-urban) categories. In terms of pollutant loadings, freeways generate the most in terms of nitrate and nitrite (4.2 lbs/acre-year or 4.7 kg/ha-year) while construction sites generate the most total phosphorus (80 lbs/acre-year or 90 kg/ha-year) (US EPA 1999).

1.1.1.1 Best Management Practices for Stormwater

Elevated nutrient concentrations in stormwater runoff have prompted the design of many best management practices (BMP's) to mitigate the problem. BMP's are systems that are designed to reduce contaminants in stormwater. A few of these systems include rain gardens, bioswales, green roofs, rain barrels, and gravel wetlands. Rain gardens, also known as bioretention filtering systems, are composed of different layers of soil implemented in layers designed to control stormwater runoff. Stormwater runoff is controlled by reducing the speed and increasing the amount of water absorbed into the ground. These systems also remove stormwater pollutants before they infiltrate into the groundwater (Anyona, 2009). Bioswales are broad ditches with slopes that are designed

to filter and hold stormwater. They are comprised of dams that slow down the velocity of incoming stormwater to allow for infiltration (Wahl, 2009). Green roofs are roofs that are covered by vegetation that are designed to consume stormwater, provide filtering of suspended solids, and reduce the amount of stormwater volume that will be delivered downstream (Rowe, 2011). Rain barrels are storage devices that retain stormwater for reuse later. The stormwater from rooftops flows directly into the rain barrels, which minimizes the volume of water that flows to drainage systems and decreases peak storm event flows (Abi Aad et al., 2009, Ando & Freitas, 2011). Gravel wetlands consist of constructed wetland cells filled with a gravel media. During small storm events, the system is designed for incoming water to flow horizontally through the gravel media, allowing contact with the root zones of wetland vegetation. Treatment then occurs through bacterial, chemical, and physical processes within the media (McCarthy, 2008).

There are two types of stormwater ponds: wet and dry (FDEP, 2010). Wet ponds stay wet most of the year, while dry ponds drain after each event. Stormwater wet ponds, or stormwater detention ponds, are a common type of BMP in Florida. Stormwater wet ponds are designed for flood mitigation (source reduction) and water quality treatment. The construction of wet ponds allows for runoff to travel off impervious surfaces for temporary storage, in order to delay and lessen peak flows for storm events (Mitchell et al., 2007). Water quality treatment is achieved mainly through sedimentation and in some cases, nutrient transformation. Another common design for a stormwater pond is a retention or dry basin. Dry basins act as settling basins that accumulate large amounts of sediments on the surface while allowing the water to infiltrate into the soil (Marsalek & Marsalek, 1997). Dry retention basin have permeable bottoms so that stormwater can infiltrate into the shallow groundwater between storm events. Both dry and wet ponds have a discharge to

surface waters, through outlet structures, when a set level in the water is exceeded. (Wahl, 2009; Stanley, 1996; FDEP 2010). Some of these outlet structures include culverts, French drains, weirs, or perforated pipes (Wanielista et. al., 1997; Emerson et al., 2005; Akin, 1990)

1.1.2 Use of Biosorption Activated Media in Stormwater BMPs

Before 1995 many municipalities used sand filters to remove sediments and nutrients, but due to the low removal efficiency of these sand filters, some researchers begin considering other types of media. Biosorption Activated Media (BAM) is a solid media used within stormwater BMPs to enhance the removal of pollutants from stormwater. Sorption is a process whereby pollutants accumulate on the solid media and are designed to remove nutrients/ Examples of media are expanded clay, tire crumb, tire chips, activated carbon, sawdust, limestone, and/or crushed shells, (Wanielista, 2015). These various media are ideal for pollutant removal, as they are non-toxic, non-degradable and have a long life expectancy (50+ years). One specific type of BAM, known as Bold and Gold (B&G), contains clay, tire crumb, and sand (CTS) and was developed by the University of Central Florida Stormwater Management Academy to remove nitrogen and phosphorus in stormwater. The composition of CTS will have between 2% and 6% of material passing between 0.075 mm openings (200 sieve). The media is primarily composed of 85% sand and 15% of other sorption materials based on volume with a total porosity of around 40% (Wen et al., 2018). The sorption materials are recycled tire and mined clay. This mix has a dry weight of 62 lbs/ft^3 (993 kg/m^3) and non-flammable up to 482 degrees Fahrenheit (250 degrees Celsius). The CTS composition has a residual water holding capacity of at least 10% and a permeability greater than 5 inches/hour (12.7 cm/hour) (*BOLD & GOLD®,* 2017).

Research results support that certain types of BAM work better than others to remove harmful nutrients through adsorption, absorption, chemical precipitation, and ion exchange. Kim et al. [2000] tested the efficiency of different types of sorption media. Two columns (40 cm long/6.4 cm in diameter) were used as a control group while the others were filled with various sorption media types for nutrient removal. One set of columns were filled with alfalfa, newspaper, and leaf mulch compost while the other experimental set of columns contained sawdust, wheat straw, and wood chips. The results of this experiment revealed that alfalfa and newspaper had a 100% nitrate (NO_3^-) removal efficiency (from a secondary effluent sample). Sawdust, wheat straw, and wood chips also resulted in removal efficiencies that were greater than 95%. Increasing the hydraulic retention time through the media could have resulted in a better removal efficiency. Birch et al. [2005] experimented with another method to remove nitrogen from a stormwater infiltration basin. The basin was composed of a 1:6 mixture of zeolite along with coarse, pure quarzitic sand. The results of this experiment showed that reduction in total kjeldahl nitrogen (organic nitrogen and ammonia – NH_3) ranged from 47 – 74% and the total nitrogen removal ranged from 33 – 40%. Total phosphorus removal ranged from 37 – 67%. Schipper et al. [2005] performed experiments using a mixture of pine sawdust and excavated soil. This method resulted in a 97.2% nitrate removal rate (approximately 1.4 g N/m^3 per day).

BAM was also used in a nutrient removal analysis study in a north-central Florida stormwater basin, in a karst region, located 1.2 mi (1.9 km) southwest of Silver Springs. The subsurface of this region consists of a surficial aquifer containing sand, silt, and clay, an intermediate layer of just clay, above the Floridan aquifer. The stormwater basin is located in a residential community with a watershed area of about 34.8 ac (14.1 ha). The goals of this study were to sustain the flood

control capacity of the stormwater infiltration basin, lower the nutrient loading to groundwater, and minimize construction and design costs while increasing the economic feasibility (O'Reilly et al., 2012). Two sub-basins were designed: one built for the purpose of nutrient reduction (south basin) and the other as a flood control basin (north basin). The south basin was formed (bottom to top) by placing 0.30 ft (0.10 m) of sand, 1 ft (0.30 m) of BAM, and 0.5 ft (0.15 m) of native soil. The BAM mixture was comprised of a 1:1.9:4.1 volume mixture of tire crumb, silt and clay, along with sand. Tire crumb increases the sorption capacity, while silt and clay increase the ability for the BAM to retain moisture. The sand helps to confine the permeability. The purpose of the 3 different layers (sand, BAM, and native soil) was to increase the soil moisture capacity, reduce the oxygen dispersion, and increase the capacity of adsorption/absorption (O'Reilly et al., 2012). The top layer of natural soil provided an organic carbon source to be used during denitrification. Sampling was done at depths of 1.6, 2.9, and 4.3 ft (0.5, 0.9, and 1.3 m) below the ground surface. Water samples were collected to measure metal ions, nutrients, and organic carbon concentrations from June 2007 to August 2010. The water samples determined that total dissolved nitrogen was nearly composed of all nitrate and total dissolved phosphorus was nearly composed of all phosphate throughout the monitoring period. Two samples were collected before construction with nitrogen concentrations of 0.11 and 0.37 mg/L. After construction, the nitrogen concentration ranged from 0.16 to 0.34 mg/L. There were nitrate losses ranging from 0.01 to 0.94 mg/L during the period after the BAM was installed. Nitrate samples collected at depths where the BAM layer was to be installed were higher than 0.5 mg/L before construction. These samples ranged from 0.06 to 0.23 mg/L post-construction. Approximately, 88% of the treatment volume was accomplished in the nutrient reduction basin. This design showed that nutrient reduction was achieved at a low cost, but more hydrological and water quality monitoring is needed to assess the

long-term capability of the nutrient removal (O'Reilly et al., 2012). Median phosphorus concentrations showed that there were between 70 and 90% decreases in total dissolved phosphorus from pre-construction to post-construction. Average concentrations of total nitrogen, total dissolved nitrogen, total phosphorus, and total dissolved phosphorus were 1.15, 1.1, 0.09 – 0.29, and 0.13 mg/L, respectively in urban areas. These values were used in the study to compare to see if the BAM was removing nutrients efficiently. The lowest phosphorus concentration was found 2.9 ft (0.88 m) deep (lower level of BAM). These results suggest that the BAM worked well in removing phosphorus, because of the addition of tire crumbs. In addition, the life expectancy for total dissolved phosphorus is 16 years versus 2.1 years for nitrate removal, supporting that BAM is potentially more effective for phosphorus removal.

1.1.3 Karst Hydrogeology

BAM used within stormwater BMPs may be effective to removing nutrients from surface water before it infiltrates to groundwater. Maintaining quality of groundwater sources is important to regulatory agencies in Florida because of reliance on groundwater for water supply. Groundwater from the Floridan aquifer is also discharged as surface water into springs, which are particularly abundant in Florida due to the thick limestone in the subsurface (Stamm, 2008) Florida has over 30 first magnitude springs (flow greater than 100 ft^3/s or 2.8 m^3/s) and over 700 identified springs that are labeled as karst springs (Scott, et al., 2004) which occur in the presence of karst aquifers. Karst is a term that is used to describe landscapes containing caves, conduits, and groundwater systems that develop on soluble rocks: limestone, marble, and gypsum (Ford & Williams, 2013). These landscapes allow for water and sediments to be easily transported through the subsurface (Pronk et al., 2006). Karst aquifers form when acidic rain, containing carbon dioxide, falls onto

the Earth's surface penetrating into areas rich in limestone. This carbonate solution penetrates the surface and dissolves the carbonate rock in the Earth's surface. Temperature and partial pressure of the atmosphere in relation to the groundwater determine the level of dissolved carbon dioxide. The carbonate solution depends on the presence of groundwater flow which helps to create underground voids. Dissolved carbonate rocks and the movement of groundwater is commonly referred to as the potential for karst development (PKD). Karst development is enhanced by the amount of rainfall, surface flow, the partial pressure of carbon dioxide in the soil, and the hydraulic gradient provided by the changes in elevation (between the beginning of the karst recharge area and the downstream spring) (Bakalowicz, 2005). Karst aquifers are formed around these heterogeneous voids or conduits. Conduits are large fractures that lead to large cave channels. Karst conduit diameters can range from on the order of a few centimeters to meters or kilometers (Goldscheider & Drew, 2007). Flow in conduits is different from the flow through regular soil matrix. Two types of flow can occur through karst features (Atkinson, 1977); slow flow in conduits occurs through small karst fissures or fractures, while turbulent flow, often described as conduit flow, occurs in larger, irregular conduits ranging in sizes from 10 mm to 1 m or greater (Bonacci, 1993). In larger conduits, conduit flow is often described as turbulent, ranging on the order or 100 m/hr or greater (Goldscheider & Drew, 2007). Recent sediment transport studies discovered an important subsurface feature called phreatic conduits. These conduits are located below the water table and have conduit gradients in the direction that produce saturated flow conditions (Husic et al., 2017).

To characterize groundwater flow in karst regions certain parameters are needed. These parameters include porosity, hydraulic conductivity, transmissivity, groundwater velocity, and groundwater

flow rate. Porosity is defined as the percentage of empty space occupied by the water or air (voids) in the total volume of rock (Goldscheider & Drew, 2007). Porosity dictates the water storage and movement in the aquifer and is directly related to the hydraulic conductivity, which is related to the velocity. The hydraulic conductivity and velocity depend on the shape and amount of pore space (voids) in the sediment. There are two types of geological porosities. Primary porosity was initially formed from the development of rock, while secondary porosity is the porosity after this development caused by the movement of tectonic plates (enhanced the overall porosity of the rock). Transmissivity is the hydraulic conductivity multiplied by the thickness of the aquifer. It equals the parallel flow rate through a vertical strip of the aquifer. In karst regions, this parameter has a different meaning because the hydraulic conductivity takes on no value with conduit flow (Goldscheider & Drew, 2007).

Geographical structures, like folds and faults, can greatly impact groundwater drainage patterns. Faults are defined as fractures in earth's crust along which movement has occurred and can alter the porosity of the aquifer to create karst valleys. Surface water that is present in these valleys (swallow holes) sinks underground to form swallets, or underground streams and is now considered groundwater but eventually emerges again as surface water when it is discharged at the spring (White, 2002). However, due to these swallow holes, karst aquifers are vulnerable to contamination. Due to the presence of swallets, karst watersheds often carry large loads of sediment (Drysdale et al., 2001). These contaminants can easily reach the groundwater where they are rapidly transported over long distances by way of conduits (Goldscheider, 2005). Owing to the fact that karst aquifers are being contaminated, methods are being conducted on how to map out these complex systems. Other challenges like mapping the limits and extent of these karst systems,

defining structural discontinuities, and localizing preferential pathways must also be addressed (Chalikakis et al., 2011). The transport of contaminants and sediment in karst systems remains the most unstudied aspects of karst in need of research (White, 2002). Geophysical methods, including electromagnetic methods, ground penetrating radar, microgravity, seismic methods, and electrical resistivity have been applied in karst areas for decades (Zhu et al., 2011).

1.1.3.1 Methods for Characterizing Karst Hydrogeology

Electromagnetic methods can provide information on the horizontal changes in the karst features that are near the surface such as fractures and lateral connections. This equipment is lightweight and provides fast measurements and is useful in delineating the limits for karst systems. Electromagnetic methods are able to define certain boundaries between carbonate rock and natural clay and silt deposits (Lange, 1999). He et al. [2006] used an integrated passive source electromagnetic method along with a controlled source audio-magnetotelluric (CSAMT) method to map the geologic structures in karst regions in China. Chalikakis [2006] used time domain electromagnetic methods to map the deep karst regions in northern Greece. Vogelsang [1987] using electromagnetic methods to locate faults, fractures, and contact zone in a karst region, however, it was noted that there were difficulties in interpreting the data for more complex systems. Guerin & Benderitter [1995] used electromagnetic methods to locate a conduit in a karst region but discovered that the data needed to be adjusted using resistivity results to determine the exact depths.

Defining structural discontinuities and localizing preferential pathways can be done be by using ground penetrating radar (GPR), microgravimetry, electrical resistivity, and through seismic

methods. GPR and microgravimetric surveys are tools that can be used to map out karst features. GPR is a technique in which radio waves are employed to map underground structures. It sends a pulse through the ground and records the echoes that result from that pulse. However, it cannot penetrate clay soils, which are commonly found in karst regions (Roth & Nyquist, 2003). Microgravimetry is used to detect subsurface cavities or densities by measuring small changes in the force of earth's gravity at geological structures. The determination of gravity provides an understanding of the subsurface. A study was implemented in an area in western Switzerland in 2001 in which these tools were used to map out a karst area (Beres et al., 2001). First GPR was conducted across four profiles in the area of a known cave. At each measurement point, 16 vertical stacks were placed for the purpose of collecting the desired signal to noise ratio. Microgravimetric measurements were made every 2 meters along the same GPR locations, where two readings were taken at each station. The GPR data showed continuous horizontal reflections with small diffractions, which were interpreted to be limestone beds. GPR data were then modeled to improve the interpretation of where the cavities were located. This study proved that GPR is an excellent tool for detecting subsurface cavities. Microgravimetry is slower than GPR but is also a method used for karst mapping. Microgravimetry in this study shows caves that corresponded to the GPR data at certain locations. Beres et al. [2001] concluded that microgravimetry is ideal where the landscape is more conductive. However, combining both methods proves to be a good approach because it improves the constraints of each of the methods if they were used separately (Beres et al., 2001).

A study was done in central Nepal where gamma rays and electrical resistivity profiles were used to map out karst features (Gautam et al., 2000). For electrical resistivity, it is assumed that water

in underground voids has a lower resistivity than the surrounding rocks and air in underground voids has a higher resistivity than the surrounding rocks. Sound and image techniques were both used. The equipment included a terrameter for imaging and a resistivity meter for sounding. For electrical imaging, a double dipole array was used, which consisted of a transmitter electrode and a receiver electrode. Measurements were made several distances apart. The objective of this was to capture a two-dimensional coverage of the subsurface by using vertical and horizontal profiling. The gamma-ray spectrometer was used to map the uppermost part of the river. Higher gamma ray readings were shown directly over depressions and karst structures are known to have high gamma activity due to the increased circulation of the emission along fractures in the subsurface. It was then interpreted that elevated readings are attributed to the presence of subsurface channels, or swallets, in the study area. Areal mapping of the Powerhouse area (area consisting of many major caves) revealed zones that were interpreted to be subsurface channels and the caves revealed a high resistivity that was attributable to karst features in the subsurface structure (Gautam et al., 2000).

A study was done, using electrical resistivity, in a landscape characterized by many sinkholes and sinking streams in Kentucky (Zhu et al., 2011). Three different types of resistivity methods were deployed: surface two-dimensional survey lines, quasi-three-dimensional resistivity, and a time-lapse survey. The 2D surface survey used electrodes close to the sinkholes to detect low resistivity anomalies. The quasi 3D survey used parallel and 2D survey lines to try and detect a conduit in a 2D profile of the site. The time-lapse survey is another way to detect low resistivity anomalies by using the same 2D survey lines to detect resistivity changes in the subsurface over time. Data from these three methods were used in conjunction with *AGI's EarthImager 2D and 3D* software. The

study was successfully able to locate a major conduit. Low resistivity anomalies were linked with moisture zones in the subsurface but could not be distinguished between water-filled conduits or water-bearing zones. The quasi 3D and time-lapse survey provided additional information but essentially confirmed the information from the 2D survey. The quasi 3D and time-lapse survey were more useful in eliminating the bad targets. An electrical resistivity survey along with a cone penetration test was used to delineate collapsed sinkhole areas (Kaufmann & Quinif, 2001). McGrath et al. [2002] used an integrated microgravity and electrical resistivity survey to identify underground voids in southern Wales. Electrical resistivity is still a very useful tool in providing information for potential drilling targets (Zhu et al., 2011). Reflections in seismic data show structural information in karst systems. The reflections help to determine the vertical and horizontal boundaries (Chalikakis et al., 2011). Weak seismic reflections could be due to uneven reflectors or a high level of noise which show weak karst features. This seismic refraction method was used to evaluate the fractures in the subsurface above a coal mine in Illinois (Johnston & Carpenter, 1998). Seismic results were compared to resistivity results in karst regions (Sumanovac & Weisser, 2001). The seismic results were valid for depths greater than 100 meters but for shorter depths of interest, the uneven reflectors limited the usefulness of the results.

1.1.4 Tracer Tests in Karst Environments

The main advantage of these geophysical methods is that they are minimally intrusive and cheaper than direct drilling. However, these methods do not locate the desired target directly (Zhu et al., 2011). Conducting a tracer test can provide valuable information about the underground connections in karst systems (Goldscheider & Drew, 2007; Kincaid et al. 2012). Conservative tracers can be used to determine the velocity and direction of groundwater flow through an aquifer.

Tracers are described as any substance that is carried passively by water, which will ultimately provide information about the groundwater direction/velocity as well as the potential contaminants. (Davis, et al, 1980). Various types of substances can be used as tracers, but the ideal tracer for a groundwater study is one that is easily detected in water and does not change the natural direction of the water flow. Ideal tracers are inexpensive, stable (chemically), and are conservative (remain as constant fluid particles) while traveling through water (Wilson et al., 1986). To choose a tracer there are several components that must be taken into consideration. For example, for tracer tests intended to portray the groundwater movement or the flow of stable and mobile contaminants, conservative tracers such as uranine or eosin should be selected (Goldscheider & Drew, 2007). In karst systems anions, and cations are conservative as well as fluorescent dyes, such as rhodamine.

Once tracers are administered, withdrawn samples must be analyzed in a lab. A filter fluorimeter or fluorimeter is used when the water contains a fluorescent dye. The intensity of the fluorescent light is directly proportional to the amount of fluorescent substance present (Wilson et al., 1986). The results of tracer tests are illustrated using a breakthrough curve, which is a graphical representation of time *versus* tracer concentration (usually in ppm or ppb). The breakthrough curve shows the behavior of the tracer over a specific time period. The components of the breakthrough curve (Fig 1) include the rising limb (rise), peak, and recession limb (fall).

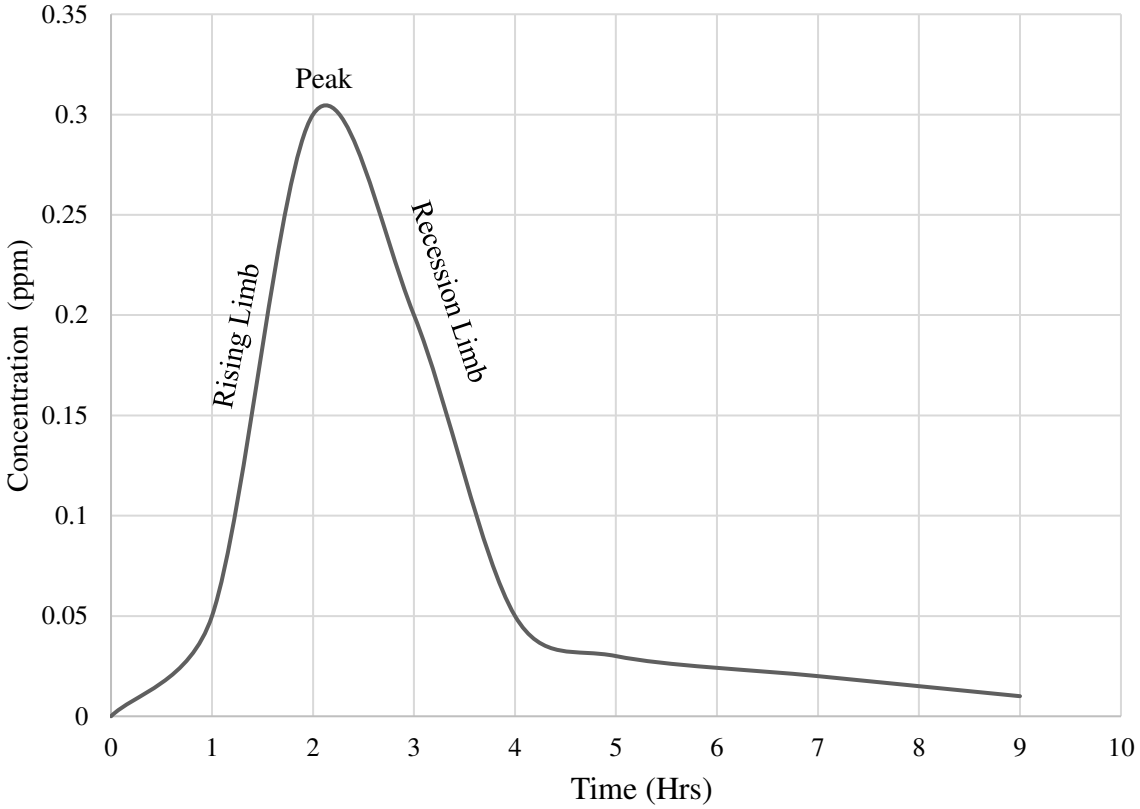

Figure 1: Sample Breakthrough Curve

The time and concentration of the peak are easily determined from continuous recordings of data. The time of the last detection is difficult to determine because it depends on the tracer, groundwater system, and monitoring/sampling intervals. Velocities, however, cannot be read directly from the breakthrough curves but can be calculated when the time to peak on the curve and the distances are known.

1.1.4.1 Dye Tracer Studies in Florida Karst Systems

A tracer study in the Wekiva River Basin used sulfur hexafluoride (SF6) to trace the movement of the groundwater (FDEP, 2016). SF6 was used as a tracer because it is not toxic, can be detected at

very low concentrations, non-reactive in groundwater, and can be injected in low amounts and still be detected on a chromatograph. Before the SF6 is to be injected wells, tracer wells needed to be installed. The location of the tracer wells was based on the impacting nitrogen sources. These wells were located at a higher elevation from the springs because of the known flow of the groundwater. The SF6 was then injected into each well under pressure. The first well was located west of Rock Spring (northwest of Wekiva Springs) in an agricultural area that could cause nitrogen to infiltrate into the groundwater. Approximately 2.1 lbs (9.3 N) of SF6 was injected into the first well and then it was chased by air until all the tracer was through the screen of the well. The second well was located southwest of Wekiva Spring in a residential area that contained septic systems. Approximately 0.85 lbs (3.8 N) of SF6 was injected into the second well and then alternately chased with purified air.

The 2.1 lbs (9.3 N) of injection of the SF6 into the first well was seen at Rock Spring within seven days of the injection. The detection time is then converted into a travel time of 980 ft/day (299 m/day), given the distance from Rock Spring (approximately 1.3 miles (2.1 km) W-NW). The 0.85 lbs (3.8 N) of injection of the SF6 into the second well took a much longer time. The tracer was detected in Wekiva Springs 50 days after injected. This detection time was converted into a travel time of 137 ft/day (41.8 m/day), given the distance from Wekiva Spring (approximately 1.3 miles (2.1 km) SW). This study just shows how tracers can be used to determine travel times and relate this back to nitrogen travel time to the springs.

Another tracer study was conducted in accordance with the City of Tallahassee's wastewater spray field (Kincaid et al., 2012). Unlike the previous study, this study used three different tracers

injected into three wells that were located in a swallet on the north side of the spray field on the southeast side of the property. The tracers that were used were three fluorescent dyes: phloxine-B (Acid Red 92 – AR92), uranine (Acid Yellow 73 – AY73), and eosin (Acid Red 87 – AR87). The main objective of this study was to figure out which springshed, either St. Marks or Wakulla River, to which the groundwater that was flowing from the wastewater facility discharges and to record the travel time as defined by injecting a specific tracer. Other objectives include using these tracers to evaluate the hydraulic properties of the aquifer in a karst environment. Separate tests were conducted to measure different parameters. A near field test was conducted to measure flow paths and the velocities across the wastewater facility. The purpose of this near-field test was to analyze the tracer between wells. An intermediate test was performed to look at the tracer movement from the sinkhole to the spring and finally, a far field test was conducted which includes analyzing the tracers between wells, wells and springs, and swallet to springs.

In the near field test, a tracer was injected along the north side of the site and sampling points were chosen at lower elevations from the injection point near the southern boundary. Five kilograms of phloxine-B were injected into three wells. The dye was mixed with 35 gallons (133 liters) of water initially and then followed by another 210 gallons (795 liters) of water as a chaser. This large volume of chase water is to make sure that the tracer encounters the aquifer. This huge volume of water has no influence on the natural flow patterns of the groundwater because of the large volume of water in the Floridan aquifer. Sample intervals were then set beginning with two hours during the first two weeks, then four hours, then six hours, and lastly twelve hours as time progressed. The purpose of the intermediate field test was to identify any sinkholes that could be used as tracer injection points. This test was quickly abandoned because no sinkholes were identified. In the far

field test, four injections were performed. In the first injection, 60 kilograms of eosin was injected into a creek upstream of a swallet. The other three injections were injected into the same wells as the near-field test. Twenty kilograms of uranine was injected into each well. Sampling was the same as the near-field test as well.

The samples were then collected and analyzed in a lab using a spectrofluorophotometer. Samples were collected at nine wells across the area of study (four in St. Marks River watershed, two in St. Marks River, and five in the Wakulla River watershed). These sampling points were analyzed for the amount of tracer detected. The fluorescent dyes were detected at five of the wells and five of the springs. The springs include Wakulla, Sally Ward, Indian, and two other small spring. The uranine and eosin were detected at high concentrations in the Wakulla watershed. The travel time from the injections located in the Wakulla watershed was determined from the breakthrough curves. The peak concentration occurred approximately 60 days after injection for the far field test and 65 days for the near field test. Low values were recorded in terms of mass or tracer recovery. The mass recovery for uranine and eosin was between 12-50% and 5-19%, respectively. Mass recovery is based on the conservative nature of the tracer, meaning that it will not react with water or absorb substrate and that the flow to the sampling points and the concentration of the tracer has been measured accurately. Complications can arise when all three tracers are chemically conservative but might be affected by microbiological decay. Next, the flow to sampling points is sometimes difficult to measure. Hydraulic meters are sometimes installed to measure the water velocity every fifteen minutes. These velocities are then converted into a flow rate through the use of the continuity equation ($Q = AV$) where Q is the flow rate (m^3/s), A is the cross-sectional area (m^2), and V is the velocity (m/s). Tracers that traveled through spring discharges that were not

sampled (causing a longer travel time than the sampling period) and tracers that did travel to the correct sampling ports were at concentrations that were less than the detection limit caused a low tracer recovery.

Groundwater velocities are then calculated from the tracer tests by dividing the distance between injection and sampling point by the tracer travel time that is recorded. The velocities for eosin between injection point and the sampling stations, between 1.3 – 10.5 miles (2.1 -16.9 km) ranged from 103 ft/day (31.4 m/day) to 998 ft/day (304 m/day). Due to this data, it is clear that in karst regions the velocities are unpredictable although when tracers are injected into swallets the velocities are usually faster. This study shows that groundwater flows SW toward Wakulla Spring between 671 and 977 ft/day (205 and 298 m/day). None of the three tracers were recovered in the St. Marks River watershed during the fourteen months. Lastly, the tracer curves of phloxine-B and uranine show that when swallets are full of groundwater, flow is decreased through shallow depths in the aquifer.

A tracer study was done in Ocala, Florida to determine the direction and flow rate of groundwater movement in the Floridan aquifer (Knochenmus, 1967). This study discusses how rhodamine dyes tracers are not affected by the sunlight. This should not raise cause for concern because the dye will be introduced underground (Knochenmus, 1967). In the upper part of the aquifer there consists an area composed of cavernous limestone. The flow paths through this limestone have not been clearly defined in the past and tracer studies have had limited success. In the 1960s, fluorescein dye was injected at Ocala Cavern and further detected at Wolf Sink, 1.3 miles (2.1 km) to the north. The dye reached peak concentration after nine days. Therefore, the estimated velocity from

the breakthrough curve is 0.8 ft/min (4×10^{-3} m/s). But discrepancies arose because the concentration was sampled at Wolf Sink on the second day and then the ninth day. Because of the large difference in time between sampling days, it is a possibility that all the dye could have reached the sink in the third day which would give it a velocity of 1.6 ft/min (8×10^{-3} m/s). If all of the dye was seen on the ninth day, then the velocity would be 0.5 ft/min (3×10^{-3} m/s). The 0.8 ft/min (4×10^{-3} m/s) velocity is just an interpolation.

More recently, there has been a study in the same area in August 2011. This study had two objectives. The first objective was to identify the pathways and travel times between specific locations and Silver Springs while the second was to identify possible sources of nutrient contamination and travel directly to Silver Springs. Task one of the study dealt with data collection of the site area, task two dealt with a groundwater dye tracer to look at potential karst systems and calculate the travel times to the spring, and task three dealt with the risk assessment for task two.

The locations for dye introduction in task one were Ocala Civic Theatre property (small sinkhole), Tuscawilla Park drainage well, Orange Lake Sink, Pontiac Pit (sink), and Spanish Palms. Fluorescein was injected at Orange Lake Sink, eosin at Tuscawilla Park, rhodamine at Ocala Civic Theatre, and sulfur-rhodamine B (SRB) at Pontiac Pit. Fluorescein was detected at Reddick Elementary School Well (4.2 miles (6.9 km) south from the detection point) at a concentration of 79.1 parts per billion (ppb). This concentration was detected fourteen days after injection. Rhodamine was detected within five to ten days after injection at the Silver Spring gauge vent. This rhodamine was detected in 20 of the 29 vents that were located at Silver Springs. This detection was approximately 1.4 miles (2.3 km) from injection which means the calculated travel

time was between 700 and 1400 ft/day (213.4 and 426.7 m/day). Eosin was detected at a vent approximately 10 months after it was injected and SRB was detected at a location 2.4 miles (3.9 km) away in a time span between 50 and 57 days. The information from the Ocala Civic Theatre tracer study is particularly important, as it allows for understanding of groundwater flow velocities within karst conduits near a spring. However, flowpaths taken by stormwater entering a stormwater management basin may take flowpaths that include flow through karst conduits and more typical matrix flow in unsaturated soils and aquifers. How flow/contaminants travel along with the cost effectiveness of several Best Management Practices (BMPs) n karst regions are still questions that remain to be answered.

1.2 Thesis outline

Stormwater runoff, treatment within BMPs, and the environment of freshwater springs are closely connected within regions of karst hydrogeology. The overall objective of this thesis is to analyze the connection between surface stormwater and groundwater flows as stormwater travels through a BMP near a freshwater spring within a karst environment located in Silver Springs, Florida. Flow paths and travel times of groundwater in a karst environment are estimated in Chapter Two, based on results of a tracer test. Chapters Three and Four assess the hydrologic performance of two novel stormwater BMPs, blanket filters and vertical reactors. In Chapter Three, presented is an analysis of capture efficiency of blanket filters and vertical reactors and describes the design, construction, and hydrologic monitoring of the stormwater BMPs. Lastly, Chapter Four evaluates the hydraulic performance of the blanket filters and the potential effectiveness at removing nutrients from shallow groundwater.

CHAPTER 2: FLOW PATHS AND TRAVEL TIMES OF SHALLOW GROUNDWATER IN A KARST ENVIRONMENT

2.1 Abstract

In recent years, loadings of nutrients have increased in natural water resources due in part to non-point source pollution associated with stormwater runoff. Increased nutrients in stormwater runoff may infiltrate with stormwater to affect quality of groundwater, and in areas of karst hydrogeology, may travel quickly to re-emerge in surface water bodies or springs. The objective of this research is to investigate potential flow paths and travel times of shallow groundwater in a karst environment, in the vicinity of a high-magnitude freshwater spring. A conservative tracer was injected into a shallow surficial aquifer within a stormwater management basin near Silver Springs, in north-central Florida. Sampling was undertaken in a wellfield, at distances from 12 – 45 m, surrounding the tracer injection site and just downstream of Silver Springs, 1.16 km away from injection site. Subsurface velocities observed in the basin ranged from 0.1 m/d to 1.4 m/d. Several pulses of tracer were observed at Silver Springs, and velocities from the injection well to the springs ranged from 2.3 m/d to 13.5 m/d. The high variability in observed velocities may reflect a continuum of potential flow pathways stormwater may travel between the stormwater management area and Silver Springs, including flow through karst conduits. The presence of karst features may decrease the retention time of groundwater in aquifers, which may influence nutrient transformations. Understanding such potential pathways and travel times of stormwater pollutants from the surface to groundwater bodies and springs may help environmental managers in design of best management practices for preserving water quality in karst environments.

2.2 Introduction

In recent years, loadings of nutrients have increased in surface water and groundwater bodies, partially due to runoff from urbanized areas. Stormwater runoff may contain high concentrations of nutrients and other pollutants, so there is concern that stormwater runoff should be treated before it infiltrates and becomes groundwater (Paul & Meyer 2001; Roy & Bickerton, 2011; Halstead et al., 2014) which may be particularly salient in areas of karst hydrogeology. Karst features, such as air-filled caves, conduits, sinkholes, and underground streams, are known to define the west-central Florida region (Tihansky & Knochenmus, 2001; Knowles et al., 2010; Ford & William, 2013). Karst landscapes allow for water and sediments to quickly travel through the subsurface (Pronk et al., 2006) and can range from small rock cavities to enormous caves (Tihansky, 1999). Most of the karst features in the Floridan aquifer are contained within Ocala Limestone (Florea et al., 2009) and are known as mantled karst. Mantled karst is defined by carbonate rocks being buried deep beneath the surface but can be detected by the presence of sinkholes or other depressions (Tihansky, 1999). Not much is known about subsurface caves in west-central Florida, because of the fact that they can be buried greater than 45 m below the land surface (Florea, 2006). Geophysical methods, including ground penetrating radar (GPR), a reflection technique that uses electromagnetic radiation (Lane, 1986), have been applied in karst areas for decades (Zhu et al., 2011) for the purpose of mapping these complex systems.

Groundwater tracer studies are often used to analyze transport characteristics in karst environments. For instance, macropore dominance in karst environments was shown through the use of dye application in experimental plots in northern Switzerland (Weiler & Naef, 2003).

Einsiedl (2005) used uranine and bromide to analyze the slow groundwater flow in epikarst aquifers (subsurface zones near the surface) in Germany, estimating groundwater velocities of 2592 m/d for both tracers. Pronk et al. (2009) described groundwater velocities ranging from 346 – 432 m/d, by tracing flow paths of uranine injected directly into a shallow hole and traced to two nearby springs in Switzerland. Both Einsiedl (2005) and Pronk et al. (2009) depicted different groundwater velocities in completely different karst environments. A study in the Wekiva River Basin in Florida used sulfur hexafluoride (SF6) to trace the movement of groundwater to a nearby spring (FDEP, 2016), indicating highly variable groundwater velocities, ranging from 42 – 299 m/d. Kincaid et al. (2012) used three different fluorescent tracers (phloxine B, eosin, and uranine) to identify groundwater flow paths away from wastewater spray field. Again, a large range of velocities were recorded, ranging from 31 – 298 m/d. Most importantly, this study demonstrated the need for more advanced wastewater treatment in the region due to relatively fast groundwater velocities observed. Knochenmus (1967) described how fluorescein, a fluorescent dye, works well as a groundwater tracer in cavernous limestone, prevalent in Ocala, Florida. Fluorescent dyes are effective groundwater tracers because they are large organic molecules that allow for detection at low concentrations (Flury & Wai, 2003; Magal et al., 2008). In Ocala, Florida, McGurk et al. (2012) observed variable groundwater velocities, ranging from 213 – 427 m/d, when rhodamine WT dye was injected to an open sinkhole, a direct surface connection to subsurface karst conduits.

Florida has over 30 first magnitude springs (flow greater than 2.8 m^3/s) and over 700 identified springs that are labeled as karst springs (Scott et al., 2004). Because groundwater is discharged as surface water in Florida's springs, which are important areas for local ecology and recreation, excess nutrients in groundwater can cause eutrophication in springs, toxicity, changes in the natural

habits of many animals, and even lead to mortality of aquatic organisms (Jacoby et al., 2008). Understanding connections between potentially contaminated surface waters, groundwater, and spring discharges can help managers to devise adequate protection for springs. This study will help analyze two components of groundwater movement in a karst environment, conduit flow and matrix flow. The objective of this study is to investigate the flow paths and travel times of shallow groundwater between a stormwater management basin and a first-magnitude spring in a karst environment.

2.3 Methodology

2.3.1 Study Area

The Silver Spring springshed (Fig. 2, approximately 3108 km^2) is located in north-central Florida at approximately 23 m above sea level. The climate of the Silver Springs basin is humid subtropical with warm, rainy summers and mild, dry winters. Mean annual temperature is 22 °C and mean annual precipitation is approximately 1520 mm (National Oceanic and Atmospheric Administration, 2017). Land use in Silver Springs basin has historically consisted of undeveloped and agricultural lands but has shifted to increased urban and suburban land uses, including numerous retirement communities and golf courses, associated with a population growth of approximately 275% from 1970 to 2000 (Phelps, 2004). Silver Springs is the largest inland spring in the state of Florida with a mean discharge of approximately 23 m^3/s (Spechler & Schiffer, 1995).

The study is conducted within a 0.3-ha dry stormwater management basin (Basin 9B, Fig 2), located close to Silver Springs State Park, within 0.57 km of the main vents of Silver Springs. Stormwater runoff enters Basin 9B through culverts from surrounding roadways and leaves the basin by infiltration through the basin bottom. Analysis of bulk samples indicates that surface soils within Basin 9B are poorly graded sand containing little silt and clay (Chang et al., 2015). Surface infiltration rates in the basin exceed 25.4 cm/hr. However, soil texture changes with depth, such that hydraulic conductivity likely decreases with depth. Based on soil boring analyses, soils are characterized as sandy from 1.1 – 1.7 m, clayey sand from 1.1 – 1.7 m, and lime rock from 1.7 – 3.0 m (Chang et al., 2015). GPR surveys detected nine anomalies interpreted to be karst features in Basin 9B, at depths from 1.5 – 2.1 m below the land surface (Chang et al., 2015). Based on 18 months of on-site monitoring, depth to the surficial aquifer fluctuates between 1.5 m and 1.8 m below grade. The regional groundwater flow direction is nominally from west to east across Basin 9B, in the direction of Silver Springs. However, shallow groundwater may flow in alternate directions in response to local controls.

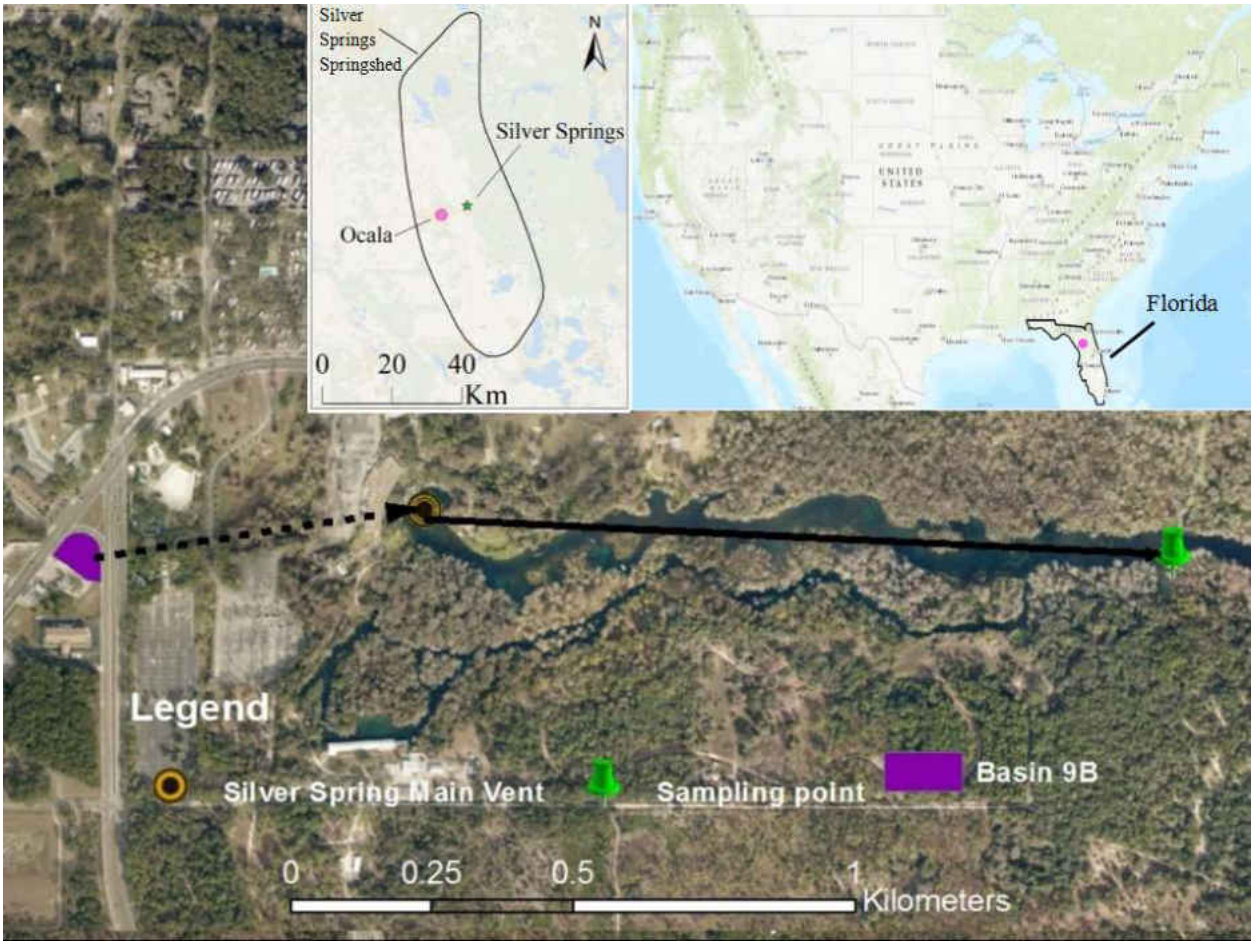

Figure 2: Study Site

2.3.2 Field Methodology

A network of observation wells was installed in Basin 9B. Twelve 3.8 cm diameter wells were drilled to a depth of 3.0 m below grade. Approximately 7 kg of standard 20% rhodamine WT dye (specific gravity 1.15) was injected into Well 0 at 5:30 am on July 25th, 2017 (Fig 3a). Rhodamine WT is cost-effective, easily detected, has a high sensitivity, conservative, and is low in toxicity (Smart & Laidlaw, 1977). The tracer was chased with 1420 L of water, delivered at a rate of 0.25 L/s (Fig 3b).

(a) *(b)*

Figure 3: (a) Dye being injected; (b) Chaser being added

Sampling stations were established to monitor groundwater in each of the twelve wells and surface water in the Silver River, approximately 1.73 km away (Euclidean distance) from the injection well and approximately 1.16 km downstream of the main Silver Springs vents (Fig 2). At the Silver River sampling station, a Sigma 900Max portable pump sampler (Fig 4) with an array of 24 bottles (575 mL each) was installed. Samples of 200 mL of spring water were withdrawn at intervals and transferred to smaller collection bottles for analysis.

Figure 4: Pump Sampler set up along the Silver River

A combination of hand pumps, peristaltic pumps, and pump samplers were used to simultaneously sample wells. Groundwater was pumped from each well into 125 mL bottles. Wells were sampled at short intervals (every 1 – 4 hours) immediately after the dye was injected and then gradually increased (to once a day and once a week) as time progressed from the time of injection. Additionally, water samples at Silver Springs were sampled at short intervals (every 1 – 2 hours) immediately after the dye was injected and then gradually increased (to once a week and once every other week) as time progressed from the time of injection. Samples were immediately stored in a dark, cool environment (26.5 L cooler) to preserve the concentration of rhodamine. Samples were transported to the lab, where they were filtered through a 0.2-micron nylon membrane (Fig 5). After filtration, tracer concentration was detected using a Turner Designs Aquafluor® Handheld Fluorometer and Turbidimeter (minimum detection limit of 0.4 ppb; dynamic reading range between 0 – 400 ppb; reading temperature between 5 - 40° C). Samples were tested in

triplicate and the triplicate mean of the raw data was calculated. Sampling concluded 9 months after injection.

Figure 5: Filtration set up using a 0.2-micron nylon membrane

Standard solutions of known rhodamine concentrations from 1 to 400 ppb were created and tested to create a calibration curve (Fig A1.1; Appendix I), following the methodologies outlined in the University Nebraska -Lincoln Chem 116 Lecture on Calibration (Powers, 2009).

Concentrations were plotted over time to discern peak concentrations in each sampling location. Time of peak concentration was used to calculate groundwater velocities (V) between Well 0 and the sampling locations (Eq. 1):

$$V = \frac{d}{t} \qquad (1)$$

where d is the Euclidean distance of the sampling location from Well 0 (m) and t is the time elapsed from the time of tracer injection to detection of peak concentration in the breakthrough curve (days). We assume that water travels through the subsurface from Well 0 to the main vents

of Silver Spring (the dashed line in Fig 2) and further transport to the Silver River sampling location occurs through open channel surface flow (the solid black line in Fig 2).

2.4 Results

Rhodamine was detected in several basin observation wells within four months of tracer injection, and in the Silver River 42 days following injection (Fig. 6). Tracer was not detected in Wells 9-11 (Fig 7). The fastest travel times within the basin were observed in wells 7 and 8, which are in line with the direction of predominant groundwater flow, between 18 - 25 m to the northeast of the injection site. Tracer appeared in wells 7 and 8 approximately two weeks after injection in (15 – 17 days), indicating subsurface velocities between 1.19 – 1.41 m/d (Fig 6). Tracer was next detected 35 days after injection in well 1, with velocity of 0.35 m/d. Well 1 was in closest proximity to the injection site, at 12. 5 m but located southeast of the injection well and not in the primary direction of groundwater advection. At 128 days, tracer was observed in wells 4, 5 and 6, which were due east to southeast of the injection site. Tracer traveled the 21 – 25 m from the injection site to wells 5 and 6 at approximately 0.15 – 0.17 m/d (Table 1). However, in the same time, tracer traveled 42 m to well 4, with velocities similar to those observed in well 1. Tracer moved more slowly (0.09 – 0.13 m/d) to wells 2 and 3 and was detected at 219 days (Fig 6).

In regard to the Silver River sampling location, tracer traveled from Well 0 through unknown subsurface flow paths and discharged at the main or secondary vents before traveling as open channel flow to the sampling location. Assuming a bulk flow velocity of 0.21 m/s in the Silver River (Odum, 1957), the likely travel time as open channel flow (~90 minutes) is negligible as compared to the subsurface travel time. The first peak tracer concentration occurs in the Silver

River at 42 days. The main vents at Silver Springs are located a Euclidean distance of 570 meters away from the injection well (Table 1). Using equation 1 this gives a velocity of approximately 13.5 m/d. A second peak of rhodamine concentration occurs 115 days after injection, indicating velocity of approximately 4.94 m/d. A third possible peak of rhodamine concentration occurs 177 days after injection resulting in a velocity of approximately 3.22 m/d. Finally, a fourth peak of rhodamine is detected 246 days after injection, with a velocity of approximately 2.32 m/d. The slowest groundwater velocity observed downstream of the spring was still faster than the fastest subsurface velocity observed in the stormwater basin.

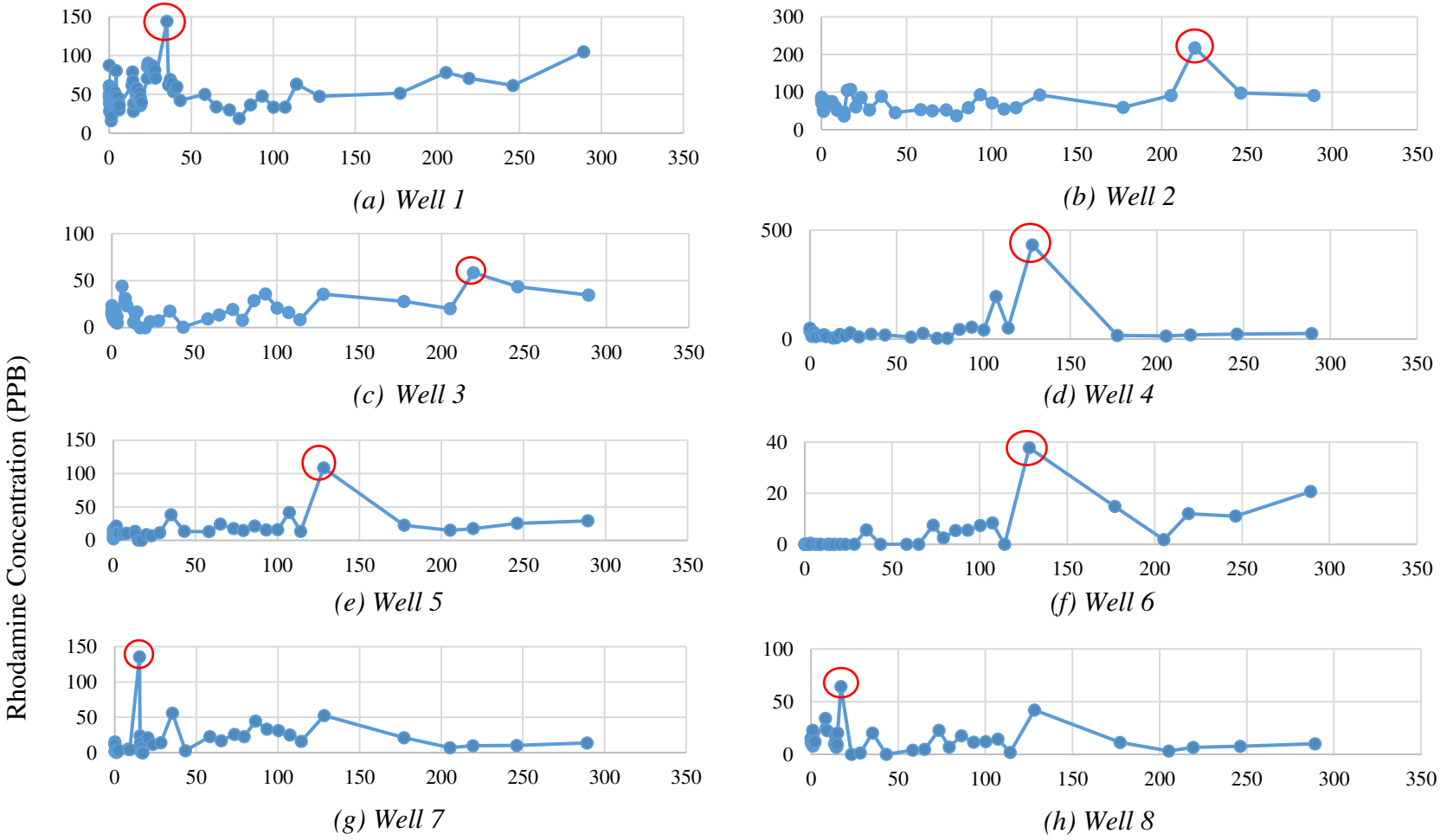

Figure 6: Breakthrough Curves for Wells with Discernable Peaks (a) Well 1 (b) Well 2 (c) Well 3 (d) Well 4 (e) Well 5 (f) Well 6 (g) Well 7 (h) Well 8

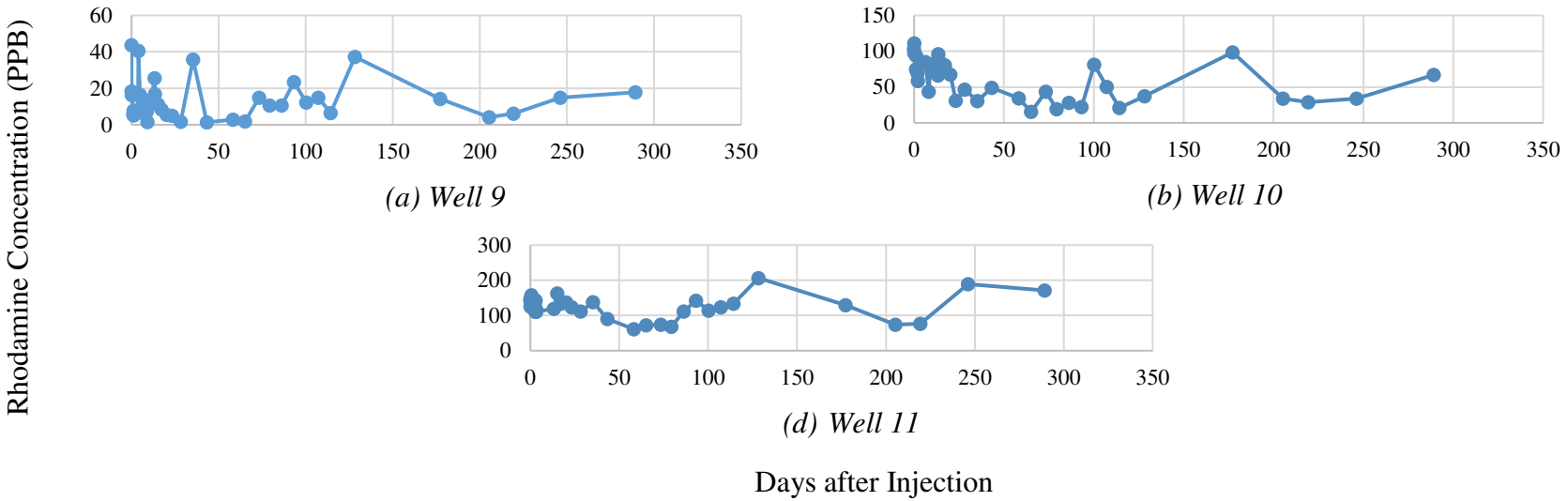

Figure 7: Breakthrough Curves for Wells with No Discernable Peaks (a) Well 9 (b) Well 10 (c) Well 11

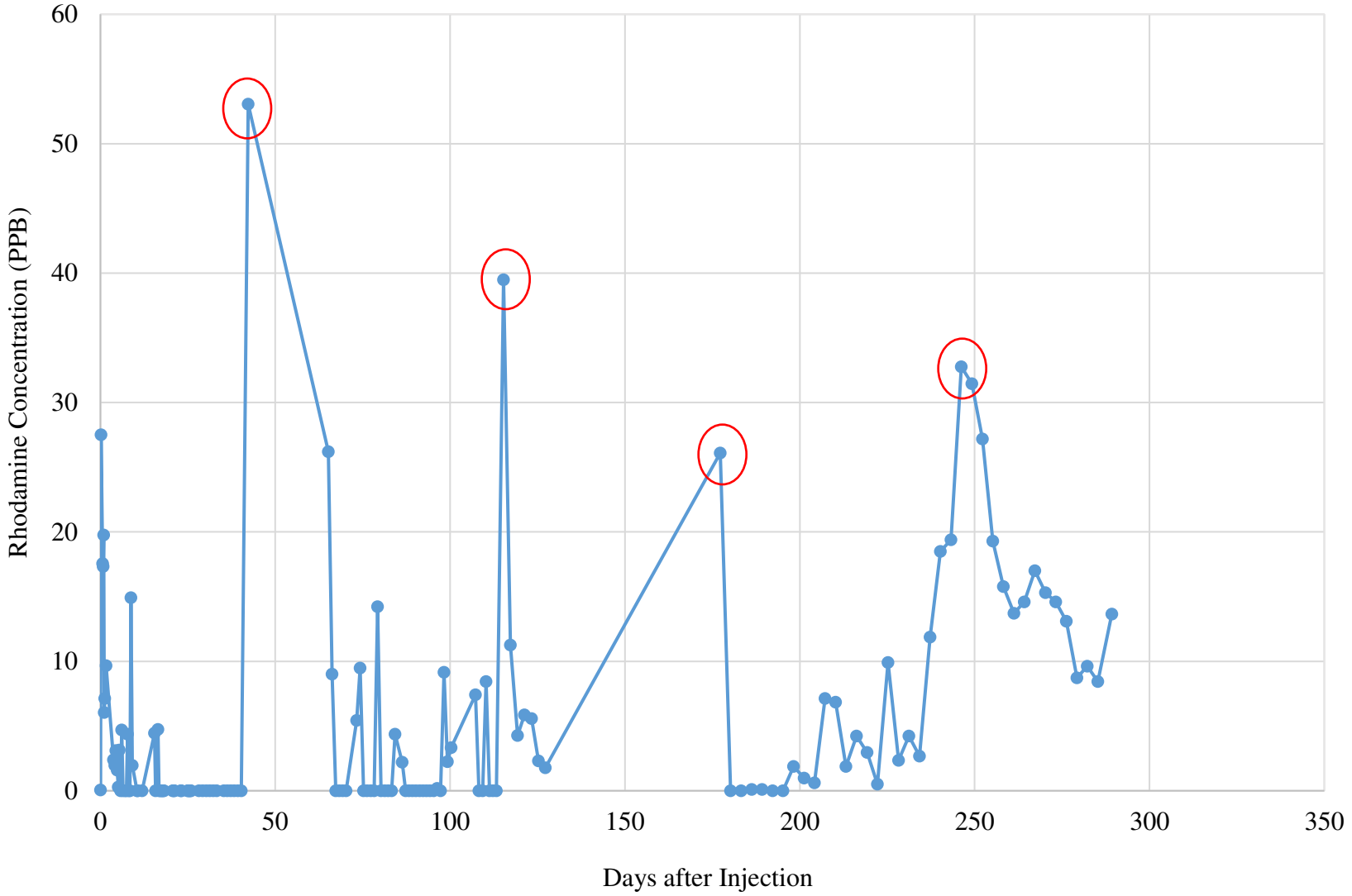

Figure 8: Breakthrough Curve for Silver Springs

Table 1: Summary of Well Velocities in Basin 9B

Well Number	Distance from Injection Well (m)	Time of Peak Concentration (days)	Velocity (m/d)	Velocity (m/s)
1	12.5	35	0.35	4.05×10^{-6}
2	20.5	219	0.09	1.04×10^{-6}
3	29.0	219	0.13	1.50×10^{-6}
4	42.7	128	0.33	3.81×10^{-6}
5	21.4	128	0.17	1.97×10^{-6}
6	24.4	128	0.19	2.20×10^{-6}
7	18.3	15	1.19	1.38×10^{-5}
8	24.4	17	1.41	1.63×10^{-5}
9	36.6	-	-	-
10	35.1	-	-	-
11	42.7	-	-	-
Silver Springs (main vents)	570	42	13.5	1.56×10^{-4}
		115	4.94	5.72×10^{-5}
		177	3.22	3.73×10^{-5}
		246	2.32	2.69×10^{-5}

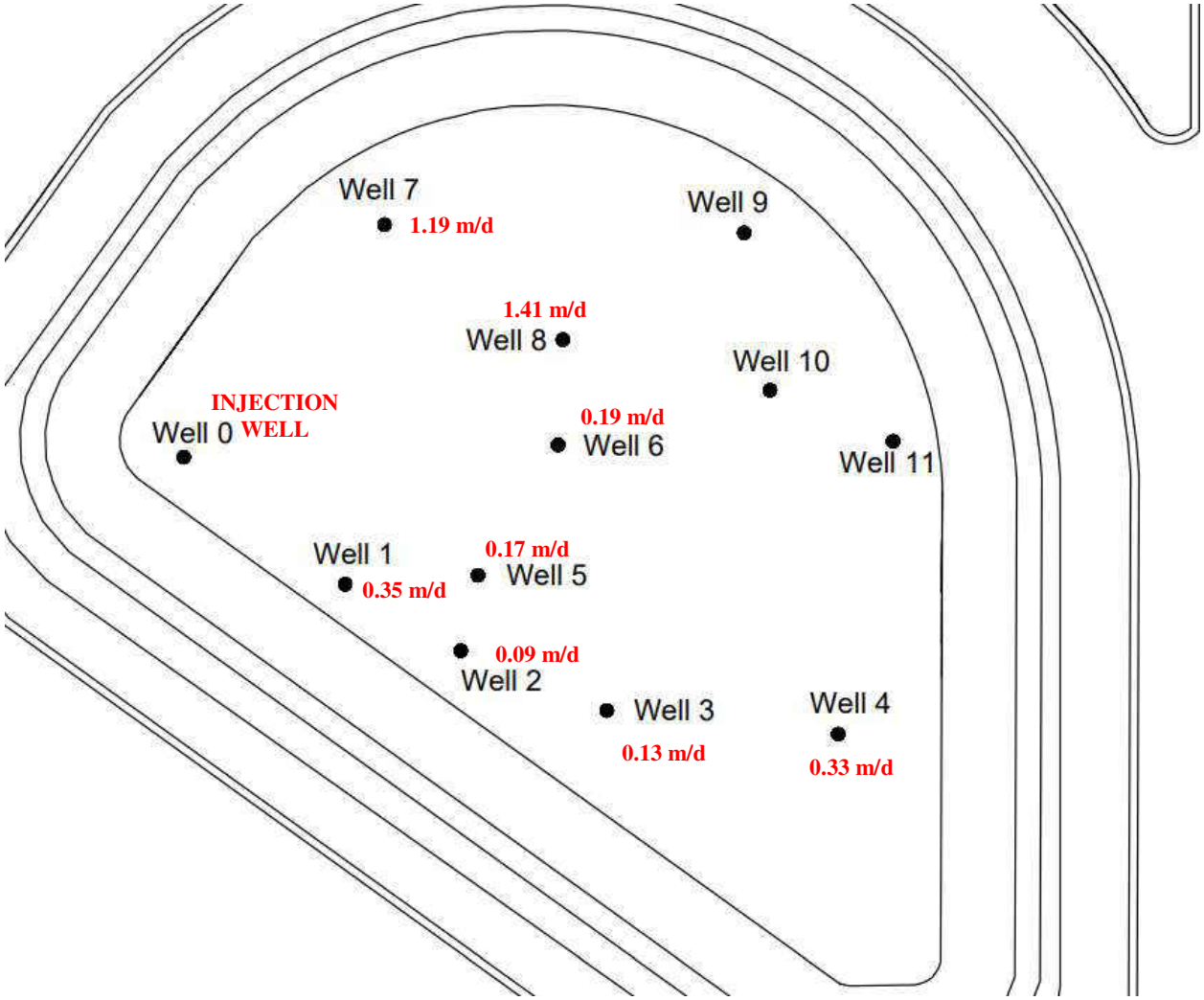

Figure 9: Wells and Observed Subsurface Velocities in Basin 9B

2.5 Discussion

Tracer traveling through the subsurface from well 0 to the Silver Springs traveled at the fastest observed velocity (Table 1). Indeed, the slowest groundwater velocity observed downstream of the spring was greater than the fastest subsurface velocity observed in the stormwater basin. Tracer was not directly injected into a karst feature (e.g. swallet), but into the surficial aquifer. It is likely that after injection, the tracer moved in the direction and at the speed of local groundwater flow within the surficial aquifer, from west to east across the site. This behavior is confirmed by the earliest indication of tracer in the wells east of the injection point. A range of velocities are observed in the wellfield in Basin 9B, with the fastest velocities observed in the wells to the northeast of the injection well (wells 7 and 8) and the slowest velocities observed in wells to the southeast of the injection well (wells 2 and 3). Observed velocities reflect the material properties of the aquifer and characteristics of groundwater flow in response to local potentiometric gradients. Subsurface velocities in Basin 9B range from 10^{-5} to 10^{-6} m/s, which corresponds with hydraulic conductivities of coarse to fine sand and silty sand (Dingman, 1994), and sandy loam, loam, and clay loam (Selker et al., 1999). Recorded subsurface velocities in the basin are thus consistent with what would be expected in basin soils, which were classified on the surface as sand with little to no fines, with greater proportions of fine material at greater depths (Chang et al., 2015).

It is likely that subsurface velocities observed within Basin 9B wellfield broadly reflect flow through a saturated, relatively homogeneous surficial aquifer. However, it is possible that the faster subsurface velocities recorded in the basin may also reflect interaction with karst features and/or preferential macropore flow. Karst aquifers are known to have flow patterns that resemble a

branching pattern, reflecting structures that form within karst aquifers (Howard & Groves, 1995; Siemers & Dreybrodt, 1998). Types of preferential flow include macropore flow, unstable flow, and funnel flow. Macropore flow is the movement through fissures or cracks, unstable flow is caused by different textural layers in the subsurface, and funnel flow refers to the horizontal direction of water caused by these textural differences (Hendrickx & Flury, 2001). Each of these processes could be occurring within the subsurface of Basin 9B and may cause variability in velocities. For instance, the earlier detection of tracer at well 4 as compared to wells 2 and 3 may be explained by preferential flow paths. The tracer moving with the bulk groundwater flow would reach wells 2 and 3 before well 4 due to their closer proximity to the injection point. Yet, high concentrations of tracer are observed at well 4 while concentrations at wells 2 and 3 remain relatively low.

The first peak in the Silver Springs sampling data is detected 42 days after tracer injection, with peak concentration of 53 ppb (Fig 8). Based on velocities calculated from this time, peak velocity of tracer to Silver Springs is more than nine times the greatest velocity observed in the wellfield in Basin 9B. Subsequent peaks occur at longer intervals, but the slowest velocities detected at the spring still outpace the greatest velocities observed in the basin. There are two gaps in the Silver Springs data. The first gap occurs between 42 and 65 days after dye injection (Fig 8) due to a hurricane (Irma) that affected the study site. Due to the storm, high levels of precipitation fell on the study site between September 8th and September 13th, 2017 (between 45 and 50 days after dye injection). It is possible that during the storm, tracer concentrations may have risen beyond the peak concentration observed at 42 days, 53 ppb. Indeed, when monitoring resumed after the storm at 65 days after injection, tracer concentrations are still well above background, at over 26 ppb. A

second gap in Silver Springs data, attributed to equipment failure, occurs between 130 and 176 days after tracer injection. Here again, tracer concentrations were above background (26 ppb) when monitoring resumed, perhaps suggesting a third peak in tracer delivery to the spring. A potential fourth peak, with concentration of 33 ppb, may be seen at 246 days after tracer injection. Each pulse of tracer observed at the Silver River may indicate a unique flow path that tracer, and thus stormwater, may take between the injection point and the spring. We posit that the faster travel times may be representative of heterogeneous flow paths that include flow through karst conduits in the subsurface between the injection well and Silver Springs. This can be illustrated by analyzing the full range of velocities in Basin 9B (0.09 – 1.41 m/d). Had the tracer moved at these recorded velocities, it would have taken between 404 – 6333 days for the tracer to reach the main vents of Silver Springs if it only traveled through the soil matrix. Pulses of tracer seen much earlier in the spring indicate that heterogenous flow paths exist between the basin and the spring, and that these flow paths may transport water, and any dissolved constituents, at a much greater rate than may be expected in a homogeneous aquifer.

Subsurface velocities observed in this study can be compared to those recorded in other karst areas near springs in Florida. In Wekiva Springs subsurface velocities were observed to be between 42 – 299 m/d, at depths ranging from 27 – 57 m deep (FDEP, 2016). In Wakulla Spring subsurface velocities between 31 – 298 m/d were observed when fluorescent tracers were injected into wells ranging from 23 – 73 m deep (Kincaid et al., 2012). Both Einsiedl (2005) and Pronk et al. (2009) depict fast subsurface velocities (2592 m/d and 346 – 432 m/d, respectively) in different karst environments. These tracers above were directly injected into the Floridan aquifer (FDEP, 2016; Kincaid et al., 2012), epikarstic conduit (Einsiedl, 2005), or swallow holes (Pronk et al., 2009)

which have direct links to karst features. The tracer in Basin 9B was injected into shallow depths in the surficial aquifer. The dye traveled through the surficial aquifer and the intermediate confining layer before possible hitting a conduit/macropore in the Upper Floridan Aquifer. This is possible reason the subsurface velocities are magnitudes lower in Basin 9B. The dye was not injected into one of these karst features shown in the previous studies. The same is seen in a study in Silver Springs where a conservative tracer was injected directly into a sinkhole and traced to Silver Springs at velocities ranging from 213 – 427 m/d (McGurk et al., 2012). Sinkholes have direct connections to karst features that accelerate groundwater velocities. The velocity of this study is more than twenty times greater than the velocities observed to from Basin 9B to Silver Springs. These studies reveal velocities that are much larger than velocities seen in Basin 9B due to the presence of karst features.

2.5.1 Proposed Conceptual Model

Based on results of the conservative tracer study, we propose a conceptual model (Fig 10) for the transport of stormwater from Basin 9B to discharge in Silver Springs. We propose that after infiltration, stormwater may travel to the spring through a combination of flow through a porous and relatively homogeneous soil matrix and through heterogeneous macropores or conduits in the underlying karst geology.

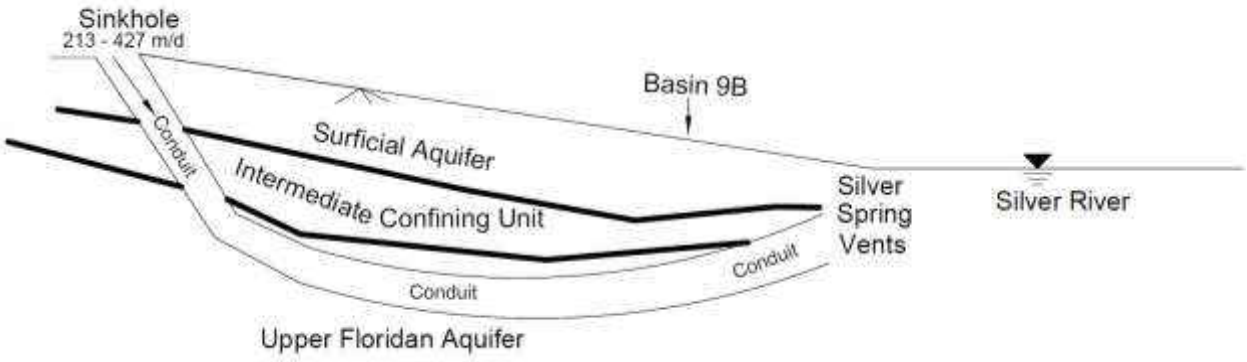

Figure 10: Proposed Conceptual Model

Runoff entering the basin quickly infiltrates through the permeable surface of the stormwater basin, and percolates into the shallow surficial aquifer. Within the surficial aquifer, water moves both horizontally and vertically. Data from the observation wellfield in the surficial aquifer indicate that shallow groundwater moves in tortuous flow paths but mainly in the northeast direction toward the main vents at Silver Spring at a velocity between 1.19 – 1.41 m/d. The larger range of velocities is broadly consistent with the fourth observed peak tracer concentration, appearing downstream of the spring 246 days after injection. If we assume the slowest tracer peak is indicative of shallow groundwater movement through a homogeneous matrix, this suggests a mean travel velocity of 2.32 m/d, which is slightly greater than speeds observed within the surficial aquifer (Durden, 2012). However, the tracer was first detected downstream of the spring 42 days after tracer injection, suggesting availability of alternative and faster flow path between the surficial aquifer and the spring. Water following these faster flow paths likely traveled through a combination of homogeneous porous matrix flow and faster preferential flow through karst macropores. While assuming that the runoff moves both horizontally and vertically there is a continuum of possible flow paths. The groundwater can move diagonally (at angles between the

horizontal and vertical directions) as well due to the natural elevation changes between Basin 9B and the main vents of Silver Springs. It can be assumed that the first peak in the breakthrough curve to Silver Springs is due to the vertical movement of dye through the subsurface until the dye interacts with karst macropores/conduits. The second and third peaks are representative of diagonal flow patterns within the subsurface before interacting with karst features in the subsurface. The last peak is mainly representative of horizontal flow through porous media within the surficial aquifer with some interaction with karst features as seen by the close range of the faster velocities in the well field and the slower velocities to Silver Springs. Horizontal flow through porous surficial aquifer and vertical flow to conduit are potential end-members where pulses of tracer are seen in the wellfield in Basin 9B and at the main vents of Silver Springs.

If it is assumed that the fastest velocity seen at the springs traveled vertically between the surficial and Upper Floridian aquifer, then the mean vertical hydraulic conductivity within the intermediate confining unit layer may be estimated. McGurk et al. (2012) observed flow velocities within karst conduits in the vicinity of Silver Springs ranging from 213 – 427 m/d. Tracer traveling from the injection site at similar speeds would have reached the spring sampling location in 1 – 3 days. Therefore, the tracer may have moved between the surficial and Upper Floridian aquifers in approximately 39 – 41 days, suggesting a mean vertical groundwater velocity on the order of 1.56 – 1.64 m/d. Alternatively, a karst feature may have been encountered anywhere between the surficial aquifer or confining layer. The estimate of vertical hydraulic connectivity of the intermediate confining unit between the surficial aquifer and Upper Floridian aquifer suggested by the proposed conceptual model is dissimilar to vertical hydraulic connectivity estimated by data provided by the St. Johns River Water Management District (SJRWMD) due to the presence of

many vertical rock fissures and sinkholes which connect the upper intermediate confining unit directly to the Upper Floridan aquifer. In the vicinity of Basin 9B, the thickness of the surficial aquifer and the intermediate confining unit are 10.5 m and 9.1 m, respectively (Durden, 2012). SJRWMD dataset estimates the vertical hydraulic conductivity of the surficial aquifer as approximately 0.51 m/d, which is similar to our conceptual model.

2.5.2 Implications for Management

This study provides valuable information about the speed at which groundwater is traveling, through the subsurface, to Silver Springs in a karst environment and the retention time that may be expected in aquifers. Silver Springs is an area of concern because of the high incoming nutrient concentration which is causing eutrophication. The velocities can be related to the transport of contaminants, suggesting retention time available for nutrient transformations in the aquifer. Albertin et al. [2012] describes that certain nutrient transformations, to reduce pollutants, take place in aquifers with long retention times, or soil matrix flow. Karst aquifers decrease retention time, thus changing nutrient transformations. Subsurface velocities observed in this study can be used to calibrate a three-dimensional subsurface model to understand groundwater flow and possibly how fast nutrients and contaminants move in the aquifer once they infiltrate through the surface. Once the flow pathways of nutrient travel are known specific steps can be taken, like implementing protection zones or furthermore installing green infrastructure (low impact development), and stormwater best management practices (BMPs) to combat the problem.

2.6 Conclusion

Flow paths and travel times of shallow groundwater were analyzed through the injection of rhodamine into a stormwater management basin to better understand groundwater flow in a karst environment. A range of different velocities are observed within the surficial aquifer below the basin ranging from 0.09 – 1.41 m/d. The fastest velocity travels to wells 7 and 8, in the northeastern direction (toward the main vents in Silver Springs), while the slowest velocity travels to well 2 and 3, in the southeastern direction of the injection well. However, there are some locations in which the velocity does not coincide with the rest of the observed velocities due to the branching patterns of conduits in karst environments. Four different potential pulses of dye are observed at Silver Springs which could indicate different flow paths that tracer may take between the injection point and the spring. The tracer may travel through the soil matrix before hitting a conduit. We hypothesize that the faster travel times may include flow through karst conduits between the injection well and Silver Springs. The dye would take anywhere between 404 and 6333 days to arrive at Silver Springs if the dye was assumed to travel only through the soil matrix. Pulses of dye at Silver Springs are seen much earlier due to the presence of karst conduits. These velocities can be used in a three-dimensional subsurface model to possibly understand speed and direction of groundwater flow as well as the nutrients/contaminants that are present in the incoming stormwater that penetrates through the ground surface. Also noting that the interaction with karst features decreases the time stormwater is retained in aquifers, thus altering expected nutrient transformations. Once the flow pathways of stormwater travel are understood from the surface to the spring, specific steps can be taken to preserve water quality like implementing protection zones

or installing green infrastructure (low impact development) or bio-sorption activated media (BAM) in karst environments.

CHAPTER 3: HYDRAULIC INSTRUMENTATION OF BLANKET FILTERS AND VERTICAL REACTORS AND THE ASSESSMENT OF THE CUMULATIVE CAPTURE EFFICIENCY

3.1 Introduction

Stormwater runoff has become an increasing issue across the nation due to the elevated nutrient concentrations from urban/residential areas. Many best management practices (BMP's) have been implemented to alleviate the problem of elevated nutrient concentration. A few of these systems include rain gardens, bioswales, green roofs, rain barrels, and gravel wetlands. Stormwater ponds, or stormwater management basins, are a common type of BMP in Florida. Stormwater management basins are designed for flood mitigation (source reduction) and water quality treatment. The construction of these stormwater management basins allow for runoff to travel off the roads and highways in order to weaken the peak flow for storm events (Mitchell et al., 2007). Stormwater basins act as settling basins that accumulate large amounts of sediments on the surface while allowing the water the percolate into the soil (Marsalek & Marsalek, 1997). Biosorption Activated Media (BAM) is also another type of BMP used to remove harmful pollutants from stormwater. BAM can be used in conjunction with these stormwater management basin to work together to greatly reduce the amount of nutrient before percolating into the groundwater. These stormwater management basins along with BAM has been studied greatly in lab or small field experiments (Kim et al., 2000; Birch et al., 2005; Schipper et al., 2005) but have not been analyzed hydrologically in terms of its main purpose, which is to collect runoff. Our objective is to estimate the cumulative capture efficiency of incoming runoff after a given storm event.

3.2 Methodology

Biosorption Activated Media (BAM)-based stormwater treatment systems were implemented in two stormwater management basins (Basin 9B and Basin 2). These two treatment systems were implemented to study the design of BAM-based treatment alternatives for testing BMP's under different hydrogeological conditions, in hopes of reducing the nutrient concentration of incoming stormwater runoff (Chang et al., 2015). A blanket filter design was implemented in Basin 9B, while a vertical reactor system was implemented in Basin 2. Both treatment systems were composed of BAM recipes consisting of clay, tire crumb, and sand, with added iron fillings (aerobic media mix) for nitrogen and phosphorus removal.

3.2.1 Construction of Blanket Filters

Two blanket filter BMPs were installed in Basin 9B off State Road 35 and State Road 40 in Marion County (Fig 11) denoted 9B West and 9B East. The west and east BAM filters are located between 3 – 6 ft (0.9 – 1.8 m) and 1 – 4 ft (0.3 – 1.2 m) below grade, respectively. Each filter is comprised of two layers. The top layer consists of a nitrifying soil layer, composed of parent material meeting the specification that no more than 1% of the material is finer than 0.075 mm. The bottom layer of the filters is comprised of a denitrifying BAM layer. The nitrifying soil layer is 3 ft (0.9 m) deep in the West filter and 1 feet (0.3 m) deep in the East filter. The denitrifying BAM layer is 3 ft (0.9 m) deep in both the West and East filter (Fig 12).

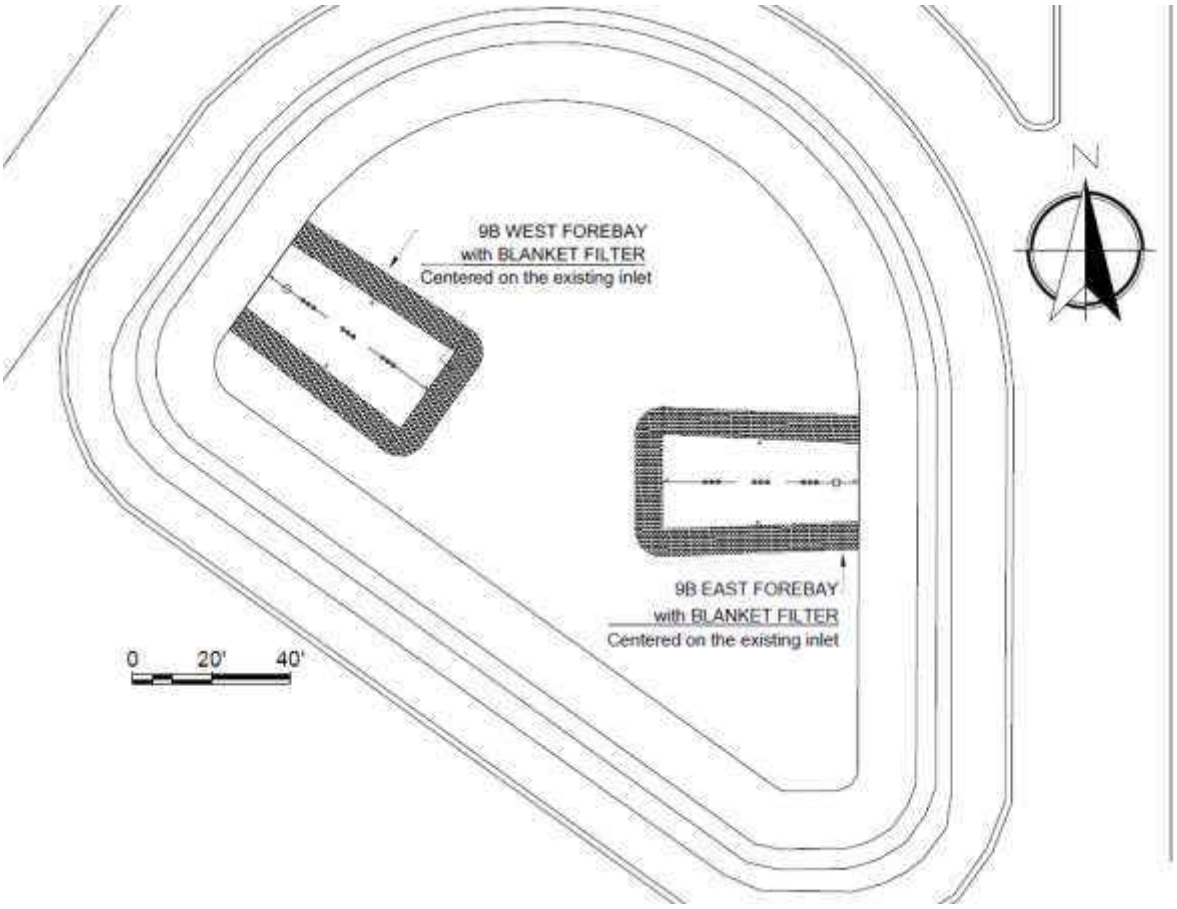

Figure 11: Plan View of Blanket Filters in Basin 9B

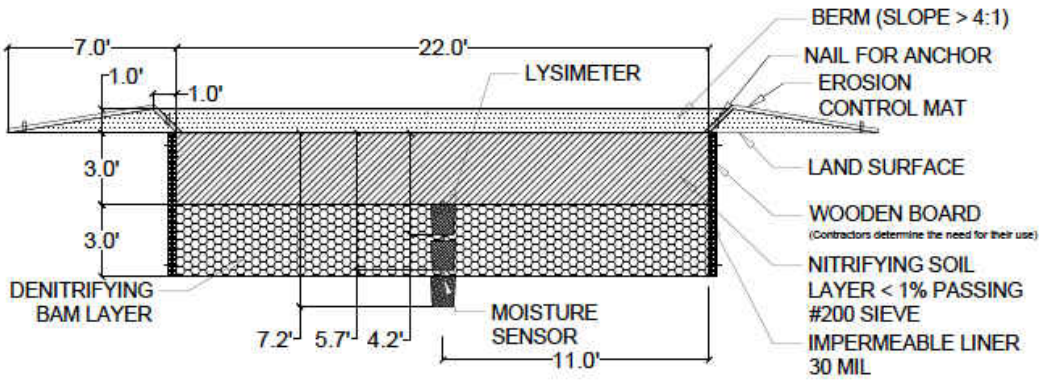

(a)

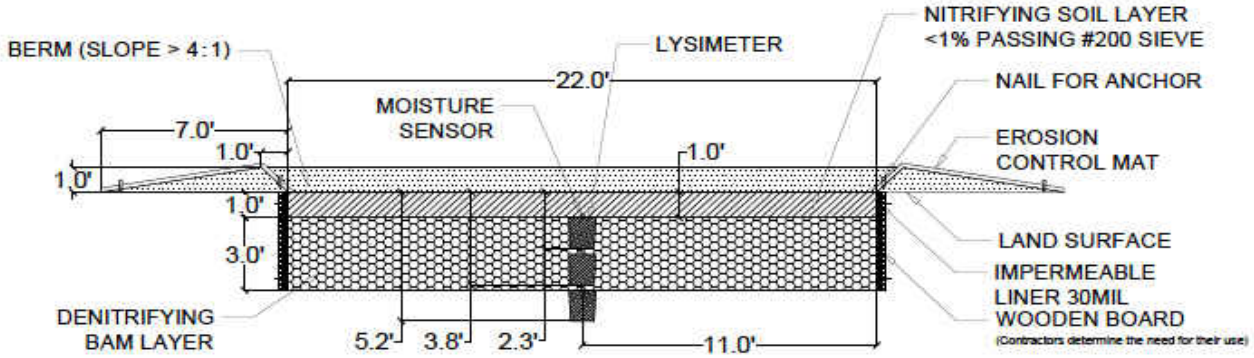

(b)

Figure 12: Cross section view of blanket filters (a) West (b) East

Each filter was installed along the centerline of an existing stormwater inlet in Basin 9B (Fig 11). An impermeable liner was installed around the sides of each filter with the support of a wooden board to prevent lateral spreading but allow for vertical infiltration (Fig 12). A berm was built around each filter using the excavated soil. Water will enter each BMP from the inlets and be contained within the forebay (bermed) area. If more water flows into the treatment area that can be contained within the forebay, the excess water will flow over the berms onto the natural soil around each of the filters.

Figure 13: Construction of Blanket Filers

3.2.2 Construction of Vertical Reactors

A vertical reactor system was installed in Basin 2 off State Road 35 in Marion County. Basin 2 is a 2.88-ac (1.2-ha) dry stormwater management basin located in a residential area with a large wooded area (Fig 14).

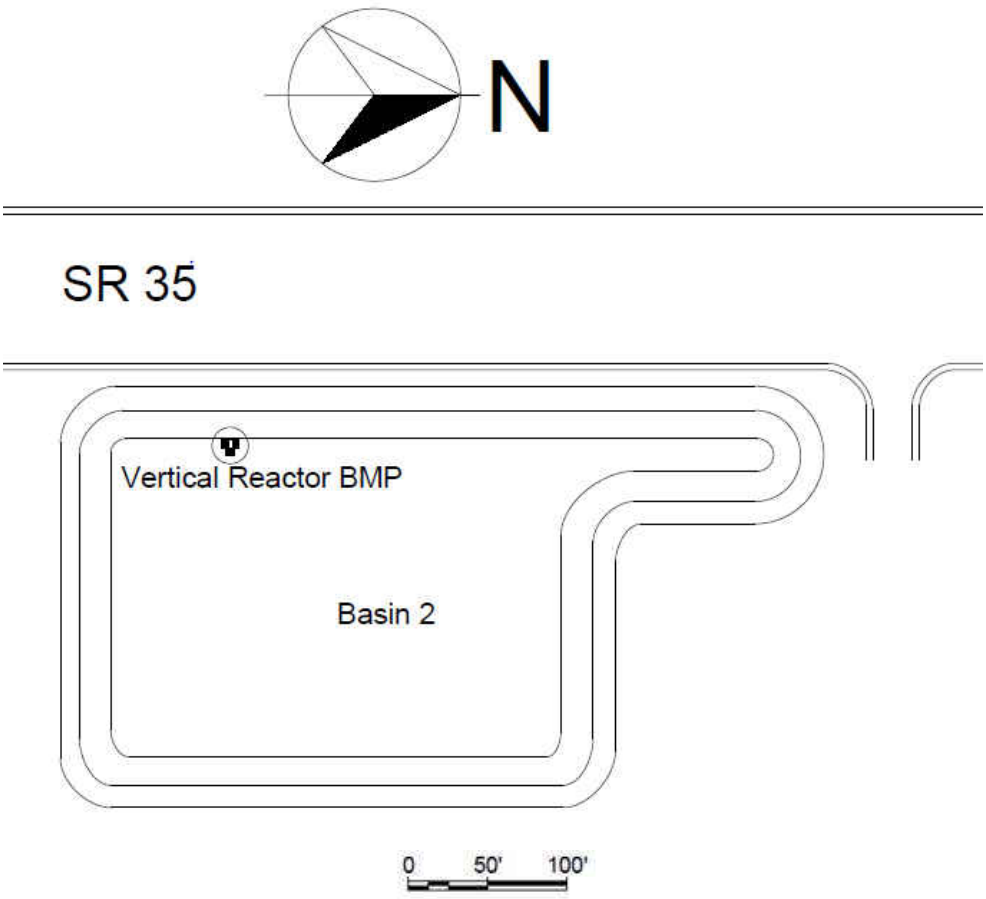

Figure 14: Plan View of Basin 2

Based on 18-month on-site monitoring the groundwater table depth was recorded to be greater than 25 ft (7.6 m). Soil samples were collected from the basin and tested using a sieve analysis to determine the soil characteristics near the ground surface. Based on the analysis results, the soil was classified as poorly graded sand with little or no fines. Analysis of bulk samples indicates sandy soils from the ground surface to a depth of 26 ft (7.9 m) and a groundwater water table of 24.2 ft (7.4 m). (Chang et al., 2015).

This treatment system consists of a central holding basin, and pairs of vertical reactors, denoted S1 through S6, attached to three sides of the holding basin (Fig 15 and 16).

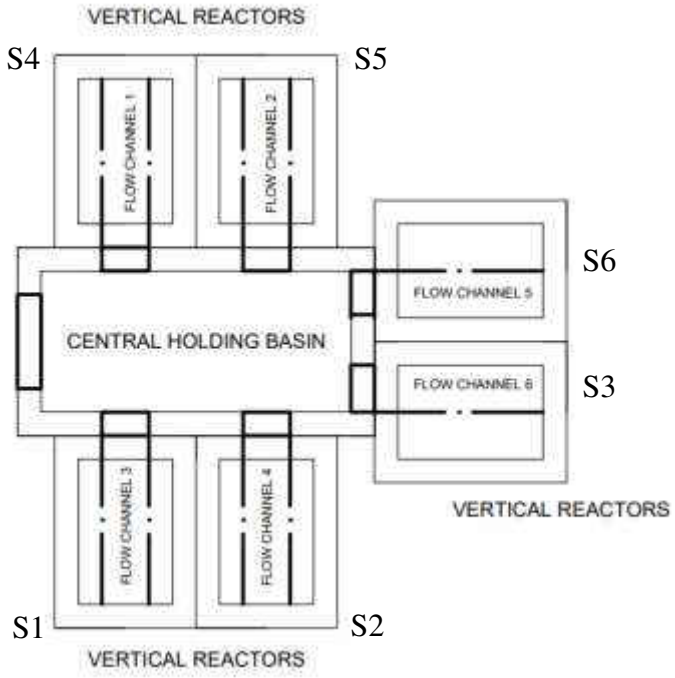

Figure 15: Plan View of Vertical Reactors

Figure 16: Construction of Vertical Reactors

The system was installed adjacent to the stormwater discharge pipe to facilitate direct flow into the inlet of the central holding basin. Once stormwater flowed into the central holding basin it

would then be distributed into each of the surrounding vertical reactors (symbolized by the bolded cutouts in the central holding basin in Fig 15). Each set of vertical reactors encompasses a different objective. Two sets of vertical reactors (S1 and S4) consist of BAM; two sets (S2 and S5) consist of aerobic media, to be provided by UCF; and the final two sets (S3 and S6) consist of BAM and the aerobic media to remove nitrogen and phosphorus. The water that has traveled all the way through reactors disperses into the surrounding nature soil.

3.2.3 Hydraulic Instrumentation

Hydraulic equipment was deployed in Basin 9B and Basin 2 to determine the hydraulic performance of each of the blanket filters and vertical reactors. A tipping-bucket rain gauge and data logger (MADGETECH Rain 101A Data Logger) were established on site in Basin 9B. The tipping bucket is 8 in (20.4 cm) in diameter and records increments of 0.01 in (0.02 cm) of precipitation to an accuracy of within 4% over rainfall intensities from 1 – 6 in (2.54 - 15.24 cm) per hour. The rain gauge and pressure transducers were installed in June 2017. However, the rain gauge was damaged when faulty housing allowed water to enter the data logger. The data logger was replaced in September 2017. On site precipitation data from July 5th until the time of equipment replacement were not recorded. Calibrated radar rainfall data (St. Johns River Water Management District) were used to estimate precipitation during the period of missing precipitation data.

In the blanket filters in Basin 9B, soil moisture sensors (ONSET 10HS Soil Moisture Smart Sensor) were installed at various depths to record the volumetric water content of surrounding soil. Soil moisture sensors were calibrated in the BAM between 0 to 0.570 m^3/m^3 with an accuracy of

0.033% for soils between 32 – 122 degrees Fahrenheit (0 – 50 degrees Celsius). Each sensor was connected to a HOBO USB Micro Station Data Logger where data were stored. The data loggers have the capacity to hold up to five soil moisture sensors, so in total 18 soil moisture sensors were installed with four data loggers. The logging interval for the soil moisture sensors was set to 15 minutes. In the west blanket filter the soil moisture sensors were installed 3, 4.5, and 6 ft (0.9, 1.4, and 1.8 m) below grade at distances 12.5, 25, and 37.5 ft (3.8, 7.6, and 11.4 m) downstream of the inlet pipe. In the east blanket filter the soil moisture sensors were installed 1, 2.5, and 4 ft (0.3, 0.8, and 1.2 m) below grade at distances 12.5, 25, and 37.5 ft (3.8, 7.6, and 11.4 m) downstream of the inlet pipe.

Pressure transducers (TE Connectivity, TruBlue 555 Vented Level Data Logger, pressure range from 0 – 300 psi, accuracy of 0.05%) were installed to record water levels. In Basin 9B, pressure transducers were installed in PVC stilling wells close to stormwater inlet pipes. In the West blanket filter, the pressure transducer was installed 3 ft (0.9 m) below the ground surface, and in the East blanket filter, the pressure transducer was installed 4 ft (1.2 m) below ground surface (Fig 17a and b). The Basin 2 vertical reactor system is instrumented with a single pressure transducer in the central holding basin (Fig 18). Staff gauges were installed next to the stilling wells, to establish a datum against which water levels recorded by the pressure transducer are compared. Change in water level is used to compute fluxes of water entering and leaving the treatment areas.

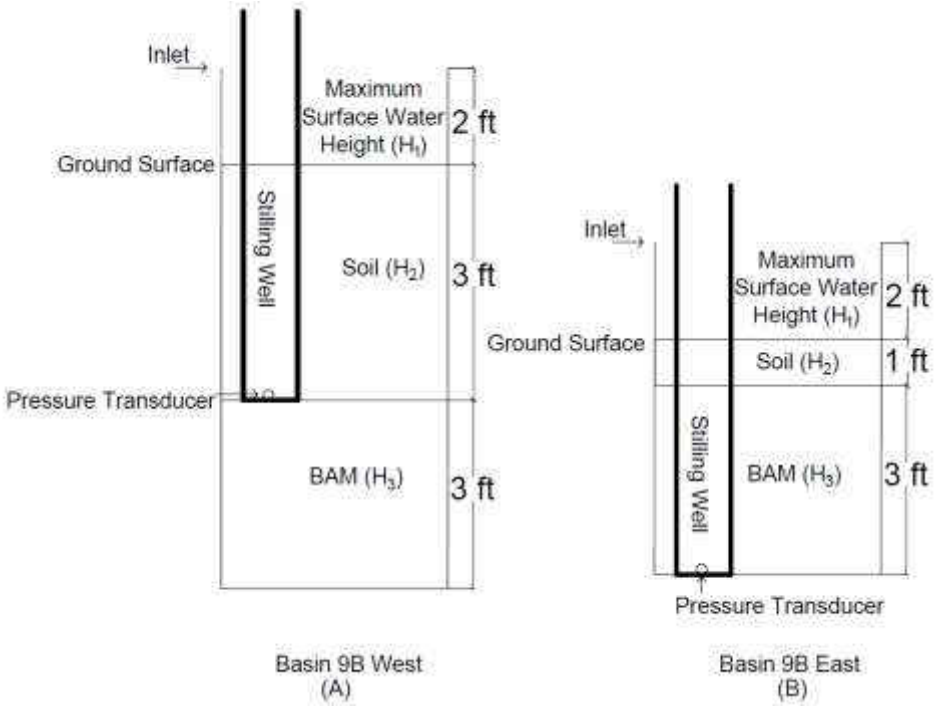

Figure 17: Cross-sectional diagram of pressure transducer locations in (a) Basin 9B West blanket filter and (b) Basin 9B East blanket filter

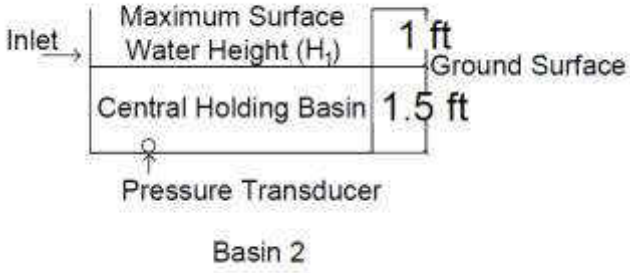

Figure 18: Cross-sectional diagram of pressure transducer location in Basin 2 Central Holding Basin

The logging interval for the pressure transducers was set to 15 minutes. These pressure transducers have the ability to measure the height of water above them which can be further used to estimate

the amount of runoff that is entering each treatment system. This information, in conjunction with rainfall data, can be used to calculate the capture efficiency for a given storm event.

3.2.4 Capture Efficiency

Change in water level given by continuous pressure transducer data is used to compute the volume of water that enters a BMP for treatment during a storm event (Q_{system}), as Eq. 2 for Basin 9B East, Eq. 3 for Basin 9B West, and Eq. 3 for Basin 2:

$$Q_{system} = A(\Delta H_1 + \phi_2 \Delta H_2 + \phi_3 \Delta H_3) \quad (2)$$

$$Q_{system} = A(\Delta H_1 + \phi_2 \Delta H_2 + \phi_3 \Delta H_3) \quad (3)$$

$$Q_{system} = A(\Delta H_1) \quad (4)$$

where A is the BMP treatment area (ft^2 or m^2), ΔH_1 is the change in height of surface water, ΔH_2 is the change in height of water in the soil layer, ΔH_3 is the change in height of water in the BAM layer, ΔH_4 is the change in height of water in the BAM using the groundwater level data , $\phi_2$is the average porosity of the natural soil and ϕ_3 is the porosity of BAM. The porosity of soil in Basin 9b (ϕ_2) is 0.34 (Das, 2008) and the porosity of BAM (ϕ_3) is 0.40 (Wen et al., 2018). For Eq. 3, the value of ΔH_3 is needed because the pressure transducer is installed to the depth of the nitrifying soil layer in the west blanket filter (3 ft or 0.9 m). Therefore ΔH_3 is calculated by subtracting the depth of the pressure transducer (3 ft or 0.9 m) from the groundwater depth. If the groundwater depth was higher than 3 ft (0.9 m) then ΔH_3 is 0 ft for Eq 3. To estimate the amount of water in the BAM layer the depth of the groundwater is analyzed. The BMP treatment area for Basin 9B West and East blanket filters is 1200 ft^2 (111 m^2) and 19.8 ft^2 (1.8 m^2) in the Basin 2 vertical

reactor. An assumption is made that each of the vertical reactors returns to field capacity before the next storm event occurs.

Capture efficiency is computed as the ratio of runoff that enters and is treated within a BMP system (Q_{system}) to the total volume of stormwater entering the retention basin through an inlet pipe during a storm event (Q_{in}) (Eq. 5).

$$Capture\ efficiency = \frac{Q_{system}}{Q_{in}} \quad (5)$$

The total volume entering the retention basin is unknown and must be estimated by continuity as Eq. 6:

$$Q_{in} = Q_{system} + Q_{out} \quad (6)$$

where Q_{out} is the volume of stormwater that bypasses the BMP when system capacity is exceeded (stormwater overtopping the bermed area).For events that do not overtop the berms we may estimate watershed contributing to the inlets of Basin 9B (Eq. 7).

$$Watershed\ Area = \frac{Q_{system}}{P} \quad (7)$$

where Q_{system} is the volume of water contained in each system, computed from the pressure transducers (ft^3) and P is the calibrated precipitation (in). This back calculation is done to calculate the watershed area (ft^2) that caused that specific volume to be seen in each treatment system. For storm events where Q_{system} does not exceed the maximum capture volume of the BMP, Q_{out} is zero and Eq. 8 applies. All stormwater entering the treatment area is treated, producing a capture efficiency of 100%.

$$Q_{in} = Q_{system} \quad (8)$$

For the events in which the stormwater entering the treatment system overtops the bermed area, the total stormwater runoff (Q_{in}) is estimated using the Soil Conservation Service Curve Number method (SCS CN), applied to the watershed area calculated using Eq. 7. Previous methods have been used to calculate runoff volumes like the American Rational Method and the Lloyd Davies method (Lloyd-Davies, 1906) but the most widely and accepted method used today is the Soil Conservation Service – Curve Number method (Mishra & Singh, 1999). The Soil Conservation Service – Curve Number (SCS CN), developed by the National Resources Conservation Service (NRCS), is commonly used by engineers for calculating the amount of runoff that is generated on a given area. The SCS CN is centered on the water balance equation and two concepts: the first concept relates direct surface runoff to rainfall, infiltration, and maximum retention while the second relates initial abstraction, or the fraction of storm depth after runoff begins, to maximum retention (Mishra & Singh, 2003). The Curve Number is used to calculate the runoff properties for a specific combination of land cover and soil group. Generally, a low curve number means there is low runoff probability, while a high curve number indicates that there is a high probability for runoff. Table 2-2a in the *'Urban Hydrology for Small Watersheds – TR-55'* shows curve numbers that characterize runoff conditions for urban, cultivated agricultural, other agricultural uses (Cronshey, 1986). This table assumes that the impervious areas are all directly connected to drainage systems. However, runoff will not occur unless precipitation is greater than the initial abstraction. Runoff from impervious areas shifts the flow of water from subsurface to surface flow (Shuster et al., 2005). This surface flow leaks as shallow/horizontal flow and then flows into nearby drainage systems. These drainage systems include roads, parking lots, and in some cases, roofs. (Boyd et al., 1993). Runoff from unconnected impervious areas (lawns, gardens, and grasslands) generally infiltrate into the soil or flow as overland flow once the soil becomes saturated. Runoff

from pervious areas is difficult to predict because it often depends on the soil type as well as the vegetation. The appendix in TR-55 contains defined soil groups as well as a list soils with their soil group classification (A, B, C, or D). Group A soils (loamy sand or silt loam) have low runoff potential when saturated and the flow of water is transferred freely throughout the soil. Group B soils (sandy clay loam) have a moderately low runoff potential when saturated and the flow of water is unobstructed. Group C soils (clay or silty clay) have a moderately high runoff potential where the flow of water is slightly restricted. Group D soils (clay) have a high runoff potential when saturated and the flow of water is very restricted (Cronshey, 1986, USDA, 2009a).

There are limitations when using the SCS CN method to predict the runoff from rainfall excess (Cronshey, 1986). Although the accepted range for curve numbers is 0 to 100 the US Department of Agriculture's CN range from 30 to 100. An additional procedure must be deployed to estimate runoff if the watershed CN is calculated to be less than 30 and runoff that accumulates on the ground as snow cannot be predicted using this method.

As previously stated, the SCN CN method is applied to calculate the amount of runoff over a particular area but it can be taken a bit further and applied to the blanket filters and vertical reactors in Basin 9B and Basin 2 given by Eqs. 9-13.

$$\frac{P^{*}-Q}{S}=\frac{Q}{P^{*}} \qquad (9)$$

In Eq. 9, Q is actual runoff (in), S is the amount maximum potential retention capacity of the watershed after runoff begins (in), and P^{*} is the effective precipitation (in). P^{*} is equivalent in volume to event flow, Q^{*}. This maximum potential retention capacity of the watershed after runoff

begins (S) is calculated by an empirical relation using a runoff curve number, as Eqs. 10 (English Units) and 11 (International System of Units):

$$S(in) = \left(\frac{1000}{CN}\right) - 10 \quad (10)$$

$$S(mm) = \frac{25400}{CN} - 254 \quad (11)$$

where CN is the runoff curve number. Given 'typical' antecedent conditions, the initial abstraction is assumed to be 20% of maximum potential retention capacity (Cronshey, 1986) as Eq. 12:

$$I_a = 0.2S \quad (12)$$

Substituting,

$$\frac{P-I_a-Q}{S} = \frac{Q}{P-I_a} \quad (13)$$

where P is the amount of rainfall. Rearranging equation 12 to solve for an event flow, Q^*, Eq. 14:

$$Q^* = \frac{(P-I_a)^2}{P-I_a+S} \quad (14)$$

Event flows are scaled by watershed area (A) to estimate total inflow volumes (V), as in Eq. 15.

$$V = Q^* \cdot A \quad (15)$$

Delineated contributing areas and curve numbers, estimated from the total drainage area to Basin 9B, are used to estimate the initial abstraction, as 3 in (7.6 cm) (Greiner, and URS, 2004a, 2004b, 2004c, 2007a, 2007b). However, we assume the production of measurable runoff during events smaller than the initial abstraction is due to runoff produced by Directly Connected Impervious Areas (DCIA), or impervious surfaces designed to drain directly to Basin 9B. The curve number for impervious surfaces is 98, which produces a maximum storage of 0.20 in (0.51 cm) and initial abstraction of 0.04 in (0.10 cm). Reliable estimates of the DCIA were not available for the two

drainage pipes draining to the west and east blanket filters so an alternate approach was used to estimate inflows from the DCIA. The watershed area is assumed to be 100% DCIA that is flowing into the stormwater management basin. To incorporate such uncertainty, we estimate inflows for events exceeding system capacity using a plausible range of DCIA. The interquartile range (IQR) of estimated DCIA given by the storm responses is assumed to approximate the true DCIA. Each range value of the IQR (Q_1 and Q_3) will be shown for events in which ΔH_1 is greater than the height of the berms.

For Basin 2 the estimate of total stormwater inflows to the vertical reactors is made using the same model. Total DCIA draining to the vertical reactor is 220×10^3 ft^2 (20×10^3 m^2) or 5.02 ac (2.03 ha) (Greiner, and URS, 2003) was used in the SCS CN Method. Impervious surfaces have a runoff curve number of 98, producing a storage of 0.20 in (0.51 cm) and an initial abstraction of 0.04 in (0.10 cm). For all the events ΔH_1 remained at this height for a minimum of 10 hours. Therefore, it safe to assume that each of the vertical reactors was to capacity at the end of a storm event. So Q_{system} equals the water in the central holding basin plus the water the pore spaces of each of the vertical reactors (approximately 40 ft^3 or 1.1 m^3).

3.2.4.1 Theoretical Maximum Capture Volume

Using the dimensions of the height of the berm, depth, and porosity of the natural soil layer, a theoretical maximum capture volume can be estimated for the East and West blanket filters (Table 2). Assuming the BAM and the soil are at field capacity at the start of inflow and neglecting infiltration out of the filter to deeper soil layers, the maximum capture volume will fill all available

pore space in the subsurface filter and a free surface of water will rise to the height of the berms. Additional water entering the treatment area will pass over the berms and will not be treated by the filter. In the vertical reactor, the maximum capture volume may be similarly approximated by the capacity of the central holding basin and reactors. This approach is a conservative estimate; actual maximum capture volumes will be greater due to deep infiltration.

3.3 Results

3.3.1 Theoretical Maximum Capture Volume

The theoretical maximum capture volumes Basin 9B West, Basin 9B East, and the vertical reactors in Basin 2 are 5200, 4400, and 87.4 ft^3 (147, 125, and 2.5 m^3), respectively (Table 2).

Table 2: Theoretical Maximum Capture Volume of BMPs

Treatment Area	**Maximum Capture Volume (ft^3)**
Basin 9B West	5200
Basin 9B East	4400
Basin 2	87.4

3.3.2 Basin 9B West Blanket Filter

The theoretical maximum capture volume of the West blanker filter is 5200 ft^3 (147 m^3) (Table 2). Over the span of a year (June 2017 – May 2018), thirty-four events produced a measurable volume change in the blanket filter (Table 5 & Figs A2.1 – A2.2; Appendix II). These events ranged from 0.1 – 2.5 in (0.3 - 6.4 cm) of cumulative precipitation. The volume of water that entered the West

blanket filter for treatment during 34 storm events ranged from $0.8 - 4.6 \times 10^3\ ft^3$ ($23 - 130\ m^3$) (Table 6; Appendix II). Based on analysis of events that did not exceed volume of the blanket filters, the DCIA draining to the West filter was estimated to be between $50 - 96 \times 10^3\ ft^2$ ($4.6 - 8.9 \times 10^3\ m^2$) for the 34 rainfall events. (Fig 19).

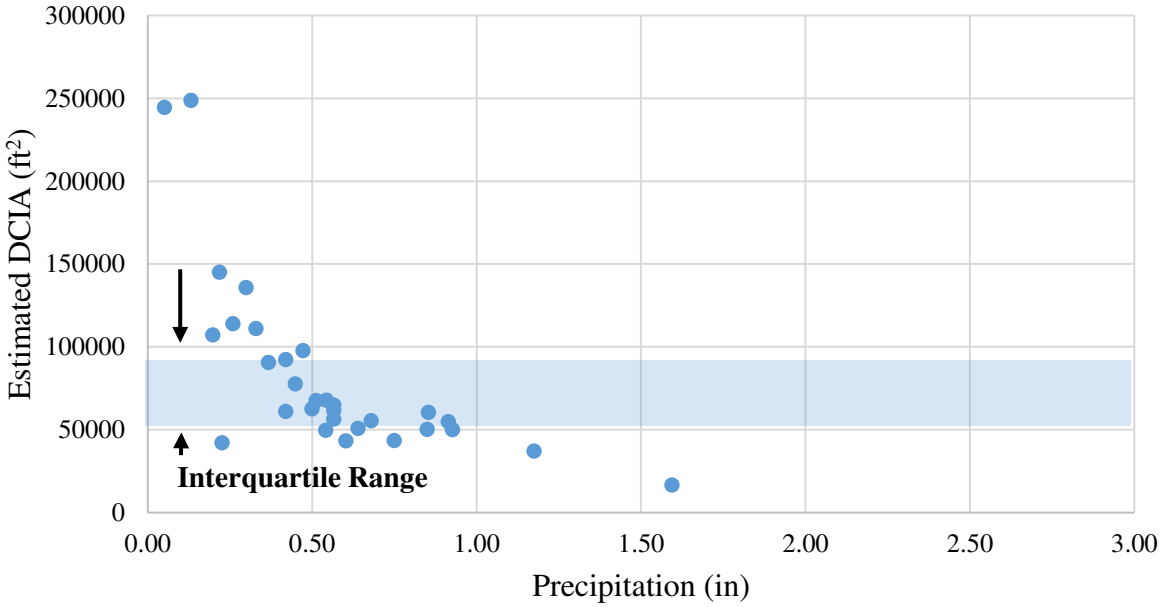

Figure 19: Estimated DCIA draining to Basin 9B West, with the interquartile range indicated

For the four exceedance events, the SCS CN Method estimated a range from $5.9 - 18 \times 10^3\ ft^3$ (167 – 510 m^3) of stormwater entered the treatment area (Q_{in}). Since the volume of stormwater in the system is known the volume that overtopped the berms and bypassed the system (Q_{out}) ranged from $1.9 - 12.4 \times 10^3\ ft^3$ (53 – 351 m^3) (Table 9; Appendix II).

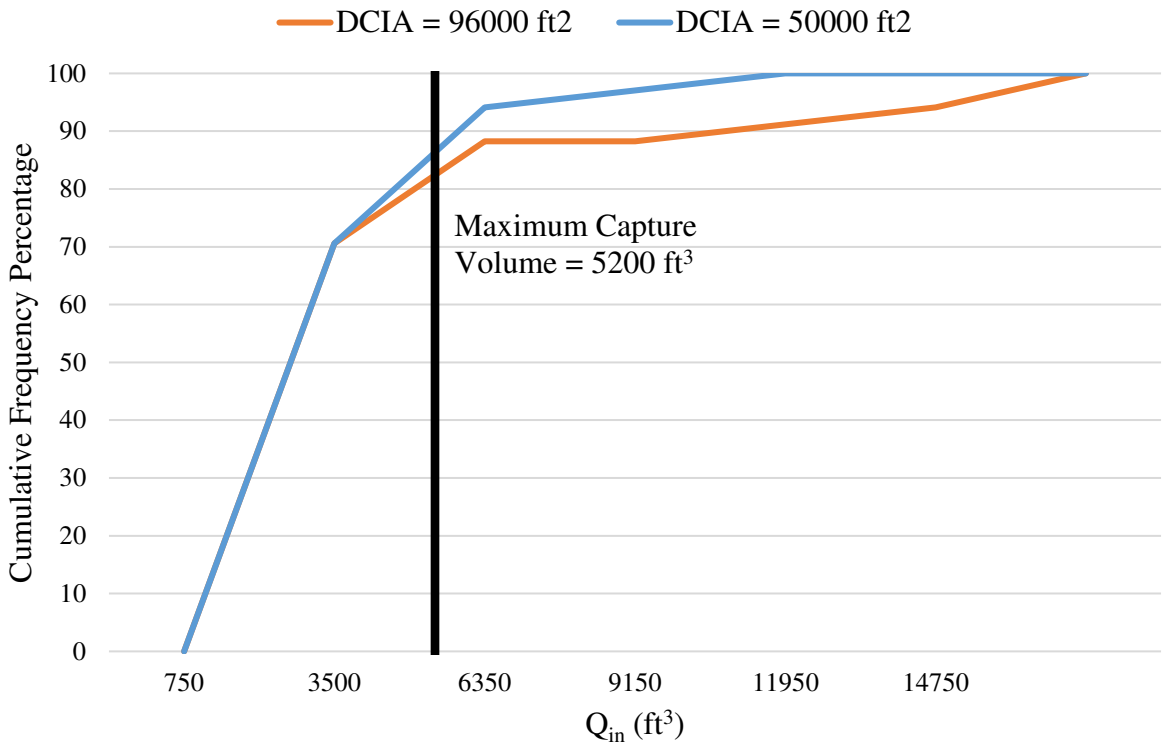

Figure 20: CDF of Basin 9B West Storm Events

When the lower bound of the interquartile range is analyzed, Q_{in} is plotted as a cumulative distribution function the events that exceeded the maximum capture volume are clearly shown and at specific ranges. Two events ranging from 5251 – 6750 ft^3 (149 – 191 m^3) and two events greater than 8250 ft^3 (234 m^3) exceeded the capacity when the lower bound of the interquartile range is analyzed (Fig 20). When the upper bound of the interquartile range is analyzed, the same exceedance of Q_{in} is shown. One event ranging from 9151 – 11950 ft^3 (259 – 338 m^3), one event ranging from 11951 – 14750 ft^3 (338 – 417 m^3), and two events greater than 14750 ft^3 (417 m^3) exceeded the system capacity (Fig 20).

At the event scale, thirty events had a capture efficiency of 100%, as filter capacity was not exceeded in these events. The four events that exceeded system capacity captured and treated

approximately 21 – 67% of incoming stormwater flows. This is a mean event flow analysis based on the events that produced surface storage. The mean event flow capture efficiency of the West filter based on events that had surface storage, over the sample period, is between 91 and 94%. Across these 34 events producing a measurable volume change in the blanket filter that total volume of water seen in the system is $9.8 \times 10^3\ ft^3$ (2780 m^3). Using the above estimation for Q_{in} the total volume of water coming into the west blanket filter ranged from $11.5 - 14.3 \times 10^3\ ft^3$ (3276 – 4057 m^3). The cumulative capture efficiency is between 68 and 85%.

3.3.3 Basin 9B East Blanket Filter

The theoretical maximum capture volume of the East blanker filter is 4400 ft^3 (125 m^3) (Table 2). Twenty-one events produced a measurable volume change in the East basin (Fig A2.3; Appendix II). These events ranged from 0.1 – 2.5 in (0.3 - 6.4 cm) of cumulative precipitation (Table 5; Appendix II). The blanket filter captured all of these twenty-one events (Fig 21). Water levels did not overtop the berms during any event recorded. The volume of stormwater in the system ranged from $2.1 - 3.1 \times 10^3\ ft^3$ $(59 - 88\ m^3)$ (Table 7; Appendix II). Therefore Q_{in} equals Q_{system} and therefore obtaining a mean event flow capture efficiency of 100% for all the events collected from June 2017 and May 2018.

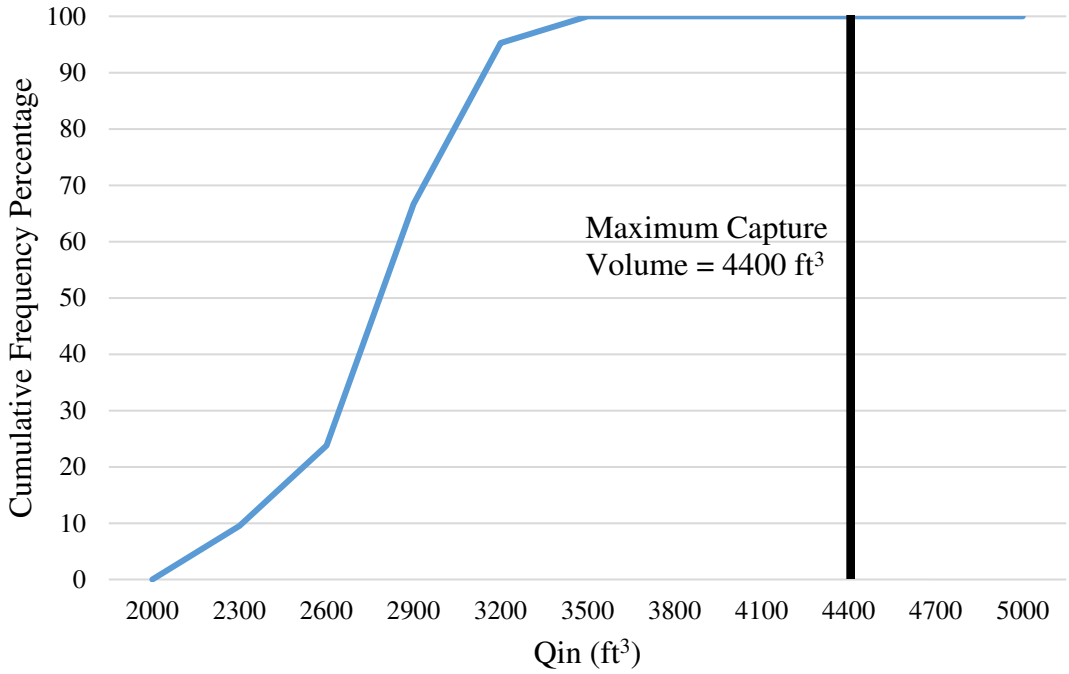

Figure 21: CDF of Basin 9B East Storm Events

None of the events in the East blanket filter overtopped the treatment system unlike in the West blanket filter so the estimates of the DCIA are not needed for the mean event flow capture efficiency but can still provide useful information. The DCIA draining to the East filter was estimated to be between $36 - 63 \times 10^3\ ft^2$ $(1.0 -\ 1.8 \times 10^3\ m^2)$ for the 21 rainfall events.

3.3.4 Basin 2 Vertical Reactor

The theoretical maximum capture volume of the vertical reactors is 87.4 ft^3 (2.5 m^3) (Table 2). Thirty-one events produced a measurable volume change in vertical reactors between June 2017 and May 2018 (Table 8 & Fig A2.4; Appendix: II). The volume of stormwater in the system was estimated to be between 49 – 115 ft^3 (1.4– 3.3 m^3).

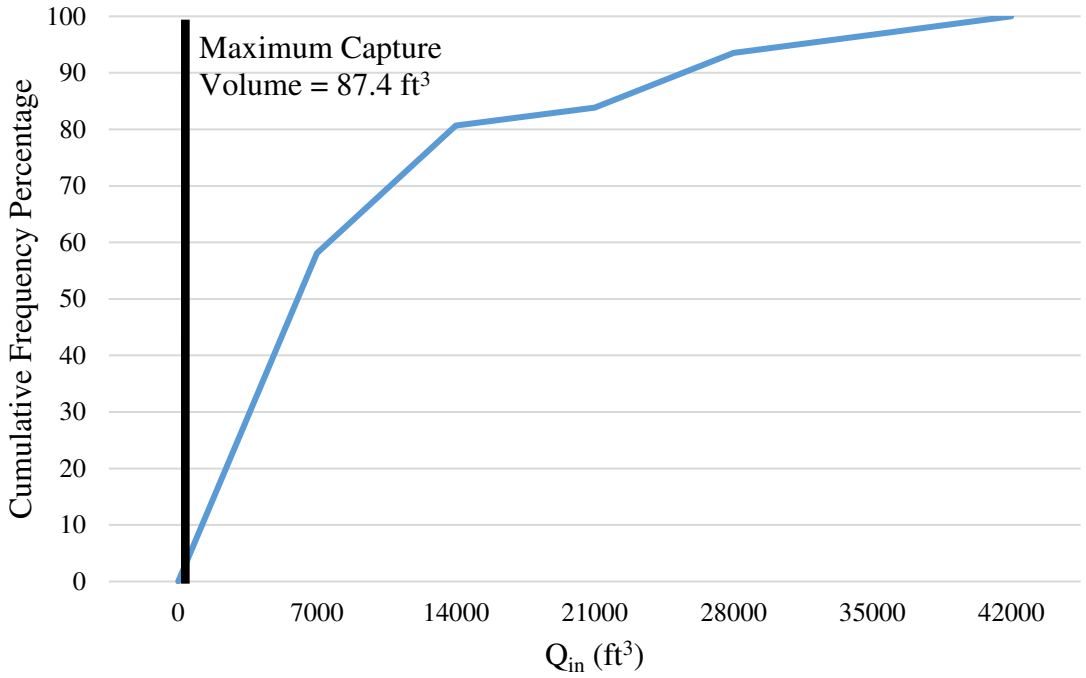

Figure 22: CDF of Basin 2 Storm Events

All of the thirty-one runoff-producing events recorded exceeded the capacity of the vertical reactors (Fig 22). These events provided very low capture efficiencies. All the events have a capture efficiency of less than 1% (Table 10; Appendix: Capture Efficiency).

3.4 Discussion

3.4.1 Hydrologic Performance of Blanket Filters

The scatter of estimated contributing DCIA areas in Figure 19 reflects the uncertainty of the SCS CN model and the calibrated precipitation estimation from the rain gauge data. Theoretically, the DCIA should not change but since reliable estimates of the DCIA for each of the west and east blanket filters was not provided this calculation was based off the volume calculated in the system, from the pressure transducers. As more and more rainfall events are analyzed, the estimate that is

being used to compute the IQR will become narrower providing more accurate calculations (hence the DCIA will become static). The analysis that is used to calculate the cumulative capture efficiency makes reasonable assumptions but as with any model, there are some small minute errors. For example, On January 29th and April 10th, the estimated height of water on the surface is 2 ft (0.6 m) and 2.2 ft (0.7 m), respectively, which is the estimated height of the berm. Theoretically, there should be a capture efficiency of 100% but due to the slope of the berm, some stormwater may be contained within the treatment area while some could overtop the berms. The calculations, using this method, show a value of Q_{system} that is greater than Q_{in}. This shows that this model may be inaccurate when the height of water on the surface and berm are equivalent. Due to this occurrence Eq. 8 is assumed for both of these events.

When comparing both blanket filter systems, Basin 9B east has the better mean event flow capture efficiency of 100%. This shows that all the runoff events from June 2017 – May 2018 are percolating downward through 1 feet (0.3 m) of parent material and then 3 ft (0.9 m) of BAM material. Basin 9B west has a cumulative capture efficiency between 70 and 90%. These capture efficiencies are high for both the east and west filters in Basin 9B which indicate that both basins are effective in capturing stormwater runoff however they are not identical. Both basins could possibly have different watershed areas which would explain the different capture efficiencies. The estimated watershed area of Basin 9B West is between $50 - 96 \times 10^3\ ft^2$ ($4.6 - 8.9 \times 10^3\ m^2$) while the estimated watershed area for Basin 9B East, although not needed, is between $36 - 63 \times 10^3\ ft^2$ ($1.0 - 1.8 \times 10^3\ m^2$). Basin 9B East has a smaller watershed area that coincides with a smaller volume of water entering the treatment system (Q_{in}) which is potentially one explanation for why there is not a storm event that exceeds the capacity of the treatment

system. Due to the design, it is also possible that the treatment systems have different infiltration rates. It is likely that BAM has a faster infiltration rate than the natural soil in Basin 9B. In Basin 9B East the BAM is installed at a shallower depth than in Basin 9B west (1 ft (0.3 m) vs. 3 ft (0.9m)). Since this is the case then the incoming stormwater will percolate into the subsurface very quickly, initially, so that the water will never reach a height that exceeds the berms in Basin 9B East.

3.4.2 Hydrologic Performance of Vertical Reactors

The maximum capture volume of the vertical reactor is small relative to volumes of stormwater draining from a large drainage area. However, this is what was expected due to the large watershed area relative to the size of the treatment area. This large watershed area correlates with a large volume of incoming stormwater. During/after a rainfall event the water remained ponded for a considerable amount of time because pore space in the vertical reactors was quickly filled. The volume of water that was too large for the system to handle. The vertical reactor system in Basin 2 was a novel design intended to treat stormwater flowing through the reactors. However, due to the small maximum capture volume, the vertical reactors would be best suited if placed next to a roof (to capture roof runoff), off a road shoulder, or in a small retention pond where there would be a small incoming volume of water flowing into the central holding box.

3.5 Conclusion

For this research, the SCS method was utilized to estimate the cumulative capture efficiency of rainfall events when incoming stormwater overtopped berms in a stormwater management basin.

In Basin 9B, pressure transducers were installed in PVC stilling wells close to stormwater inlet pipes and the transducers were directly installed in the central holding box in Basin 2. Rain gauge and radar rainfall data were used to estimate the amount of precipitation captured in each site, to utilize the SCS CN method to estimate the capture efficiency. The blanket filters in Basin 9B West and East were designed to capture and treat the majority of the incoming stormwater runoff while the vertical reactors in Basin 2 were designed to treat incoming stormwater. Therefore, Basin 9B West and East were hypothesized to have capture efficiencies close to 100%, while Basin 2 was hypothesized to have a relatively low capture efficiency (because of the large size of the basin and the small capture volume of the vertical reactors). Thirty-four events produced a measurable volume change in Basin 9B in at least one of the BMPs during the sampling period. Of these thirty-four events, four events overtopped the berms in the West blanket filter while zero events overtopped the berms in the East blanket filter. By using the SCS CN method, the total cumulative capture efficiency of the West filter over the sample period ranges from 91 to 94% while the total cumulative capture efficiency of the East filter is 100%. The blanket filters in Basin 9B are effectively treating a large portion of the incoming stormwater runoff. In regard to Basin 2, the vertical reactors were constructed on the emphasis on stormwater treatment. Therefore, the vertical reactors would be best suited if placed where there would be a small incoming volume of water flowing into the central holding box.

CHAPTER 4: HYDRAULIC PERFORMANCE OF BLANKET FILTERS AND EFFECTIVENESS AT REMOVING NUTRIENTS FROM SHALLOW GROUNDWATER

4.1 Introduction

Capturing stormwater runoff is a valuable tool for addressing the growing demand for freshwater across the globe. However, this stormwater has potential impacts that are affecting the groundwater. For this reason, the promotion of green infrastructure in stormwater management basins is becoming very important. Current approaches to stormwater management aim to treat stormwater and remove these pollutants through the use of bioretention filtering systems (Anyona, 2009), bioswales (Wahl, 2009), green roofs (Rowe, 2011), rain barrels (Abi Aad et al., 2009; Ando & Freitas, 2011) and stormwater management basins. When looking to apply best management practices (BMPs) in stormwater management basins there must be a balance between enhancing stormwater quantity and protecting stormwater quality. Stormwater management basins can contribute to elevated nutrient concentrations in groundwater in urban environments (Taylor et al., 2005). Nitrogen and phosphorus are common constituents of concern because of the environmental/health problems discussed in Ch. 1. (O' Reilly et al., 2010). Biosorption Activated Media (BAM) is an additional stormwater BMP used to remove harmful pollutants in the environment that can be used in conjunction with other BMPs. Sorption is a process where particles accumulate on certain BAM particles like expanded clay, tire crumb, tire chips, activated carbon, sawdust, limestone, and/or crushed shells, (Wanielista, 2015). One specific type of BAM, known as Bold and Gold (B&G), contains clay, tire crumb, and sand (CTS) and was developed by the University Of Central Florida Stormwater Management Academy to remove nitrogen and phosphorus in stormwater. The composition of CTS will have between 2% and 6% of material

passing between 0.075 mm openings (200 sieve). The media is primarily composed of 85% sand and 15% of other sorption materials based on volume with a total porosity of around 40%. Lab testing was done to analyze the porosity of the BAM by pouring a known volume of water into a known volume of media until saturation was reached (Wen et al., 2018). Field capacity is the upper limit of water content, seen in the field, after the media is allowed to dry (Colman, 1947; Xuan et al., 2013). In determining the field capacity as well as the saturation levels of BAM, lab/fields studies must be implemented where the BAM is saturated with incoming water and allowed to dry properly by gravity. Hood [2012] took measurements of Bold & Gold™ after complete drainage by gravity in a field scale test bed and reported the average field capacity as 40.15%. On the other hand, O'Reilly et al. [2012] estimated the field capacity of BAM to be 24% and saturation of 49% in a storm water infiltration basin near Silver Springs, Florida. In terms of nutrient removal BAM must retain a minimum residual moisture content for biofilm growth. Biofilms are species of bacteria that attach to particles in the BAM to remove nutrients through adsorption (Mah & O'toole, 2001; Pasmore et al., 2001). Naujock [2008] implemented a study in Marion County in which the minimum residual moisture content of two types of media containing tire crumb, sand, and clay was approximately 0.10 m^3/m^3 for biofilm growth. The sorption materials are recycled tire and mined clay. This mix has a dry weight of 62 lbs/ft^3 (993 kg/m^3) and non-flammable up to 482 degrees Fahrenheit (250 degrees Celsius). The CTS composition has a water holding capacity of 10% measured by porosity and a permeability greater than 5 in/hr (12.7 cm/hr) (*BOLD & GOLD®,* 2017).

In the past researchers have performed lab/site scale analysis to test the effectiveness of BAM at removing nitrogen or phosphorus. Kim et al. [2000] used eight columns (two control, six

experimental) test different type of sorption media that would be contained in BAM. The experimental columns were filled with alfalfa, leaf mulch compost, newspaper, sawdust, wheat straw, and wood chips. Alfalfa, newspaper, and leaf mulch compost were grouped together in one experiment while sawdust, wheat straw, and wood chips were grouped together in another. The results of this experiment showed that alfalfa and newspaper had a 100% nitrate removal efficiency from a secondary effluent sample. Sawdust, wheat straw, and wood chips also showed good removal efficiencies that were greater than 95%. Hood et al. [2013] showed that BAM, in a field scale test bed, is effective in removing phosphorus from highway runoff. The test bed, that represented a highway and roadside swale, removed 71% of total phosphorus and 95% of soluble reactive phosphorus (SRP). Birch et al. [2005] experimented with removing nitrogen in a stormwater infiltration basin. The basin was composed of a 1:6 mixture of zeolite along with coarse, pure quarzitic sand. The results of this experiment showed that total kjeldahl nitrogen removal ranged from 47 – 74% and the total nitrogen removal ranged from 33 – 40%. Total phosphorus removal ranged from 37 – 67%. Schipper et al. [2005] performed an experiment in which they filled a trench (35 m long, 1.5 m deep, and 1.5 m wide) with pine sawdust mixed with the soil that was excavated. In this experiment, the nitrate decreased at a rate of approximately 1.4 g N/m3 per day which was showed to be approximately 97.2% of nitrate removal. A study (Wanielista et al., 2014) was done to show how effective BAM was in removing nutrients from two ultra-urban environments (environments with large peak flows and large incoming pollutant concentrations that affect the groundwater in Florida). This study analyzed three different types of BAM mixtures: BAM mixture one (contained 55% fine expanded clay, 20% 3/8-inch expanded clay, and 25% tire crumb, BAM mixture two (25% 3/8-inch expanded clay, 50% A-3 and 25% A-2-4 silty sand), and BAM mixture three (contained 15% fine expanded clay, 15% tire crumb, 50%

A-3 sand and 20% limestone). In terms of nitrogen removal, BAM mixture one, two, and three had a removal efficiency of 26%, 14%, and 20%, respectively for simulated two-hour storm event. In the 24-hour storm event BAM mixtures one, two, and three had a removal efficiency of 48%, 21%, and 33%. Overall BAM mixture one performed the best in terms of removal total nitrogen, SRP, and total phosphorus. Greater nutrient removal is achieved when stormwater is retained in BAM for longer periods of time. However, the specific hydraulic retention times of BAM, in the above studies, was not tested along with how BAM interacts with the groundwater table. Will groundwater have the same improvements observed for infiltrating surface water? In this study, the objective is to evaluate the hydraulic performance of the blanket filters, through the use of hydrologic monitoring equipment (previously described in Ch. 3), and the effectiveness of the blanket filters at removing nutrients from shallow groundwater in Basin 9B.

4.2 Methodology

4.2.1 Hydraulic Monitoring Equipment

A network of 12 observation wells was drilled in Basin 9B for the purpose of observing the groundwater depth. The wells were drilled 10 ft (3.0 m) below grade with a 1.5 in (3.8 cm) diameter. Pressure sensors (ONSET HOBO Water Level Data Logger U20 and U20L) were installed in one of the wells to continuously monitor groundwater level and atmospheric pressure. A barometric compensation assistant is used in ONSET to create a water level depth series using the type of water (freshwater or saltwater), density, reference water level (defined here as from the ground surface to the depth of the water table) (ONSET, 2008). Pre-construction and post-

construction groundwater depths were measured in west sampling well 1 and west sampling well 2, respectively (Fig 23).

Soil moisture sensors (ONSET 10HS Soil Moisture Smart Sensor) were installed at various depths to record the volumetric water content (VWC) of surrounding soil and determine the hydraulic performance of each treatment system. Soil moisture sensors were calibrated in the BAM between 0 to 0.570 m^3/m^3 with an accuracy of 0.033% for soils between 32 – 122 degrees Fahrenheit (0 – 50 degrees Celsius). The logging interval for the soil moisture sensors was set to 15 minutes. In the west blanket filter the soil moisture sensors were installed 3, 4.5, and 6 ft (0.9, 1.4, and 1.8 m) below grade at distances 12.5, 25, and 37.5 ft (3.8, 7.6, and 11.4 m) downstream of the inlet pipe. In the east blanket filter the soil moisture sensors were installed 1, 2.5, and 4 ft (0.3, 0.8, and 1.2 m) below grade at distances 12.5, 25, and 37.5 ft (3.8, 7.6, and 11.4 m) downstream of the inlet pipe. Rainfall events were analyzed along with the volumetric water content across the entire project duration thus far and it was determined that a given event in which the soil remained dry for a long period of time followed by a large storm event would be best for analysis of the hydraulic performance.

The porosity of BAM was calculated to be approximately 40%. However, during construction and installation of the BAM in the blanket filters, compaction occurred such that maximum porosity may vary from that estimated in the lab. This is important because the volumetric water content cannot exceed the maximum porosity. Measurements were observed for several storm events between June 2017 and May 2018. The VWCs were analyzed in each basin and used to estimate hydraulic retention time.

4.2.2 Nutrient Concentrations of Shallow Groundwater

Nutrient concentration (nitrate, total nitrogen, and total phosphorus) of shallow groundwater were monitored for 11 months. A **B**efore-**After C**ontrol-**I**mpact (BACI) study was applied at 2 well locations: in close proximity to the BAM filter at the west sampling well 1/2 and further from the BAM filter at the east sampling well (Fig 23). Groundwater samples were analyzed in both locations before and after the introduction of the BAM filter (impact) to measure the potential effectiveness of the BAM blanket filter at removing nutrients from shallow groundwater. We assume that groundwater withdrawn from the east sampling well is not affected, or affected to a lesser degree, by the installation of the BAM filter as compared to water from the west sampling position, which is directly in the downstream flow path of the BAM filter. West sampling well 1 was destroyed during construction of the west blanket filter. After construction, new wells were installed. The new location of west sampling well was slightly to the northwest, just downstream of the treatment area, and was renamed west sampling well 2. The location of the east sampling well was unaffected by construction.

Peristatic pumps (Masterflex L/S Digital Standard Drive, Easy-Load II Head for Precision Tubing, pump range from 0.0012 to 2300 mL/min, 8.8 m of suction lift) were used to pump approximately 100 mL of groundwater into sample bottles for triplicate testing. These bottles were then labeled with their appropriate well location (west or east) and date and brought back to the lab for testing. A spectrophotometer (HACH DR6000 UV Spectrophotometer with RFID Technology, accuracy of less than 1%) was used to test concentrations of nitrate, total nitrogen, and total phosphorus. Testing proceeded as described in Hach, [2015, 2017].

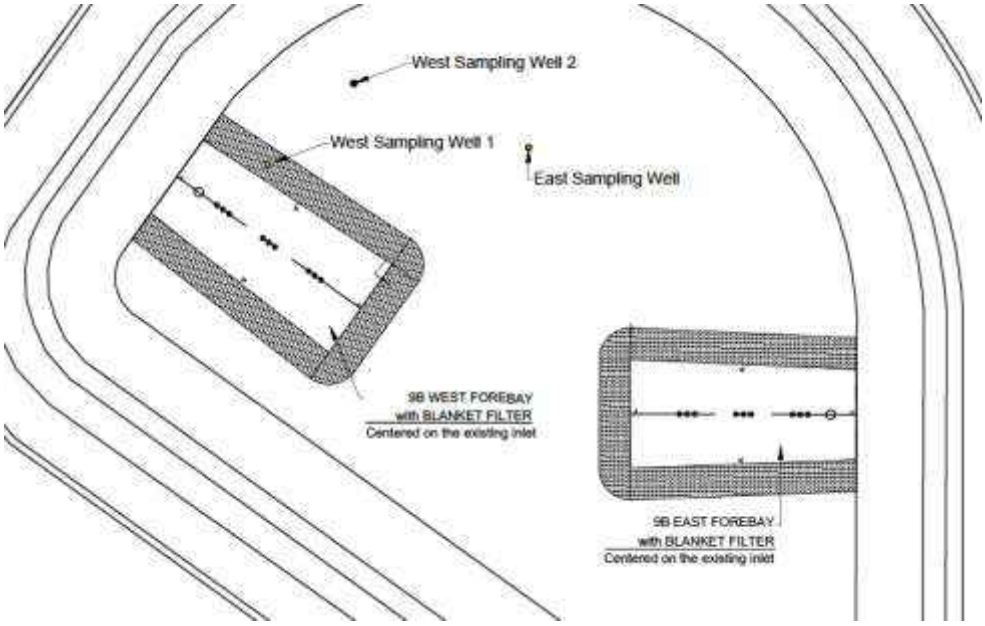

Figure 23: Groundwater sampling well locations

The first groundwater samples were collected in November of 2016, approximately 6 months before construction. Subsequently, groundwater samples were collected in December, January, March, and April before construction started in May of 2017. Groundwater samples were halted from May through July during construction and installation of new observation wells. Well sampling resumed in August of 2017 and monthly sampling proceeded until May of 2018.

4.3 Results

4.3.1 Groundwater Depth

The mean groundwater depth in Basin 9B during the dry season (January – April 2017) was 5.6±0.35 ft (1.7±0.11 m) below the ground surface (Fig 24). Before Hurricane Irma, the mean wet season (July – early September) groundwater depth is 4.9±0.62 ft (1.5±0.19 m). Between

September 10th and September 12th, Hurricane Irma caused a sharp increase in groundwater level. Between these dates, there was a cumulative precipitation of 2.3 in (5.8 cm) which caused an average of 0.1±2.09 ft (0.03±0.64 m) of water above the ground surface with a maximum water level of 2.2 ft (0.7 m) of water above the ground surface on September 11th. After Hurricane Irma, the mean wet season (mid – September to October) groundwater depth is 1.4±0.36 ft (0.4±0.11 m). The mean groundwater depth in the 2017 dry season is 0.7 ft (0.2 m) lower than the mean groundwater depth in the 2017 wet season. After Hurricane Irma, groundwater depth started to decline. From November 2017 to April 2018 (dry season), the mean groundwater depth is 3±0.51 ft (0.9±0.16 m) below the ground surface which is 2.6 ft (0.8 m) higher than the 2017 mean dry season depth.

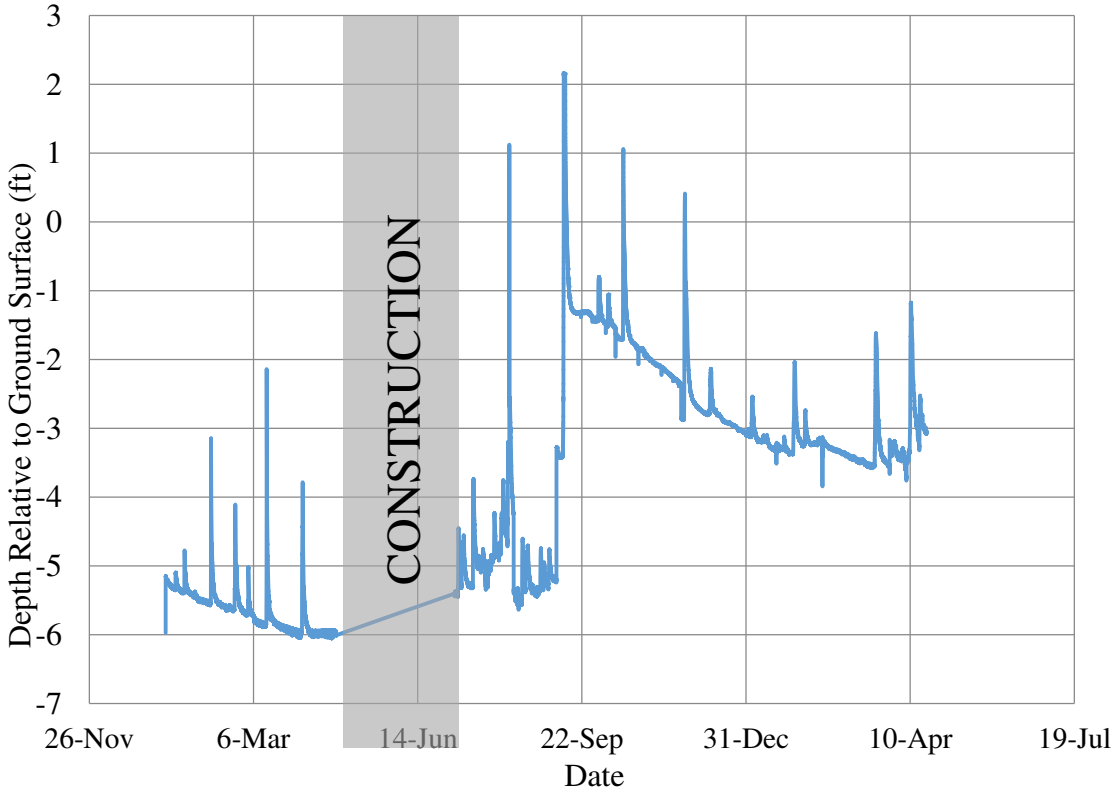

Figure 24: Depth to Surficial Aquifer

Groundwater levels indicate that following construction, the west BAM filter, located 3 to 6 ft (0.9 to 1.8 m) below grade, and the east BAM filter, located 1 to 4 ft (0.3 to 1.2 m) below grade, was at least partially saturated 77% of days.

A quality assurance/quality control (QA/QC) procedure was done for the soil moisture sensors. The sets of soil moisture sensors below grade at distances 12.5 and 25 ft (3.8 and 7.6 m) downstream of the inlet pipe experience equipment failure thus the soil moisture sensors 37.5 ft (11.4 m) downstream were analyzed. The field capacity and the saturation of the soil moisture sensors in the east basin are approximately 0.20 and 0.46 m^3/m^3, respectively Data points were removed in the east basin due to data logger failure (August 22nd to September 20th, 2017) and an exceedance in the maximum porosity/saturation (February 7th to February 15th, 2018) (Fig 25).

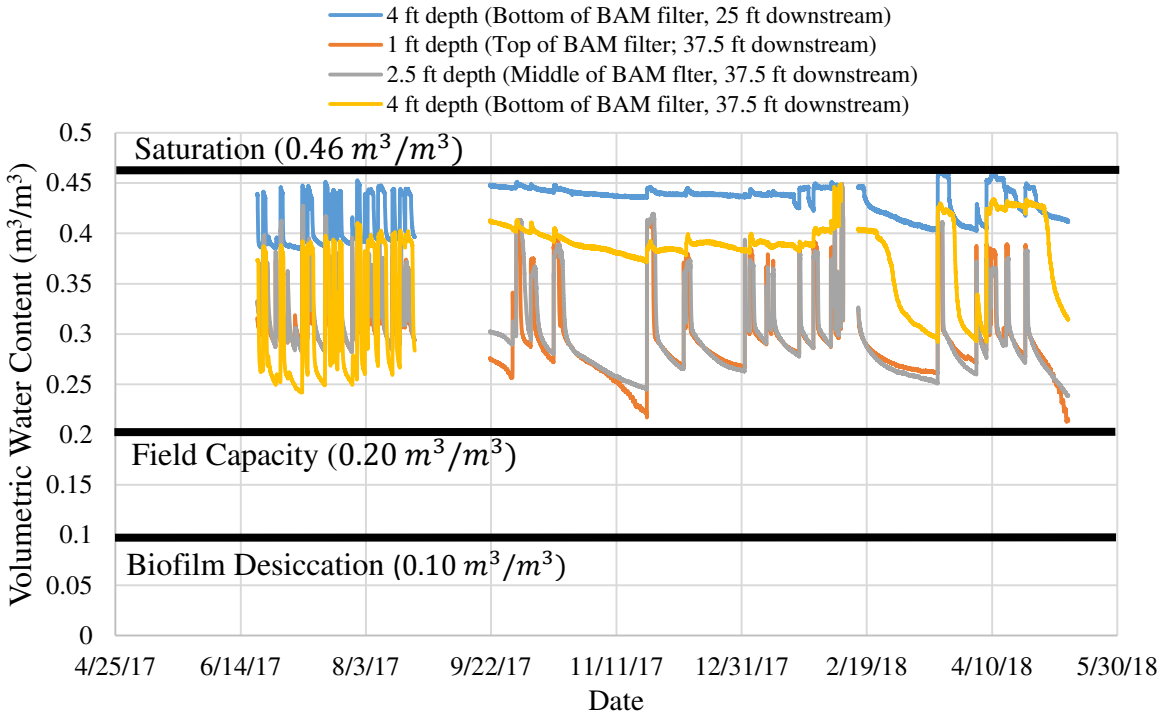

Figure 25: Basin 9B East Soil VWC

Prior to August 22nd, there are several increases and decreases in the VWC on the soil due to the occurrence of many storm events. If the peaks in are counted (Fig 25), then approximately 16 storm events occurred over a period of 62 days. The fact that the storm events occurred so close together made it difficult to determine the long-term hydraulic retention time of the BAM layer. However, we observe that across these many events, BAM drained quickly from near-saturation to well below saturation. After September 20th, approximately 17 storm events occurred in a period of 231 days. A decrease in storm events is seen because Florida was entering the dry season (November to April).

Soil moisture sensors deployed in the west blanket filter experience more failures than in the east blanket filter. The field capacity and the saturation of the soil moisture sensors in the east basin are approximately 0.20 and 0.45 m^3/m3, respectively. Data points were removed in the west blanket filter due to data logger failure (August 22nd to September 20th, 2017) and an exceedance in the maximum porosity/saturation (February 7th to February 15th, 2018) (Fig 26). It is much harder to determine when a storm event occurs in the west blanket filters because the increase and decrease in the volumetric water content are not clearly shown as in the east blanket filter. The volumetric water content seems to fluctuate around the same value of 0.35 m^3/m^3.

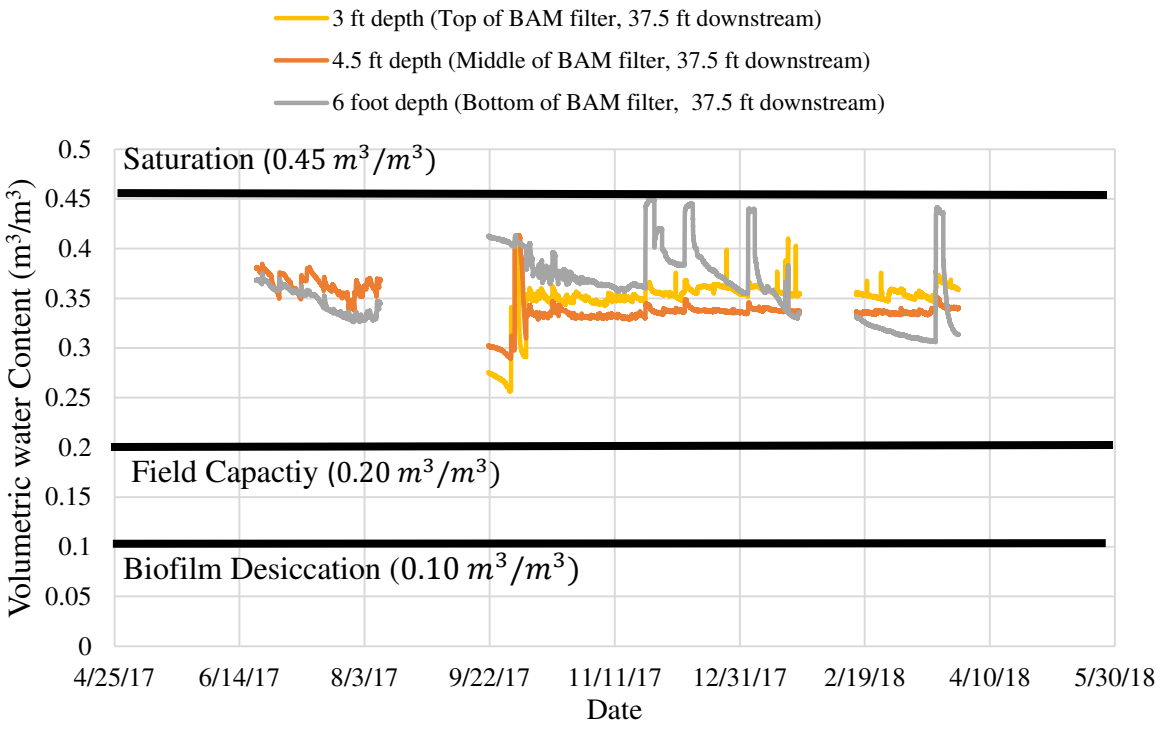

Figure 26: Basin 9B West Soil VWC

Approximately 4 clear peaks can be seen in the Fig 21 that correlate with storm events. The VWC in the west basin were scattered with readings well above the maximum porosity so therefore the east basin was carried through for further investigation.

On October 17th, 2017, there was an estimated volume of precipitation of 0.9 in (2.3 cm). This amount of rainfall caused nearly 1 ft (0.3 m) of water to be seen on the surface in Basin 9B east (Fig 28). Following this event, no precipitation was observed until November 23, 2017, and the soil layers were able to drain for 35 days, the longest drainage period available during the period of hydrologic monitoring. During the Oct 17th storm event, the soil moisture sensors were near saturation or the maximum porosity of the BAM. Soil moisture sensors 1, 2.5, and 4 ft (0.3, 0.8,

and 1.2 m) deep in the east blanket filter have volumetric water contents close to the known porosity of BAM (Fig 27). The water then flowed through the system and the upper layers of BAM became unsaturated in the days following the storm event. During the 35-day draining period the shallow soil moisture sensors, 1 – 2.5 ft (0.3 – 0.8 m) deep, in the east basin return back to field capacity (Fig 27). The deeper sensor remained near saturation, for 35-days, until the next storm event. If we look at the groundwater depth we can see that it is above at depth of 4 ft (1.2 m) from October 17th until November 23rd meaning that water was occupying all of the pore spaces in the deeper level of the BAM. The contour plot (Fig 28) shows a dark pink color, indicative of a VWC near 0.4 m^3/m^3, a depth of 4 ft (1.2 m) while the shallower depths change from dark blue, 0.37 m^3/m^3, to light blue, 0.25 m^3/m^3, during the 35-day period. The water successfully percolates to a depth of at least 2.5 ft (0.8 m) for this storm event and subsequent storm events (Fig 28).

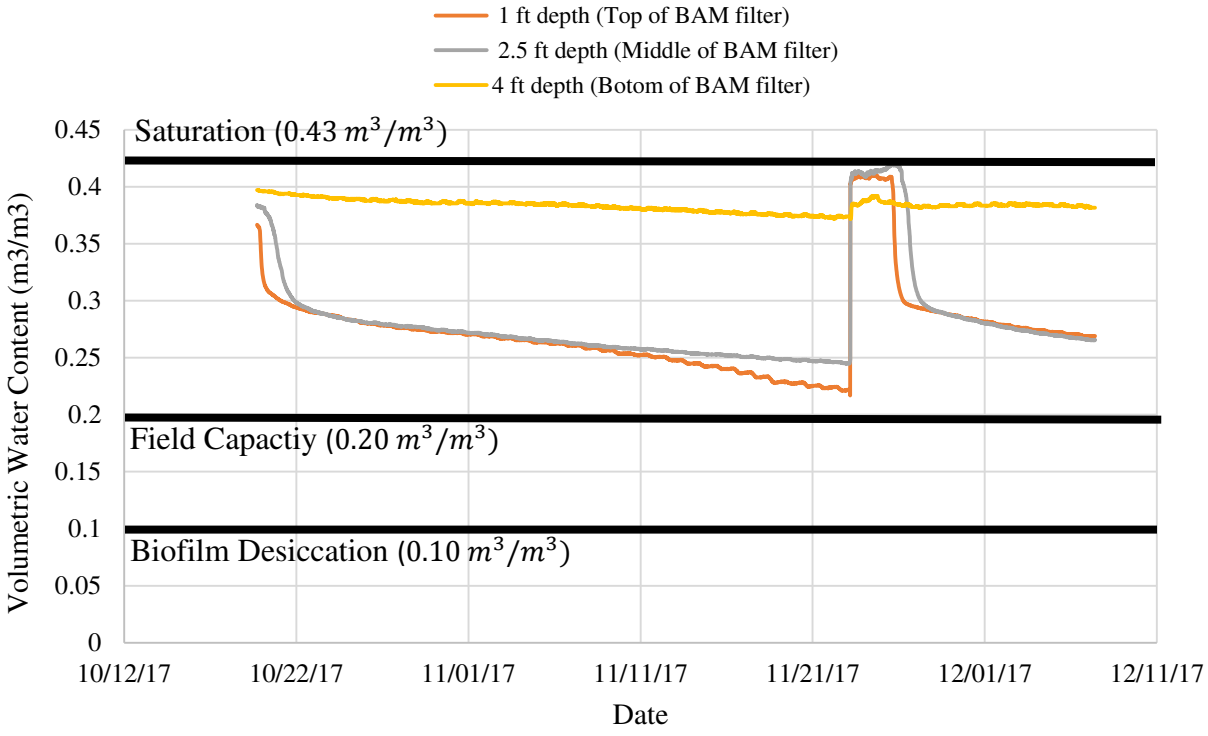

Figure 27: Basin 9B East Water Content (single storm event)

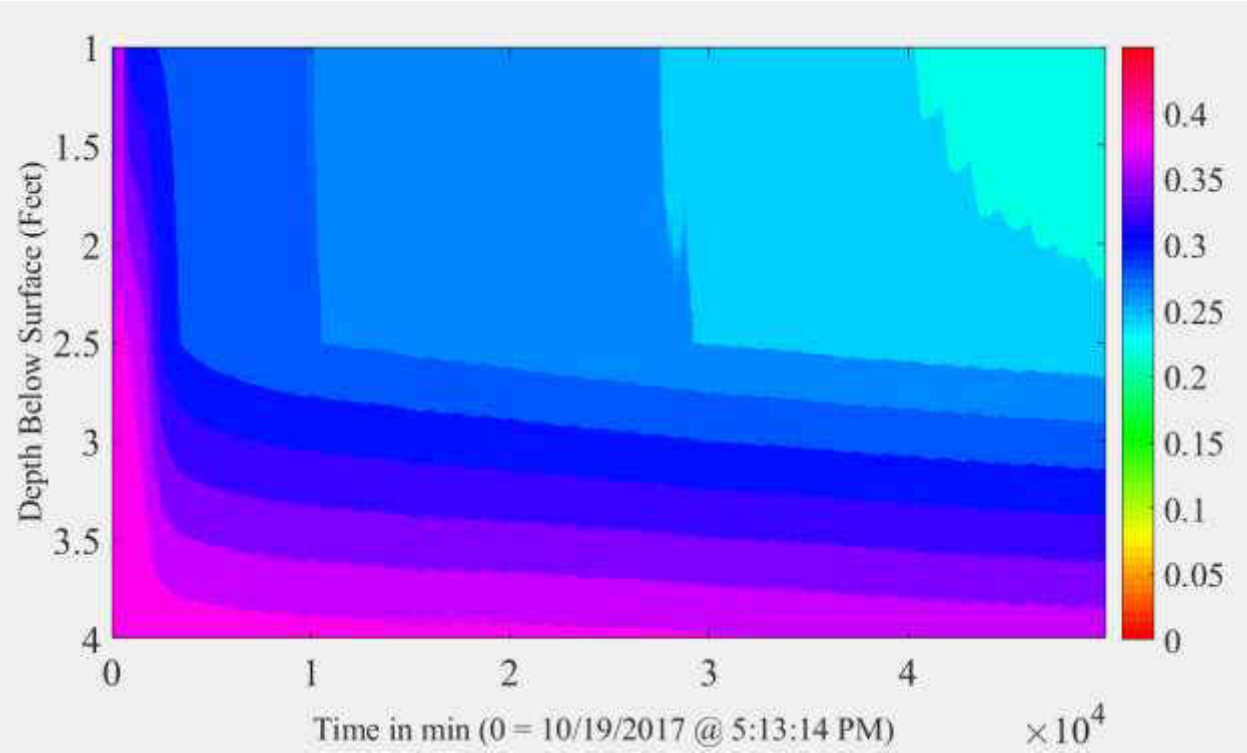

Figure 28: Basin 9B East Contour Plot of Single Storm Event

4.3.2 Nutrient Concentrations of Shallow Groundwater

4.3.2.1 Total Nitrogen and Nitrate

The value of total nitrogen (TN), in the west and east sampling wells, ranged from as low as 0.20 to as high as 9.00 mg/L (Table 3). Due to the variable range of TN, these concentrations will be discarded during analysis because they were labeled as inaccurate. However, they will still be shown in the table to show that samples were still collected on these days.

Table 3: Total Nitrogen and Nitrate Concentrations

Time Period	Date	TN/Nitrate concentration (mg/L)	
		Treatment	Control
Pre-Construction (Before)	11/8/16	0.20 (TN)	0.90 (TN)
	12/14/16	9.00 (TN)	2.30 (TN)
	1/11/17	2.33 (TN)	1.27 (TN)
	3/6/17	2.15	0.42
	4/25/17	0.18	0.27
Post-Construction (After)	8/14/17	1.10	0.15
	10/12/17	0.28	0.16
	11/16/17	0.08	0.22
	1/18/18	0.08	0.13
	2/15/18	0.56	0.14
	3/28/18	0.94	0.09
	5/11/18	0.49	0.20

The mean 'before' nitrate concentrations in west sampling well 1 and the east sampling well are 1.17±1.39 and 0.35±0.11 mg/L, respectively. The mean 'after' nitrate concentrations in west sampling well 2 and the east sampling well are 0.46±0.42 and 0.16±0.04 mg/L, respectively.

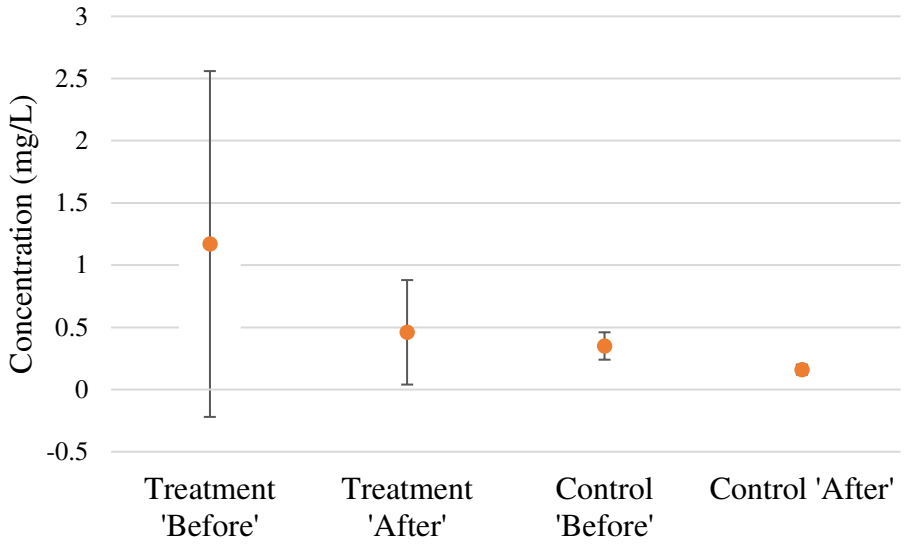

Figure 29: Nitrate Concentration (Mean ± Standard Deviation)

There is a mean decrease of 0.71 mg/L and 0.19 mg/L in the nitrate concentration in the west and east sampling well, respectively. There is a large variability in the nitrate concentrations in the 'treatment before' condition. The mean plus one standard deviation in the 'treatment after' condition is approximately the same concentration as the mean of the 'treatment before.' The control/east sampling well does not seem to fluctuate as much as the west sampling wells but a decrease in the mean nitrate concentration can still be seen (Fig 29). Unlike the nitrate concentration, the total phosphorus (TP) concentrations are assumed to be accurate throughout the whole duration so boxplots were able to be used to show a comparison between the 'before' and 'after.'

4.3.2.2 Total Phosphorus

Table 4: Total Phosphorus Concentrations

Time Period	Date	TP concentration (mg/L)	
		Treatment	Control
Pre-Construction (Before)	11/8/16	0.34	0.25
	12/14/16	2.03	1.84
	1/11/17	0.64	0.29
	3/6/17	1.17	0.31
	4/25/17	0.79	0.37
Post-Construction (After)	8/14/17	0.59	1.30
	10/12/17	0.48	1.09
	11/16/17	0.29	3.10
	1/18/18	3.97	2.12
	2/15/18	0.29	1.12
	3/28/18	0.43	0.51

The values of TP range from 0.34 to 2.03 mg/L during the 'before' period and from 0.29 to 3.97 mg/L during the 'after' period (Table 4). The boxplot (Fig 30) is showing the full distribution of the date with the red and blue dots showing the mean and outliers of each data set, respectively.

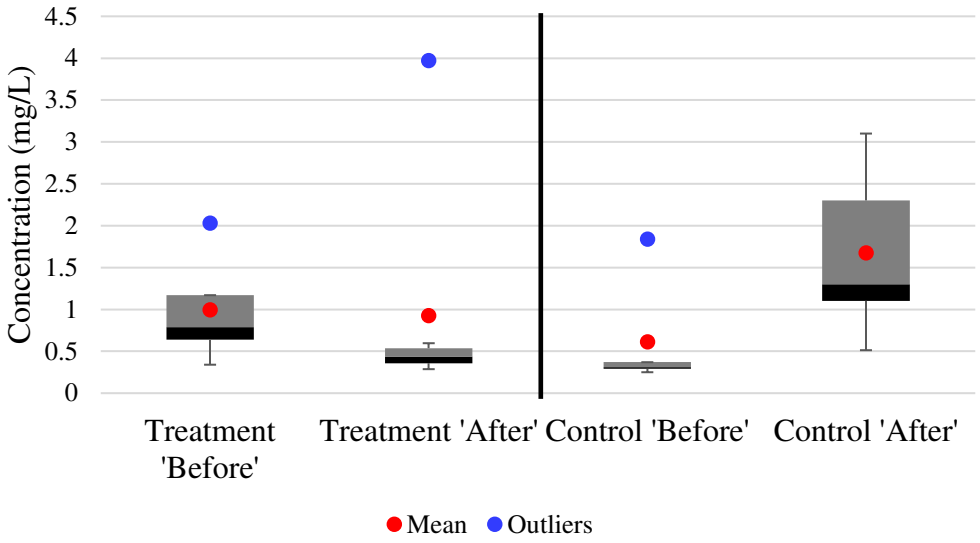

Figure 30: Total Phosphorus Boxplots

The average 'before' TP concentration in west sampling well 1 and the east sampling well is 0.99±0.65 mg/L and 0.61±0.69 mg/L, respectively. The average 'after' phosphorus concentration in west sampling well 2 and the east sampling well is 0.93±1.35 mg/L and 1.67±0.92 mg/L, respectively.

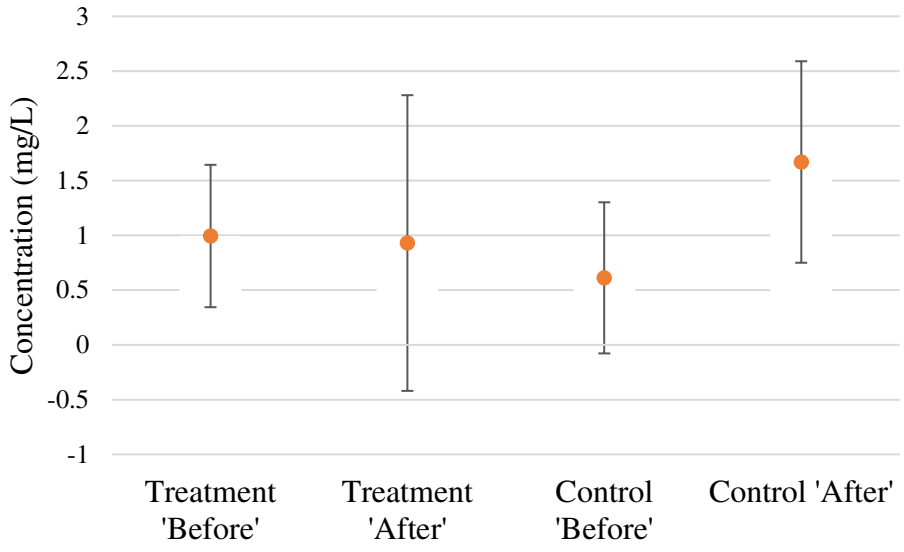

Figure 31: Total Phosphorus Concentration (Mean ± Standard Deviation)

The near-stagnant TP concentration between west sampling wells 1 and 2 and the increase in TP concentration in the east sampling well is clearly depicted (Fig 31). There is a mean decrease of 0.07 mg/L and an increase of 1.05 mg/L in the total phosphorus concentration in west sampling well 1 and 2 and the east sampling well, respectively. The TP concentration in the east sampling well more than doubles. There is a much larger variability in the 'after' conditions of both wells. However, there is some overlap in distributions of 'before' and 'after' TP concentrations in the Treatment well (Fig 32), suggesting that this level of change may or may not be significant.

4.4 Discussion

4.4.1 Hydraulic Performance of BAM in Blanket Filters

The mean groundwater depth in the dry season is higher in 2018 than in 2017. This is due to the fact 2017 was historically a dry year (NOAA, 2018) also including that Hurricane Irma brought

down heavy precipitation right before the start of the dry season in 2018. The groundwater reached a maximum water level height of 2.2 ft (0.7 m) of water seen on the ground surface. The groundwater depth has been slowly declining since Hurricane Irma but still has not reached a depth of 5.6 ft (1.7 m) that is what before the implementation of the blanket filters.

Once a storm event occurs the BAM layer reaches a saturation level close to the maximum porosity that was assumed (greater than lab tests due to field compaction). When the incoming storm water flows through the BAM layer and is allowed to return to field capacity the values seen (Figs 25 – 27) are more comparable to the field study in Silver Springs by O'Reilly et al. (2012) (field capacity = 24%) and approximately 20% lower to the test beds values reported by Hood (2012) (field capacity = 40%). Higher field capacities are indicative of an increase in the biological activity in the media layers (Hood, 2012). Clear depictions of how the water content changes throughout a single storm event days are shown in a contour plot (Fig 28). There is an increasing volumetric water content from light blue to blue to pink. The contour plot never shows the yellow color, indicative of biofilm desiccation. Shortly after the storm event on October 17th, 2017, all the soil moisture sensors appear to be saturated, as evident by the pink color. As time progresses a transition in shown, in the soil moisture sensors at shallow depths, from dark pink to light blue. The soil moisture sensor 4 feet (1.2 m) deep remained near saturated during this 35-day period (October 17th – November 23rd, 2017). The hydraulic retention is difficult to calculate for events because of the facts the storm event occurs so frequently. However, the soil moisture sensors in the east blanket filter show the BAM at shallow depths being able to return to its field capacity while the BAM at deeper depths remains saturated. There is a rather steep peak in the VWC during a storm event followed by a steep and then gradual decline in the VWC after a storm event. This

could be due to a quick infiltration rate at shallow depths (natural soil layer) in the east blanket filter. After the storm event occurs on November 23rd, 2017, fifteen days pass before the next storm event occurs so the BAM layer does not become completely dry. The volumetric water content is greater than 0.20 m^3/m^3 before the next storm event (Fig 27). The volumetric water content does remain above 0.10 m^3/m^3 through the whole monitoring period which shows that biofilm desiccation is not likely to occur. Field implementation of BAM suggests that the BAM stays wet enough for biofilm growth.

4.4.2 Nutrient Concentrations of Shallow Groundwater

Soil moisture monitoring confirms that incoming stormwater percolates vertically through the BAM blanket filters (Figs 25 – 26) and into the surficial aquifer. Tracer testing within the surficial aquifer beneath Basin 9B (detailed in Ch. 2) confirms that the local groundwater flow direction is to the east-northeast, towards Silver Springs, which is similar to the regional groundwater flow direction (Shoemaker et al., 2004). The groundwater depth that has been monitored is assumed to be uniform across Basin 9B, thus it has been interacting with the BAM filter in both basins since Hurricane Irma (September 10 – 12th, 2017). Therefore, incoming shallow groundwater is often flowing through the west BAM filter.

Groundwater samples taken just east of the west filter (west sampling well 2) should represent shallow groundwater that has just flowed through the filter. The east sampling well has remained in the same position from pre to post-construction of the blanket filters. However, it is not a perfect control because we cannot guarantee that the water being pumped and analyzed from this well has had no influence by the blanket filters, it is only assumed. Although we do not have comparable

time periods were have reason to believe that nitrate concentrations change with seasonality and hydrologic extremes. Higher nitrate concentrations are observed at deeper groundwater table depths while lower nitrogen concentrations are observed at shallow depths in the west sampling well. The mean nitrate concentration has decreased in the west sampling but there is a large range of variance. There is much scatter around the means for nitrate and total phosphorus. There are only three months on 'before' nitrate data which make it to say for certain in there is a correlation between the groundwater depth and the nitrate concentration. Continued monitoring would need to be done to determine if in fact the nitrate concentration is truly decreasing, and a smaller standard deviation would help in this.

In regard to TP there has been continuous monitoring for five months pre-construction and seven months post-construction. There is an increase in the TP concentration in the control well (east sampling well) from 'before' to 'after' (Fig 32), suggesting that factors external to the BAM filter treatment may have elevated TP concentrations in incoming groundwater. There exists an outlier in the 'before' at 1.84 mg/L which is similar to the quartile 3 (75% of the data) of 2.30 mg/L. The interquartile range (middle 50% of data) is 1.11 mg/L higher in the 'after' than in the 'before.' The introduction of iron fillings would assist in the decrease of TP concentration. Values are much more comparable in the treatment well (west sampling wells). The interquartile range is 0.36 mg/L higher in the 'before' than in the 'after.' However, the TP concentration in the west sampling wells essentially does not change from 'before' to 'after' when considering the means due to the large spread in concentrations that are seen. Both the 'before' to 'after' have outliers shown at 2.03 and 3.97 mg/l, respectively.

4.5 Conclusion

In our study, the objective is to evaluate the hydraulic performance of the blanket filters, through the use of hydraulic equipment and the effectiveness of the blanket filters at removing nutrients from shallow groundwater in Basin 9B. Soil moisture sensors were a major component in using the volumetric water content to determine the hydraulic retention time of a single storm event. The VWC in the east basin shows step increases and decreases in the time during and directly after storm events which is suggestive of quick infiltration rates near the surface or in the 1 ft (0.3 m) of natural soil above the 3 ft (0.9 m) of BAM. The hydraulic retention for the storm event on October 19th, 2017 is approximately 35 days. Retention times for other events were hard to compute because of the large frequency of storm events. This back to back occurrence of many storm events is shown rather than hydraulic retention times. However, retention times can vary based on the depth of BAM and the incoming flow rate of the water. Previous studies revealed nitrogen removal percentages in many ranges: 26 – 46% (Wanielista et al., 2014), 47 – 74% (Birch et al., 2005), and 97.2% (Schipper et al., 2005). Overall, no clear conclusion can be shown if the BAM is working effectively in removing nitrogen from shallow groundwater or not due to the large spread in the data however, there is evidence that biofilm desiccation does not occur (VWC always greater than 0.10 m^3/m^3). Field implementation of BAM suggests that there will always be bacteria present to remove incoming nutrients.

CHAPTER 5: CONCLUSION

The overall objective of this thesis is to analyze the hydrologic performance of innovative stormwater BMPs and investigate the connections between the BMPs and groundwater flows to freshwater springs within a karst environment. In recent years, concentrations of nutrients have increased in surface and groundwater resources, due in part to nonpoint source pollution from urban development associated with stormwater runoff. The elevated nutrient concentrations found in stormwater runoff has prompted the design of BMPs to mitigate the problem. The hydrologic performance of two novel stormwater BMPs containing Bio-sorption Activated Media (BAM) was assessed in terms of capture efficiency, hydraulic retention time, and effectiveness in removing nutrients from shallow groundwater. Blanket filters were built in Basin 9B while vertical reactors were built in Basin 2. The blanket filters in Basin 9B West and East were designed to capture and treat the majority of the incoming stormwater runoff while the vertical reactors in Basin 2 were designed to treat smaller volumes of incoming stormwater. The total cumulative capture efficiency was minimal mainly because the vertical reactors because the system capacity was not well aligned with the watershed area of Basin 2. The total cumulative capture efficiency of the West filter over the sample period ranges from 92 to 95% while the total cumulative capture efficiency of the East filter is 100%. Blanket filters in Basin 9B are effectively treating a large portion of the incoming stormwater runoff.

The hydraulic performance of the blanket filters was evaluated through the use of hydraulic equipment and by analyzing the effectiveness of the blanket filters at removing nutrients from shallow groundwater. Soil moisture sensors were a major component in using the volumetric water

content to determine the hydraulic retention time of a single storm event. The volumetric water content in the east basin shows steep increases and decreases in the time during and directly after storm events which are suggestive of quick infiltration rates near the surface or in the 1 ft (0.3 m) of natural soil above the 3 ft (0.9 m) of BAM. The hydraulic retention for the storm event on October 19th, 2017, is approximately 35 days. Retention times for other events were hard to calculate because of the large frequency of storm events. Frequent occurrence of storm events in the data depicts times in between storm events rather than hydraulic retention times. In terms of nutrient removal, no clear conclusion can be drawn on if the BAM is working effectively due to the large spread in the data. Continued hydrologic monitoring will continue throughout the duration of the project. The data and analysis presented here was based on the information gathered to date (June 2017 – May 2018).

Flow paths and travel times of shallow groundwater in a karst environment were investigated through the use of a tracer study in Basin 9B. A range of different velocities is seen with the fastest velocity traveling in the northeastern direction, and the slowest velocity traveling in the southeastern direction from the injection well. The dye that travels to Silver Springs ultimately has the fastest velocity. There are four potential peaks in the breakthrough curve showing macropore flow (conduit) and matrix flow. Subsurface velocities observed in the basin ranged from 0.1 m/d to 1.4 m/d, while velocities from the injection well to the spring vary from 2.3 m/d to 13.5 m/d. Velocities in karst environments are known to vary greatly. Faster velocities are indicative of flow through large macropores or conduits, while slower velocities are indicative of flow through small karst fractures or cracks.

5.1 Significance and future research

Agriculture, wastewater, fossil fuels, and stormwater runoff from highways and roads are some sources of pollution to surface water bodies and groundwater. Surface water bodies are connected to groundwater sources through topography and landscapes. Due to this, surface water bodies play a significant role in groundwater systems. Additional nitrogen and phosphorus, in surface water bodies, have been shown to cause eutrophication (excessive algae growth). This algae growth prevents sunlight from penetrating down into the depths of the water, which causes plant and wildlife decay by decreasing oxygen levels and releasing harmful toxins into the water. Investigators can use the information from the tracer study to relate dye velocities to nutrient velocities traveling to the main vents of Silver Springs. This shows the speed that nutrients are traveling to the springs causing eutrophication. Future work can be done using these velocities for model calibration to understand the groundwater flow direction and speed. Understanding the variable pathways and velocities stormwater may take from the surface to spring discharge as well as how karst features decrease retention times that impact nutrient transformations may assist environmental managers in preserving water quality in springs and other water bodies in karst systems.

This elevated nutrient concentration has prompted the design of many BMPs to mitigate the problem. Stormwater ponds or stormwater management basins, are the most common type of BMP in Florida. These stormwater management basins are designed to hold stormwater for the purpose of source reduction and water quality treatment. The capture efficiencies in the blanket filters in Basin 9B West and East show that BMPs can be designed with the ability to capture all of the

incoming stormwater. Investigators can use the capture efficiency results to decide where to implement these novel treatment systems. If the amount of incoming runoff volume is known, then these treatment systems can be scaled up or down, accordingly, to capture all the volume and effectively treat the stormwater percolating into the groundwater. For example, the vertical reactors would be best suited if placed off a road shoulder or small retention ponds where there would be a small incoming volume of water flowing into the central holding box.

APPENDIX I: FLUOROMETER CALIBRATION CURVE

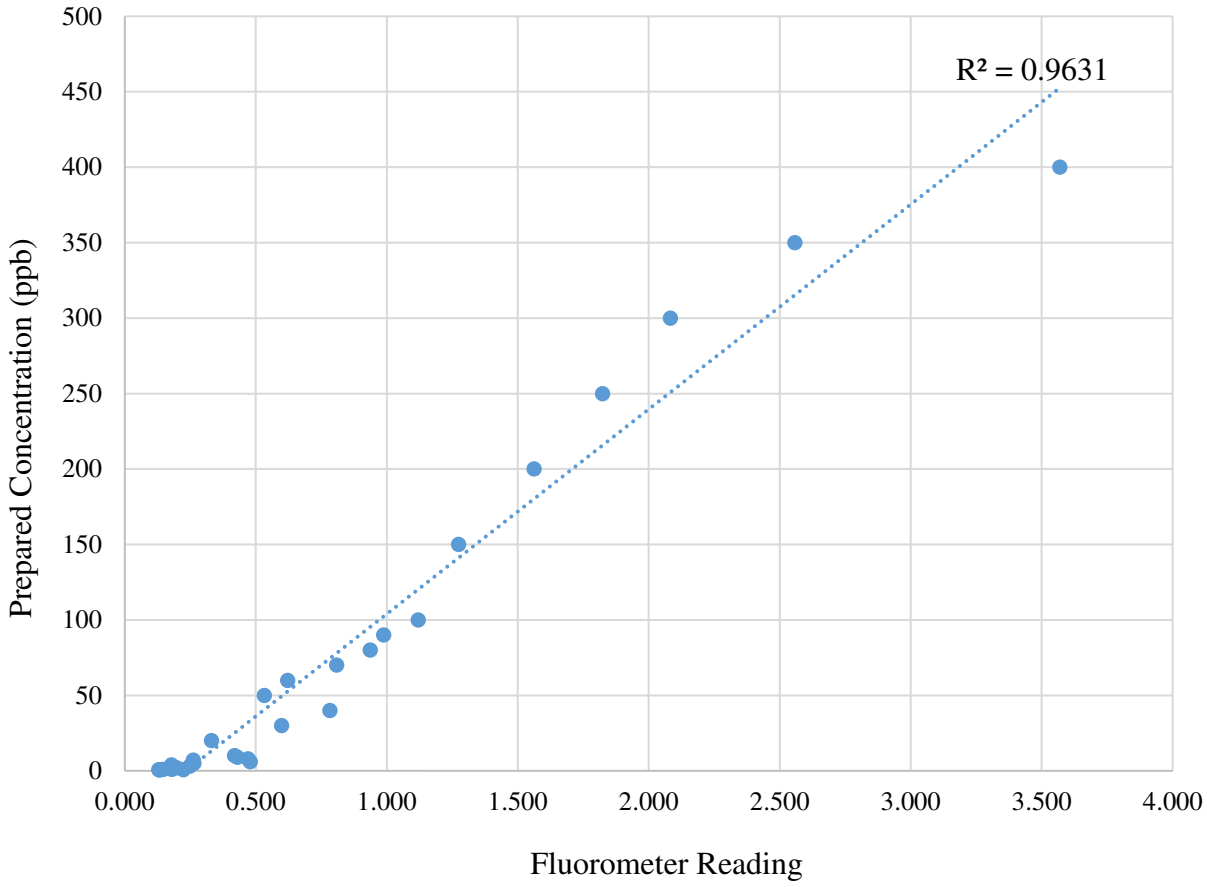

Figure A1. 1: Turner Designs Aquafluor® Handheld Fluorometer and Turbidimeter Calibration Curve

APPENDIX II: CAPTURE EFFICIENCY

Table 5: Precipitation events producing a measurable volume change in BMPs

Date	Cumulative Precipitation (in)
6/22/17	0.6
6/29/17	0.1
7/8/17	0.3+
7/10/17	0.5+
7/11/17	0.6+
7/17/17	0.9+
7/30/17	0.5+
8/3/17	0.3+
8/4/17	0.3+
8/7/17	0.9+
8/8/17	1.7+
8/16/17	0.5+
8/18/17	0.4+
8/19/17	0.1+
8/27/17	0.6+
8/29/17	0.4+
9/1/17	0.5+
9/11/17	2.3+
9/30/17	0.2+
10/7/17	0.6+
10/17/17	0.9+
10/19/17	0.1+
11/23/17	2.5+
12/9/17	0.5+
1/3/18	0.6+
1/23/18	0.2+
1/28/18	0.5+
1/29/18	1.2+
2/4/18	0.2+
3/19/18	1.6+
4/9/18	1.6+
4/10/18	0.9+
4/15/18	0.7+
4/26/18	0.4+

+ indicates calibrated radar data;

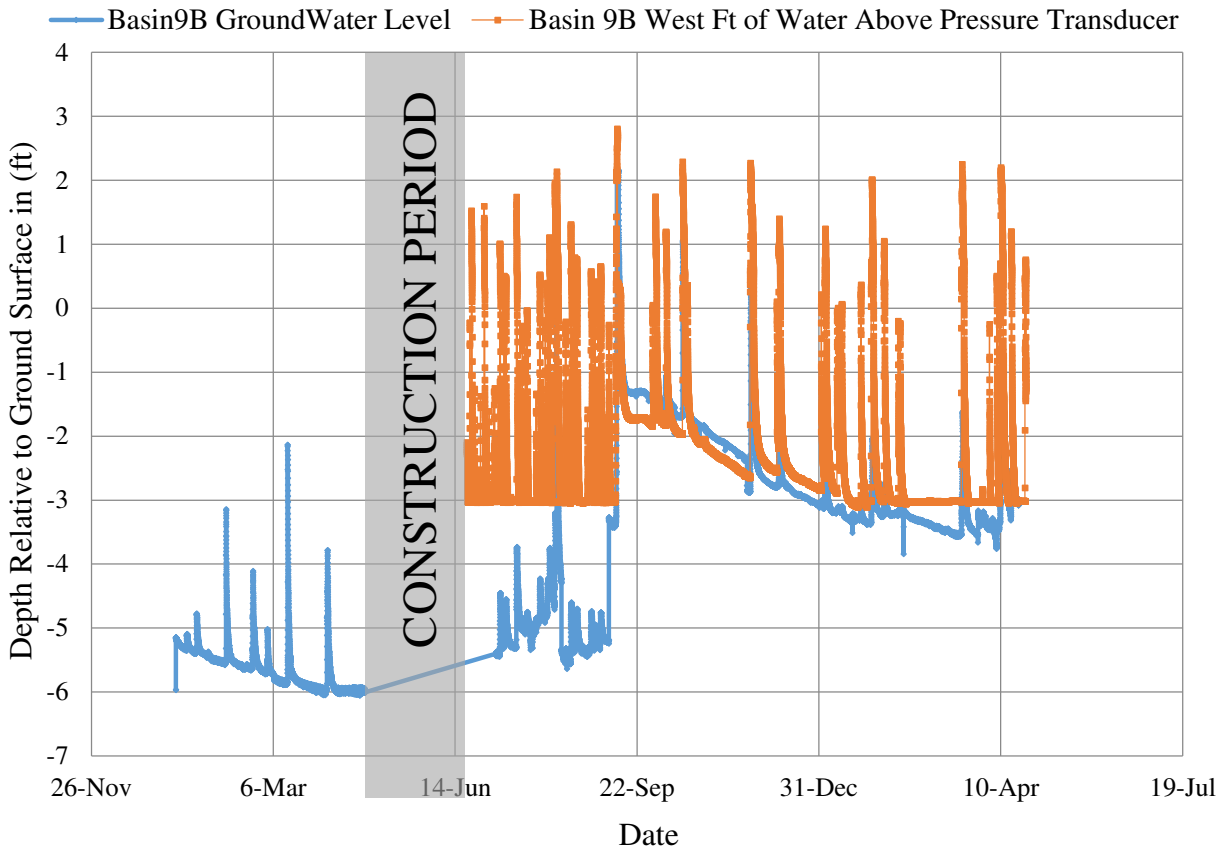

Figure A2. 1: Basin 9B West Pressure Transducer vs. Groundwater Depth

Table 6: Event inflow volumes - Basin 9B West blanket filter

Date	Cumulative Precipitation (in)	ΔH_1 (ft)	ΔH_2 (ft)	ΔH_3 (ft)	Q_{system} (ft^3)
6/22/17	0.6	1.5	3.0	-	3.1×10^3
6/29/17	0.1	1.6	3.0	-	3.4×10^3
7/8/17	0.3^+	1.0	3.0	2.0	3.3×10^3
7/10/17	0.5^+	0.5	3.0	2.2	2.8×10^3
7/11/17	0.6^+	0.5	3.0	1.8	2.7×10^3
7/17/17	0.9^+	1.7	3.0	1.8	4.2×10^3
7/30/17	0.5^+	0.5	3.0	1.6	2.6×10^3
8/3/17	0.3^+	0.4	3.0	1.6	2.5×10^3
8/4/17	0.3^+	1.1	2.7	1.3	3.0×10^3
8/7/17	0.9^+	2.0	3.0	1.5	4.3×10^3
8/8/17	1.7^+	2.1	1.8	0.1	3.2×10^3
8/16/17	0.5^+	1.3	3.0	2.2	3.9×10^3
8/18/17	0.4^+	0.8	3.0	2.2	3.2×10^3
8/19/17	0.1^+	0.8	2.2	1.9	2.7×10^3
8/27/17	0.6^+	0.6	3.0	2.1	2.9×10^3
8/29/17	0.4^+	0.4	3.0	2.2	2.7×10^3
9/1/17	0.5^+	0.7	3.0	2.2	3.0×10^3
9/11/17	2.3^+	2.8	3.0	0.0	4.6×10^3
9/30/17	0.2^+	0.1	1.8	0.0	0.8×10^3
10/7/17	0.6^+	1.2	1.8	0.0	2.2×10^3
10/17/17	0.9^+	2.3	2.0	0.0	3.6×10^3
10/19/17	0.1^+	0.4	1.5	0.0	1.0×10^3
11/23/17	2.5^+	2.2	3.0	0.0	3.8×10^3
12/9/17	0.5^+	1.4	3.0	0.0	2.9×10^3
1/3/18	0.6^+	1.2	3.0	0.0	2.7×10^3
1/23/18	0.2^+	0.4	3.0	0.2	1.8×10^3
1/28/18	0.5^+	0.7	3.0	0.3	2.2×10^3
1/29/18	1.2^+	2.0	3.0	0.0	3.6×10^3
2/4/18	0.2^+	1.1	3.0	0.3	2.6×10^3
3/19/18	1.6^+	2.3	3.0	0.1	4.0×10^3
4/9/18	1.6^+	0.7	3.0	0.3	2.2×10^3
4/10/18	0.9^+	2.2	3.0	0.0	3.9×10^3
4/15/18	0.7^+	1.2	3.0	0.1	2.7×10^3
4/26/18	0.4^+	0.8	3.0	-	2.1×10^3

$^+$ indicates calibrated radar data

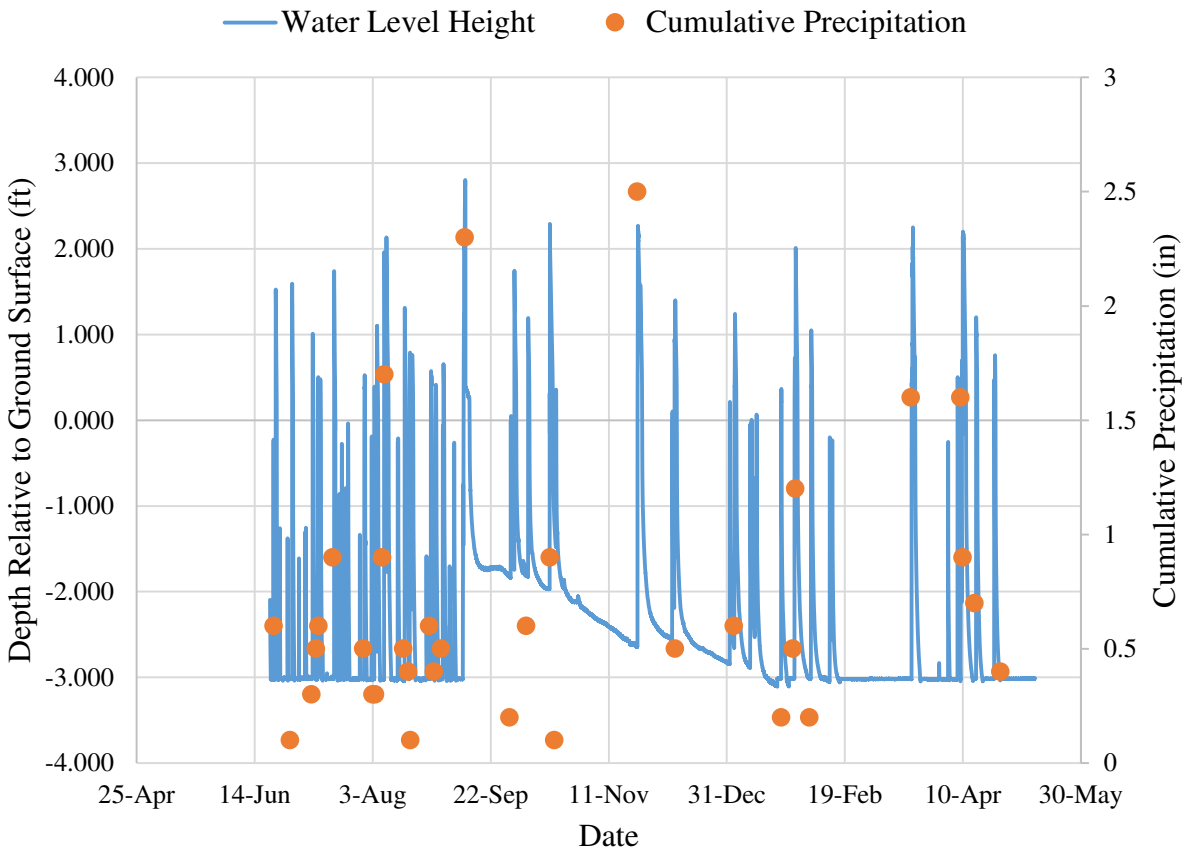

Figure A2. 2: Basin 9B West Water Level Height vs. Cumulative Precipitation

Table 7: Event inflow volumes - Basin 9B East blanket filter

Date	Cumulative Precipitation (in)	ΔH_1 (ft)	ΔH_2 (ft)	ΔH_3 (ft)	Q_{system} (ft^3)
6/22/17	0.6	0.6	1.0	3.0	2.7×10^3
6/29/17	0.1	0.7	1.0	3.0	2.9×10^3
7/8/17	0.3+	0.5	1.0	3.0	2.7×10^3
7/17/17	0.9+	0.5	1.0	3.0	2.7×10^3
8/4/17	0.3+	0.5	1.0	3.1	2.7×10^3
8/7/17	0.9+	0.8	1.0	3.0	3.0×10^3
8/8/17	1.7+	0.8	1.0	3.1	3.1×10^3
8/16/17	0.5+	0.5	1.0	3.0	2.7×10^3
8/19/17	0.1+	0.2	1.0	3.3	2.4×10^3
9/11/17	2.3+	1.2	1.0	3.0	3.4×10^3
10/7/17	0.6+	0.3	1.0	2.5	2.1×10^3
10/17/17	0.9+	0.9	1.0	2.7	3.0×10^3
11/23/17	2.5+	0.9	1.0	3.0	3.0×10^3
12/9/17	0.5+	0.4	1.0	3.0	2.5×10^3
1/3/18	0.6+	0.3	1.0	3.0	2.4×10^3
1/29/18	1.2+	0.7	1.0	3.0	2.9×10^3
2/4/18	0.2+	0.2	1.0	3.0	2.3×10^3
3/19/18	1.6+	0.8	1.0	3.0	3.0×10^3
4/9/18	1.6+	0.7	1.0	3.0	3.0×10^3
4/10/18	0.9+	0.7	1.0	3.0	2.9×10^3
4/15/18	0.7+	0.6	1.0	3.0	2.8×10^3

+ indicates calibrated radar data

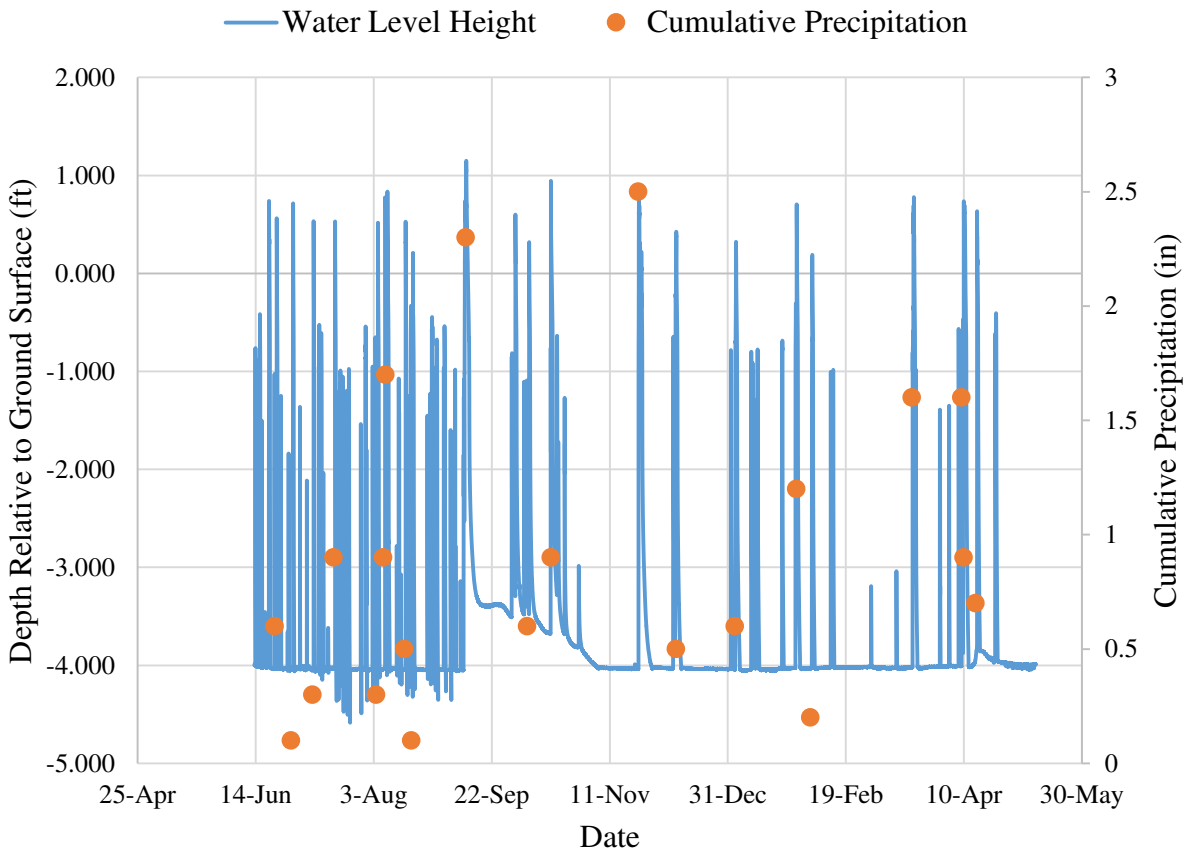

Figure A2. 3: Basin 9B East Water Level Height vs. Cumulative Precipitation

Table 8: Event inflow volumes – Basin 2 Vertical Reactor

Date	Cumulative Precipitation (in)	ΔH_1 (ft)	Q_{system} (ft^3)
6/22/17	0.6	0.8	16
6/29/17	0.1	1.5*	29
7/8/17	0.3+	0.6	12
7/10/17	0.5+	0.5	11
7/11/17	0.6+	0.5	9
7/17/17	0.9+	0.6	11
7/30/17	0.5+	0.4	8
8/3/17	0.3+	0.5	11
8/4/17	0.3+	0.5	10
8/7/17	0.9+	0.4	8
8/8/17	1.7+	0.5	10
8/18/17	0.4+	0.6	11
8/19/17	0.1+	0.5	10
8/27/17	0.6+	0.5	10
8/29/17	0.4+	0.5	9
9/1/17	0.5+	0.6	11
9/11/17	2.3+	0.5	10
10/7/17	0.6+	1.1	21
10/17/17	0.9+	3.8*	75
11/23/17	2.5+	2.3*	45
12/9/17	0.5+	0.9	19
1/3/18	0.6+	1.0	20
1/23/18	0.2+	0.9	17
1/28/18	0.5+	1.0	20
1/29/18	1.2+	1.1	21
2/4/18	0.2+	1.0	19
3/19/18	1.6+	1.1	23
4/9/18	1.6+	1.2	24
4/10/18	0.9+	1.5	30
4/15/18	0.7+	1.1	22
4/23/18	0.4+	1.1	22

+ indicates calibrated radar data; *indicates a height of water overtopping the central holding basin

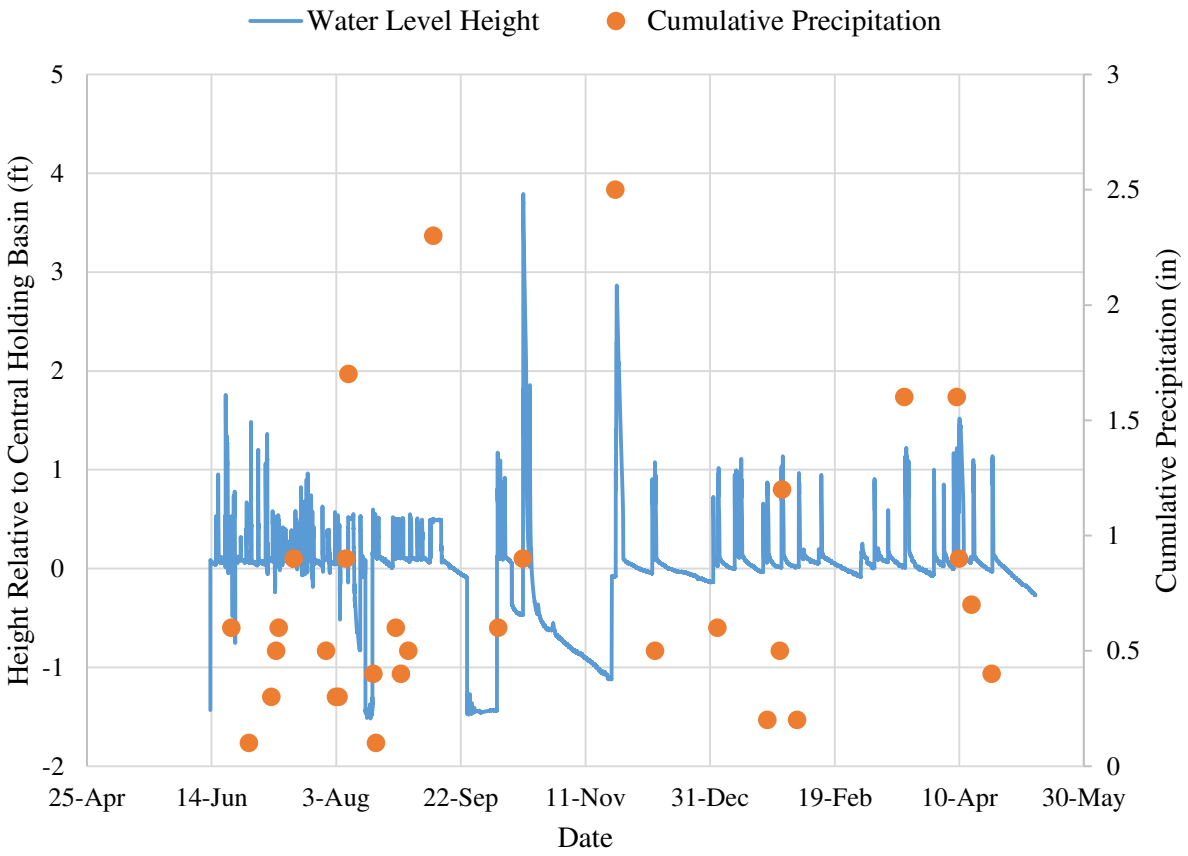

Figure A2. 4: Basin 2 Water Level Height vs. Cumulative Precipitation

Table 9: Runoff and capture efficiency for storm events in Basin 9B West

Date	Cumulative Precipitation (in)	Q_{in} (ft^3)	Q_{system} (ft^3)	Q_{out} (ft^3)	Capture efficiency (%)
6/22/17	0.6	3.1×10^3	3.1×10^3	0.0	100
6/29/17	0.1	3.4×10^3	3.4×10^3	0.0	100
7/8/17	0.3+	3.3×10^3	3.3×10^3	0.0	100
7/10/17	0.5+	2.8×10^3	2.8×10^3	0.0	100
7/11/17	0.6+	2.7×10^3	2.7×10^3	0.0	100
7/17/17	0.9+	4.2×10^3	4.2×10^3	0.0	100
7/30/17	0.5+	2.6×10^3	2.6×10^3	0.0	100
8/3/17	0.3+	2.5×10^3	2.5×10^3	0.0	100
8/4/17	0.3+	3.0×10^3	3.0×10^3	0.0	100
8/7/17	0.9+	4.3×10^3	4.3×10^3	0.0	100
8/8/17	**1.7+**	$6.2 - 12 \times 10^3$	3.2×10^3	$3.0 - 8.8 \times 10^3$	**26 - 52**
8/16/17	0.5+	3.9×10^3	3.9×10^3	0.0	100
8/18/17	0.4+	3.2×10^3	3.2×10^3	0.0	100
8/19/17	0.1+	2.7×10^3	2.7×10^3	0.0	100
8/27/17	0.6+	2.9×10^3	2.9×10^3	0.0	100
8/29/17	0.4+	2.7×10^3	2.7×10^3	0.0	100
9/1/17	0.5+	3.0×10^3	3.0×10^3	0.0	100
9/11/17	**2.3+**	$8.7 - 17 \times 10^3$	4.6×10^3	$4.1 - 12.4 \times 10^3$	**27 – 53**
9/30/17	0.2+	0.8×10^3	0.8×10^3	0.0	100
10/7/17	0.6+	2.2×10^3	2.2×10^3	0.0	100
10/17/17	0.9+	3.6×10^3	3.6×10^3	0.0	100
10/19/17	0.1+	1.0×10^3	1.0×10^3	0.0	100
11/23/17	**2.5+**	$9.6 - 18 \times 10^3$	3.8×10^3	$5.8 - 11.2 \times 10^3$	**21 - 40**
12/9/17	0.5+	2.9×10^3	2.9×10^3	0.0	100
1/3/18	0.6+	2.7×10^3	2.7×10^3	0.0	100
1/23/18	0.2+	1.8×10^3	1.8×10^3	0.0	100
1/28/18	0.5+	2.2×10^3	2.2×10^3	0.0	100
1/29/18*	1.2+	3.6×10^3	3.6×10^3	0.0	100
2/4/18	0.2+	2.6×10^3	2.6×10^3	0.0	100
3/19/18	**1.6+**	$5.9 - 11 \times 10^3$	4.0×10^3	$1.9 - 7.0 \times 10^3$	**36 – 67**
4/9/18	1.6+	2.2×10^3	2.2×10^3	0.0	100
4/10/18*	0.9+	3.9×10^3	3.9×10^3	0.0	100
4/15/18	0.7+	2.7×10^3	2.7×10^3	0.0	100
4/23/18	0.4+	2.8×10^3	2.8×10^3	0.0	100

+ indicates calibrated radar data; bold boxes indicate events that exceeded system capacity;
*height of water on surface~height of berm (Eq. 8 assumed)

Table 10: Runoff and capture efficiency for storm events in Basin 2 vertical reactors

Date	Cumulative Precipitation (in)	Q_{in} (ft^3)	Q_{system} (ft^3)	Q_{out} (ft^3)	Capture efficiency (%)
6/22/17	0.6	6.8×10^3	56	6.8×10^3	<1%
6/29/17	0.1	0.2×10^3	69	0.2×10^3	<1%
7/8/17	0.3+	2.6×10^3	62	2.6×10^3	<1%
7/10/17	0.5+	6.0×10^3	51	6.0×10^3	<1%
7/11/17	0.6+	6.9×10^3	49	6.9×10^3	<1%
7/17/17	0.9+	13×10^3	51	13×10^3	<1%
7/30/17	0.5+	5.8×10^3	48	5.8×10^3	<1%
8/3/17	0.3+	2.1×10^3	51	2.1×10^3	<1%
8/4/17	0.3+	3.1×10^3	50	3.1×10^3	<1%
8/7/17	0.9+	12×10^3	48	12×10^3	<1%
8/8/17	1.7+	27×10^3	50	27×10^3	<1%
8/18/17	0.4+	4.5×10^3	51	4.5×10^3	<1%
8/19/17	0.1+	0.5×10^3	50	0.5×10^3	<1%
8/27/17	0.6+	6.9×10^3	50	6.9×10^3	<1%
8/29/17	0.4+	3.7×10^3	49	3.7×10^3	<1%
9/1/17	0.5+	6.5×10^3	51	6.5×10^3	<1%
9/11/17	2.3+	38×10^3	50	38×10^3	<1%
10/7/17	0.6+	7.5×10^3	61	7.5×10^3	<1%
10/17/17	0.8+	12×10^3	115	12×10^3	<1%
11/23/17	2.5+	42×10^3	85	42×10^3	<1%
12/9/17	0.4+	5.0×10^3	59	5.0×10^3	<1%
1/3/17	0.6+	8.1×10^3	60	8.1×10^3	<1%
1/23/17	0.2+	1.2×10^3	57	1.2×10^3	<1%
1/28/17	0.5+	6.5×10^3	60	6.5×10^3	<1%
1/29/17	1.2+	18×10^3	61	18×10^3	<1%
2/4/17	0.2+	1.5×10^3	59	1.5×10^3	<1%
3/19/18	1.6+	26×10^3	63	26×10^3	<1%
4/9/18	1.6+	25×10^3	64	25×10^3	<1%
4/10/18	0.9+	13×10^3	70	13×10^3	<1%
4/15/18	0.7+	10×10^3	62	10×10^3	<1%
4/23/18	0.4+	4.5×10^3	62	4.5×10^3	<1%

+ indicates calibrated radar data; bold boxes indicate events that exceeded system capacity

LIST OF REFERENCES

Abi Aad, M. P., Suidan, M. T., & Shuster, W. D. (2009). Modeling techniques of best management practices: Rain barrels and rain gardens using EPA SWMM-5. *Journal of Hydrologic Engineering*, *15*(6), 434-443.

Akan, A. O. (1990). Single-outlet detention-pond analysis and design. *Journal of Irrigation and Drainage Engineering*, *116*(4), 527-536

Albertin, A. R., Sickman, J. O., Pinowska, A., & Stevenson, R. J. (2012). Identification of nitrogen sources and transformations within karst springs using isotope tracers of nitrogen. *Biogeochemistry*, *108*(1-3), 219-232.

Ando, A. W., & Freitas, L. P. (2011). Consumer demand for green stormwater management technology in an urban setting: The case of Chicago rain barrels. *Water Resources Research*, *47*(12).

Anyona, A. (2009). Stormwater Best Management Practices. *Stream of Consciousness*, 6.

Askarizadeh, A., Rippy, M. A., Fletcher, T. D., Feldman, D. L., Peng, J., Bowler, P., ... & Jiang, S. C. (2015). From rain tanks to catchments: use of low-impact development to address hydrologic symptoms of the urban stream syndrome. *Environmental science & technology*, *49*(19), 11264-11280

Atkinson, T. C. (1977) Diffuse flow and conduit flow in limestone terrain in Mendip Hills, Somerset (Great Britain). J. Hydrol. 35, 93-100.

Bakalowicz, M. (2005). Karst groundwater: a challenge for new resources. *Hydrogeology journal*, *13*(1), 148-160

Beres, M., Luetscher, M., & Olivier, R. (2001). Integration of ground-penetrating radar and microgravimetric methods to map shallow caves. *Journal of Applied Geophysics*, *46*(4), 249-262.

Birch, G. F., Fazeli, M. S., & Matthai, C. (2005). Efficiency of an infiltration basin in removing contaminants from urban stormwater. *Environmental Monitoring and Assessment*, *101*(1-3), 23-38

BOLD & GOLD® CTS REGULAR BIOSORPTION ACTIVATED MEDIA Specifications(Rep.). (2017). doi:https://ecs-water.com/stormwater-management/bold-and-gold-stormwater/

Bonacci, O. (1993). Karst springs hydrographs as indicators of karst aquifers.

Boyd, M. J., Bufill, M. C., & Knee, R. M. (1993). Pervious and impervious runoff in urban catchments. *Hydrological Sciences Journal*, *38*(6), 463-478

Brown, J. N., & Peake, B. M. (2006). Sources of heavy metals and polycyclic aromatic hydrocarbons in urban stormwater runoff. *Science of the total environment*, *359*(1-3), 145-155.

Burns, D., Vitvar, T., McDonnell, J., Hassett, J., Duncan, J., & Kendall, C. (2005). Effects of suburban development on runoff generation in the Croton River basin, New York, USA. *Journal of Hydrology*, *311*(1-4), 266-281

Colman, E. A. (1947). A LABORATORY PROCDURE FOR DETERMINING THE FIELD CAPACITY OF SOILS. *Soil Science*, *63*(4), 277-284.

Chalikakis, K., (2006) Application de méthodes géophysiques pour la reconnaissance et la protection des ressources en eau dans les milieux karstiques [Geophysical methods applied to water exploration and protection in karst environment]. PhD Thesis, Université Pierre et Marie Curie-Paris 6, France, 217pp

Chalikakis, K., Plagnes, V., Guerin, R., Valois, R., & Bosch, F. P. (2011). Contribution of geophysical methods to karst-system exploration: an overview. *Hydrogeology Journal*, *19*(6), 1169

Chang, N. B., Hossain, F., & Wanielista, M. (2010). Filter media for nutrient removal in natural systems and built environments: I—Previous trends and perspectives. *Environmental Engineering Science*, *27*(9), 689-706.

Chang, N., Wanielista, M., & Hartshorn, N. (2015). *Optimal Design of Stormwater Basins with Bio-sorption Activated Media (BAM) in Karst Environments - Phase I: Site Screening and Selection* (Rep. No. BDV24-977-12). Tallahassee, FL: FDOT.

Chang, N. B., Xuan, Z., & Wanielista, M. P. (2012). A tracer study for assessing the interactions between hydraulic retention time and transport processes in a wetland system for nutrient removal. *Bioprocess and biosystems engineering*, *35*(3), 399-406

Cronshey, R. (1986). *Urban hydrology for small watersheds*. US Dept. of Agriculture, Soil Conservation Service, Engineering Division.

Das, B. M. (2008). Advanced soil mechanics, Taylor and Francis

Davis, Stanley N., et al. "Ground-Water Tracers—A Short Review." *Groundwater* 18.1 (1980): 14-23.

Drysdale, R., Pierotti, L., Piccini, L., Baldacci, F., 2001. Suspended sediments in karst spring waters near Massa (Tuscany), Italy. Environ. Geol. 40, 1037–1050

Durden, D. (2012). DATA AVAILABILITY FOR DEVELOPMENT OF THE NORTH FLORIDA SOUTHEAST GEORGIA (NFSEG) REGIONAL GROUNDWATER FLOW MODEL IN THE AREA OF ITS POTENTIAL DOMAIN. *NFSEG Technical Team*.

Einsiedl, F. (2005). Flow system dynamics and water storage of a fissured-porous karst aquifer characterized by artificial and environmental tracers. *Journal of Hydrology*, *312*(1-4), 312-321

Emerson, C. H., Welty, C., & Traver, R. G. (2005). Watershed-scale evaluation of a system of storm water detention basins. *Journal of Hydrologic Engineering*, *10*(3), 237-242.

EPA, U. (2015). Preventing Eutrophication: Scientific Support for Dual Nutrient Criteria.

Fan, A. M., & Steinberg, V. E. (1996). Health implications of nitrate and nitrite in drinking water: an update on methemoglobinemia occurrence and reproductive and developmental toxicity. *Regulatory toxicology and pharmacology*, 23(1), 35-43

Florea, L. J. (2006). Architecture of air-filled caves within the karst of the Brooksville Ridge, west-central Florida. *Geography/Geology Faculty Publications*, 12.

Florea, L. J., Budd, D. A., & Brinkman, R. B. (2009). Caves and karst of west-central Florida. *Geography/Geology Faculty Publications*, 21.

Florida Department of Environmental Protection. Tallahassee: FDEP, 2016, *Wekiva Basin Ground Water Tracer Study for Rock and Wekiwa Springs*. Rep. no. WM926. 1-10. Print.

Florida Department of Environmental Protection (FDEP) & Water Management Districts. (2010) Environmental Resource Permit Stormwater Quality Applicant's Handbook: Design Requirements for Stormwater Treatment Systems in Florida. Retrieved from http://www.fdot.gov/roadway/drainage/files/StormwaterQualityAppHB-DRAFT.pdf

Flury, M., & Wai, N. N. (2003). Dyes as tracers for vadose zone hydrology. *Reviews of Geophysics*, *41*(1).

Ford, D., & Williams, P. D. (2013). *Karst hydrogeology and geomorphology*. John Wiley & Sons.

Gautam, P., Pant, S. R., & Ando, H. (2000). Mapping of subsurface karst structure with gamma ray and electrical resistivity profiles: a case study from Pokhara valley, central Nepal. *Journal of Applied Geophysics*, *45*(2), 97-110

Goldscheider, N. (2005). Karst groundwater vulnerability mapping: application of a new method in the Swabian Alb, Germany. *Hydrogeology Journal*, *13*(4), 555-564.

Goldscheider, N., & Drew, D. (2007). Methods in karst hydrogeology. International Contributions to Hydrogeology 26. *Int. Ass. Hydrogeologists*..

Greiner, and URS. (2003) Pond 2 Post Development Hydrology. pp. 1–39, Pond 2 Post Development Hydrology

Greiner and URS. (2004a). Stormwater Management Calculations for State Road from SR 464/CR 464 to SR 40 (Vol. 3, pp. 1 - 479, Rep. No. 238677). Orlando, FL: URS

Greiner and URS. (2004b). Stormwater Management Calculations for State Road from SR 464/CR 464 to SR 40 (Vol. 2, pp. 1 - 482, Rep. No. 238677). Orlando, FL: URS

Greiner and URS. (2004c). Stormwater Management Calculations for State Road from SR 464/CR 464 to SR 40 (Vol. 1, pp. 1 - 571, Rep. No. 238677). Orlando, FL: URS

Greiner and URS. (2007a). Stormwater Management Calculations for State Road from SR 464/CR 464 to SR 40 (Vol. 2, pp. 271 - 311, Rep. No. 238677). Orlando, FL: URS

Greiner and URS. (2007b). Stormwater Management Calculations for State Road from SR 464/CR 464 to SR 40 (Vol. 1, pp. 1 - 644, Rep. No. 238677). Orlando, FL: URS

Guerin, R., & Benderitter, Y. (1995) "Shallow Karst Exploration Using MT-VLF and DC Resistivity Methods," Geophysical Prospecting, Vol. 43, pp. 635–653.

Halstead, J. A., Kliman, S., Berheide, C. W., Chaucer, A., & Cock-Esteb, A. (2014). Urban stream syndrome in a small, lightly developed watershed: a statistical analysis of water chemistry parameters, land use patterns, and natural sources. *Environmental monitoring and assessment*, *186*(6), 3391-3414.

Hach Company. (2015). *Nitrate Cadmium Reduction Method LR Method 8192, Powder Pillows.* Retrieved from https://www.hach.com/product.detail-downloads.jsa?id=10239244800

Hach Company. (2015). *Nitrogen, Total, Persulfate Digestion HR Method 10072, Test 'N Tube Vials.* Retrieved from https://www.hach.com/product.detail-downloads.jsa?id=10239244800

Hach Company. (2017). *Phosphorus, Total-PhosVer® with Acid Persulfate Digestion Method 8190, Test 'N Tube™ Vials.* Retrieved from https://www.hach.com/product.detail-downloads.jsa?id=10239244800

He L, Feng M, He Z, Wang X (2006) Application of EM methods for the investigation of Qiyueshan tunnel, China. J Environ Eng Geophys 11:151–156

Hendrickx, J. M., & Flury, M. (2001). Uniform and preferential flow mechanisms in the vadose zone. *Conceptual models of flow and transport in the fractured vadose zone*, 149-187.

Husic, A., Fox, J., Agouridis, C., Currens, J., Ford, W., & Taylor, C. (2017). Sediment carbon fate in phreatic karst (Part 1): Conceptual model development. *Journal of Hydrology*, *549*, 179-193

Hood, A. C. (2012). Evaluation of Biosorption Activated Media Under Roadside Swales for Stormwater Quality Improvement and Harvesting.

Hood, A., Chopra, M., & Wanielista, M. (2013). Assessment of biosorption activated media under roadside swales for the removal of phosphorus from stormwater. *Water*, *5*(1), 53-66.

Howard, A. D., & Groves, C. G. (1995). Early development of karst systems: 2. Turbulent flow. *Water Resources Research*, *31*(1), 19-26

Jacoby, C. A., T. K. Frazer, and E. J. Phlips. 2008. Chapter 4: Nutrient effects on spring flora and fauna. In: Summary and synthesis of the available literature on the effects of nutrients on spring organisms and systems. Report prepared for the Florida Department of Environmental Protection. Tallahassee, FL

Johnston, M. A., & Carpenter, P. J. (1998). Use of seismic refraction surveys to identify mine subsidence fractures in glacial drift and bedrock. *Journal of Environmental and Engineering Geophysics*, *2*, 213-222.

Kaufmann O, Quinif Y (2001) An application of cone penetration tests and combined array 2D electrical resistivity tomography to delineate cover-collapse sinkhole prone areas: geotechnical and environmental applications of karst geology and hydrology. Balkema, Lisse, the Netherlands, pp 359–364

Kim, H., Seagren, E. A., & Davis, A. P. (2000). Engineering bioretention for removal of nitrate from storm water runoff. WEFTEC 2000 Conference Proceedings on CDROM Research Symposium. *Nitrogen Removal, Session*, *19*.

Kincaid, T., Davies, G., Werner, C., & DeHan, R. (2012). *Demonstrating interconnection between a wastewater application facility and a first magnitude spring in a karstic watershed: Tracer study of the Southeast Farm Wastewater Reuse Facility, Tallahassee, Florida*. Florida Geological Survey.

Knochenmus, D. D. (1967). *Tracer studies and background fluorescence of ground water in the Ocala, Florida, area* (No. 67-132).

Knowles, L., Katz, B. G., & Toth, D. J. (2010). Using multiple chemical indicators to characterize and determine the age of groundwater from selected vents of the Silver Springs Group, central Florida, USA. *Hydrogeology journal*, *18*(8), 1825-1838

Lane, E. (1986). *Karst in Florida* (No. 29). Florida Geological Survey, 1-100.

Lange, A. L. (1999). Geophysical studies at Kartchner Caverns state park, Arizona. *Journal of Cave and Karst Studies*, *61*(2), 68-72.

Lee, B. C., Matsui, S., Shimizu, Y., & Matsuda, T. (2005). Characterizations of the first flush in storm water runoff from an urban roadway. *Environmental technology*, *26*(7), 773-782.

Lloyd-Davies, D. E. (1906). ‘‘The elimination of storm water from sewerage systems.’’ Proc., Inst. Civ. Eng., London, 164, 41–67

Lyon, S. W., McHale, M. R., Walter, M. T., & Steenhuis, T. S. (2006). The impact of runoff generation mechanisms on the location of critical source areas. *JAWRA Journal of the American Water Resources Association*, *42*(3), 793-804.

Magal, E., Weisbrod, N., Yakirevich, A., & Yechieli, Y. (2008). The use of fluorescent dyes as tracers in highly saline groundwater. *Journal of Hydrology*, *358*(1-2), 124-133.

Mah, T. F. C., & O'toole, G. A. (2001). Mechanisms of biofilm resistance to antimicrobial agents. *Trends in microbiology*, *9*(1), 34-39

Majumdar, D. (2003). The blue baby syndrome. *Resonance*, 8(10), 20-30.

Mallin, M. A., Johnson, V. L., & Ensign, S. H. (2009). Comparative impacts of stormwater runoff on water quality of an urban, a suburban, and a rural stream. *Environmental Monitoring and Assessment*, *159*(1-4), 475-491.

Marsalek, J., & Marsalek, P. M. (1997). Characteristics of sediments from a stormwater management pond. *Water Science and technology*, *36*(8-9), 117-122.

Mays, L. W., ed. (2001). ‘‘Chapter 1: Introduction.’’ Stormwater collection systems design handbook, McGraw-Hill, New York.

McCarthy, J., (2008). Stormwater and Antidegradation. In *New Hampshire Stormwater Manual*. (Vol. 1, pp. 55-75). New Hampshire: Comprehensive Environmental Inc.

McGrath RJ, Styles P, Thomas E, Neale S (2002) Integrated highresolution geophysical investigations as potential tools for water resource investigations in karst terrain. Environ Geol 42:552– 557

McGurk, B. E., Davis, J. B., Stokes, J. A., Toth, D. J., Colona, W., & Butt, P. (2012). Silver Springs nutrient pathway characterization project, final report. *St. Johns River Water Management District Special Publication SJ*.

Miller, J. A. (1986). *Hydrogeologic framework of the Floridan aquifer system in Florida and parts of Georgia, Alabama, and South Carolina*. Department of the Interior, US Geological Survey.

Mishra, S. K., & Singh, V. P. (1999). Another look at SCS-CN method. *Journal of Hydrologic Engineering*, *4*(3), 257-264

Mishra, S. K., & Singh, V. P. (2003). SCS-CN Method. In *Soil conservation service curve number (SCS-CN) methodology* (pp. 84-146). Springer, Dordrecht.

Mitchell, V., Deletic, A., Fletcher, T. D., Hatt, B. E., & McCarthy, D. T. (2007). Achieving multiple benefits from stormwater harvesting. *Water Science and Technology*, *55*(4), 135-144.

National Oceanic and Atmospheric Administration. (2018, January 12). *Drought - Annual 2017*(Rep.). Retrieved June 18, 2018, from National Oceanic and Atmospheric Administration website: https://www.ncdc.noaa.gov/sotc/drought/201713

National Oceanic and Atmospheric Administration (NOAA), 2017, Climatological data annual summary, Florida, v. 121, no. 13, Ocala, FL.

Naujock, L. (2008). Development of hydraulic and soil properties for soil amendments and native soils for retention ponds in Marion County, Florida.

Odum, H. T. (1957). Trophic structure and productivity of Silver Springs, Florida. *Ecological monographs*, *27*(1), 55-112.

ONSET. (2008). *HOBOware® Pro Barometric Compensation Assistant User's Guide*. Retrieved from http://www.onsetcomp.com/files/manual_pdfs/10572-J%20Barometric%20Compensation%20Assistant%20User%27s%20Guide.pdf

O'Reilly, A. M., Chang, N. B., Wanielista, M. P., & Xuan, Z. (2010, June). Identifying biogeochemical processes beneath stormwater infiltration ponds in support of a new best management practice for groundwater protection. In *GQ10: Groundwater Quality Management in a Rapidly Changing World, Proc. 7th International Groundwater Quality Conference, Zurich, Switzerland* (pp. 13-18)

O'Reilly, A. M., Wanielista, M. P., Chang, N. B., Xuan, Z., & Harris, W. G. (2012). Nutrient removal using biosorption activated media: Preliminary biogeochemical assessment of an innovative stormwater infiltration basin. *Science of the Total Environment*, *432*, 227-242

Pasmore, M., Todd, P., Smith, S., Baker, D., Silverstein, J., Coons, D., & Bowman, C. N. (2001). Effects of ultrafiltration membrane surface properties on Pseudomonas aeruginosa biofilm initiation for the purpose of reducing biofouling. *Journal of Membrane Science*, *194*(1), 15-32

Paul, M. J., & Meyer, J. L. (2001). Streams in the urban landscape. *Annual review of Ecology and Systematics*, *32*(1), 333-365

Phelps, G. G. (2004). *Chemistry of ground water in the Silver Springs Basin, Florida, with an emphasis on nitrate*. US Department of Interior, US Geological Survey.

Powers, R., (2009). *Calibration* [PowerPoint slides]. Retrieved from http://bionmr.unl.edu/course.php?id=chem116

Pronk, M., Goldscheider, N., & Zopfi, J. (2006). Dynamics and interaction of organic carbon, turbidity and bacteria in a karst aquifer system. *Hydrogeology Journal*, *14*(4), 473-484.

Pronk, M., Goldscheider, N., Zopfi, J., & Zwahlen, F. (2009). Percolation and particle transport in the unsaturated zone of a karst aquifer. *Groundwater*, *47*(3), 361-369.

Quinlan, J. F. (1989). *Ground-water monitoring in karst terranes: recommended protocols and implicit assumptions*. US Environmental Protection Agency, Environmental Monitoring Systems Laboratory.

Rose, S., & Peters, N. E. (2001). Effects of urbanization on streamflow in the Atlanta area (Georgia, USA): a comparative hydrological approach. *Hydrological Processes*, *15*(8), 1441-1457.

Roth, M. J. S., & Nyquist, J. E. (2003). Evaluation of multi-electrode earth resistivity testing in karst. *Geotechnical Testing Journal*, *26*(2), 167-178

Rowe, D. B. (2011). Green roofs as a means of pollution abatement. *Environmental pollution,* 159(8-9), 2100-2110.

Roy, J. W., & Bickerton, G. (2011). Toxic groundwater contaminants: an overlooked contributor to urban stream syndrome?. *Environmental science & technology*, *46*(2), 729-736

Schipper, L. A., Barkle, G. F., & Vojvodic-Vukovic, M. (2005). Maximum rates of nitrate removal in a denitrification wall. *Journal of environmental quality*, *34*(4), 1270-1276.

Scott, T. M., Means, G. H., Meegan, R. P., Means, R. C., Upchurch, S., Copeland, R. E., Jones, J., Tina, R., & Willet, A. (2004). Springs of Florida. Florida Geological Survey. *Bulletin, 66*.

Shoemaker, W. B., O'Reilly, A. M., Sepúlveda, N., Williams, S. A., Motz, L. H., & Sun, Q. (2004). Comparison of estimated areas contributing recharge to selected springs in north-central Florida by using multiple ground-water flow models. *Tallahassee, FL.*

Shuster, W. D., Bonta, J., Thurston, H., Warnemuende, E., & Smith, D. R. (2005). Impacts of impervious surface on watershed hydrology: a review. *Urban Water Journal*, *2*(4), 263-275

Siemers, J., & Dreybrodt, W. (1998). Early development of karst aquifers on percolation networks of fractures in limestone. *Water resources research*, *34*(3), 409-419

Sinclair, W. C., Stewart, J. W., Knutilla, R. L., Gilboy, A. E., & Miller, R. L. (1985). *Types, features, and occurrence of sinkholes in the karst of west-central Florida* (No. 85-4126). US Geological Survey,

Sivapalan, M., Beven, K., & Wood, E. F. (1987). On hydrologic similarity: 2. A scaled model of storm runoff production. *Water Resources Research*, *23*(12), 2266-2278

Smart, P. L., & Laidlaw, I. M. S. (1977). An evaluation of some fluorescent dyes for water tracing. *Water Resources Research*, *13*(1), 15-33

Spechler, R. M., & Schiffer, D. M. (1995). *Springs of Florida* (No. 151-95). US Geological Survey,

Stamm, D. R. (2008). *The springs of Florida*. Pineapple Press Inc.

Stanley, D. W. (1996). Pollutant removal by a stormwater dry detention pond. *Water Environment Research*, *68*(6), 1076-1083.

Sumanovac, F. and Weisser, M., 2001, "Evaluation of Resistivity and Seismic Methods for Hydrogeological Mapping in Karst Terrains," Journal of Applied Geophysics, Vol. 47, pp. 13–28.

Taylor, G. D., Fletcher, T. D., Wong, T. H., Breen, P. F., & Duncan, H. P. (2005). Nitrogen composition in urban runoff—implications for stormwater management. *Water research*, *39*(10), 1982-1989.

Tarboton, D. G. (2003). Rainfall-runoff processes. *Utah State University*.

Tihansky, A. B. (1999). Sinkholes, west-central Florida. *Land subsidence in the United States: US geological survey circular*, *1182*, 121-140

Tihansky, A. B., & Knochenmus, L. A. (2001). Karst features and hydrogeology in west-central Florida—a field perspective. *US Geological Survey Karst Interest Group Proceedings. US Geological Survey Water-Resources Investigations Report*, 01-4011.

Trudgill, S. T. (1987). Soil water dye tracing, with special reference to the use of Rhodamine WT, Lissamine FF and Amino G acid. *Hydrological processes*, *1*(2), 149-170.

U.S. Dept. of Agriculture (USDA). (2009a). "Hydrologic soil groups." Chapter 7, part 630, National engineering handbook, USDA Natural Resource Conservation Service (NRCS), Washington, DC.

U.S. Environmental Protection Agency (1983). *Results of Nationwide Urban Runoff Program: Volume 1 – Final Report*, United States Environmental Protection Agency, NTIS Assession Number: PB84-185552, National Technical Information Service, U.S. Department of Commerce, Springfield, Virginia, 22161

U.S. Environmental Protection Agency (1992) NPDES Storm Water Sampling Guidance Document, EPA-833/B-92-001; U.S. Environmen tal Protection Agency, Office of Water: Washington

U.S. Environmental Protection Agency (1999). *Preliminary Data Summary of Urban Storm Water Best Management Practices*, United States Environmental Protection Agency, EPA number: EPA-821-R-99-012, Office of Water, Washington, D.C., 20460

Wahl, S. (2009). Stormwater best management practices.

Walsh, C. J., Roy, A. H., Feminella, J. W., Cottingham, P. D., Groffman, P. M., & Morgan, R. P. (2005). The urban stream syndrome: current knowledge and the search for a cure. *Journal of the North American Benthological Society*, *24*(3), 706-723.

Wanielista, M. (2015). Biosorption Activated Media Filters [PowerPoint slides]. Retrieved from http://stormwater.ucf.edu/wp-content/uploads/2015/05/5-Biosorption-Activated-Media-Marty.pdf

Wanielista, M., Chang, N. B., Randall, A., Chopra, M., Hardin, M., Jones, J., Hood, A., & Salamah, S. (2014). *Demonstration Bio Media for Ultra-urban Stormwater Treatment* (No. SMA 1660 7051).

Wanielista, M., Kersten, R., & Eaglin, R. (1997). *Hydrology: Water quantity and quality control*. John Wiley and Sons.

Ward, M. H. (2005). Workgroup report: drinking-water nitrate and health—recent findings and research needs. Environmental health perspectives, 113(11), 1607.

Weiler, M., & Naef, F. (2003). An experimental tracer study of the role of macropores in infiltration in grassland soils. *Hydrological Processes*, *17*(2), 477-493.

Wen, D., Chang, N., & Wanielista, M. (2018). *Assessing the Nutrient Removal and Recovery Potential by Using Iron Filings-based Green Environmental Media (IFGEM) for Soil Amendment*(Rep.).

White, W. B. (2002). Karst hydrology: recent developments and open questions. *Engineering geology*, *65*(2-3), 85-105.

Wilson Jr, J. F., Cobb, E. D., & Kilpatrick, F. A. (1986). Fluorometric procedures for dye tracing: US Geological Survey Techniques of Water-Resources Investigations, book 3, chap. *A12*, *34*.

Winter, T. C. (1999). Relation of streams, lakes, and wetlands to groundwater flow systems. *Hydrogeology Journal*, 7(1), 28-45.

Van der Kamp, G. (1995). The hydrogeology of springs in relation to the biodiversity of spring fauna: a review. *Journal of the Kansas Entomological Society*, 4-17.

Vesper, D. J., & White, W. B. (2003). Metal transport to karst springs during storm flow: an example from Fort Campbell, Kentucky/Tennessee, USA. *Journal of Hydrology*, *276*(1-4), 20-36

Vietz, G. J., Walsh, C. J., & Fletcher, T. D. (2016). Urban hydrogeomorphology and the urban stream syndrome: Treating the symptoms and causes of geomorphic change. *Progress in Physical Geography*, *40*(3), 480-492.

Vogelsang, D., 1987, "Examples of Electromagnetic Prospecting for Karst and Fault Systems," Geophysical Prospecting, Vol. 35, pp. 604–617.

Xuan, Z., Chang, N. B., Wanielista, M. P., & Williams, E. S. (2013). System Dynamics Modeling of Nitrogen Removal in a Stormwater Infiltration Basin with Biosorption-Activated Media. *Journal of environmental quality*, *42*(4), 1086-1099.

Zhu, J., Currens, J. C., & Dinger, J. S. (2011). Challenges of using electrical resistivity method to locate karst conduits—a field case in the Inner Bluegrass Region, Kentucky. *Journal of Applied Geophysics*, *75*(3), 523-530